Assessment of soil organic carbon dynamics in colluvial and terraced soils

Pengzhi Zhao

Thèse présentée en vue de l'obtention du grade de

Docteur en Sciences









Université catholique de Louvain

Earth and Life Institute

Louvain-la-Neuve, Belgium



April 2022

Jury members

President

Marie–Laurence De Keersmaecker, Professor, Département de géographie – Earth and Life Institute, Faculté des Sciences, UCLouvain.

Promotors

Kristof Van Oost, Professor, Département de géographie, Earth and Life Institute, Faculté des Sciences, UCLouvain, Louvain–la–Neuve, Belgium.

Sebastian Dötterl, Professor**,** Department of Environmental Systems Science, ETH Zurich, Switzerland.

Jury members

Marnik Vanclooster, Professor, Earth and Life Institute, Faculté d'ingénierie biologique agronomique et environnementale, UCLouvain, Louvain–la–Neuve, Belgium.

Zhengang Wang, Professor, School of Geography and Planning, Sun Yat–sen University, Guangzhou, China.

Johan Six, Professor**,** Department of Environmental Systems Science, ETH Zurich, Switzerland.

Acknowledgement

Four-year doctoral life transits swiftly but every single moment is crystal in my mind. I still remember my first day in Belgium, full of language, people, food that I am unfamiliar with. Being in a mood of surprise, curiousness mingled with loneliness, I spent my first week in Louvain-la-Neuve. Immediately afterwards, a brand-new life started with thousand types of beers, tasty chocolate, big-sized fries, friendly colleagues, insightful seminars, and lovely working environment. All these things will bring me back into a vivid and special memory, which means a lot for the rest of my life.

First and foremost, I would like to thank my promoter prof. Kristof van Oost and co-promoter prof. Sebastian Dötterl. Thank you, Kristof, for steering my PhD in the right direction with your constructive feedbacks and highly valued comments. You trained me to think as an independent scientist and encouraged me to challenge myself. Many thanks for your support and advice for my future career. Thank you, Sebastian, for your great help and inputs during my PhD. Thank you for allowing me to stay in your group at the University of Augsburg and ETH Zurich, where I did most of my lab work. Thank you for taking me to your group activities, and I really enjoyed the atmosphere.

Special thanks go to my jury members, prof. Marie–Laurence De Keersmaecker, prof. Marnik Vanclooster, prof. Zhengang Wang and prof. Johan Six, for the time and efforts to read this book and for your constructive comments and suggestions to improve it.

This thesis was financially supported by the joint scholarship between China Scholarship Council and UCLouvain. Further financial supports for lab analysis and travel had been given by the advance European Research Council (ERC) grant (ERC-2017-ADG 787790) and Mobility grant from Le Fonds de la Recherche Scientifique (FNRS), Belgium.

Throughout my PhD research, many people have given me extraordinary help and supports in conducting field sampling and laboratory work: Thank you Marco, our excellent technician. I really enjoyed the time we spent together doing field sampling, driving, lab analysis, cutting soil cores, sharing music and funny stories. Thank you, Laura, my big sister, who helped me a lot at the beginning of my PhD. Many thanks to the colleagues at UCLouvain (Anne, Giacomo, Simon, Alice), Augsburg University (Mario, Anton, Anna, Benjamin, Florian), ETH Zurich (Marco, Julia, Matti, Brita, Laura, Daniel), and Gent University (Joseph), for your great help with conducting lab analysis as well as data interpretation. My gratitude also goes to prof. Enheng Wang, for your continued support over the years.

My life in Belgium would have been boring without friends: Special thanks to my office mate and ex-roommate – Dr. He, and Leuven team – Man, Fei, Zhiqiang, Siyao and Dong. Many thanks to Mercator team – Big brother Pu, and Hao, Anqi, Zhipeng, Rui, Qianqian, and Wanlin. I really enjoyed the time we spent together for cooking, drinking, playing pingpang and poker. I hope we stay in touch!

Last but not least, I would like to thank my study–mate, game–mate, soulmate and, my girlfriend, Yijie. Thank you for supporting my hobbies of fishing, hiking and making videos, accompanying me through some difficult times. My great thanks go to my parents, for always supporting my decision, allowing me to pursue my dreams without hesitation.

Pengzhi Zhao

Louvian-la-Neuve, April 2022

Table of contents

Jury members ..... **I**
Acknowledgement ..... **III**
Summary ..... **IX**
List of abbreviations ..... **XI**
Chapter 1 ..... **1**
General Introduction **1**
1.1 Soil organic carbon and climate change 1
1.2 SOC stabilization mechanisms 2
1.3 Key environmental factors influencing SOC stabilization 3
1.3.1 Climatic and soil geochemical factors 3
1.3.2 Role of human activities 5
1.4 Problem statement 12
1.5 Objectives and research questions 13
1.6 Outline of thesis 14
Chapter 2 ..... **17**
Factors controlling SOC stability in colluvial soils under contrasting climate and soil weathering conditions **17**
Abstract 17
2.1 Introduction 19
2.2 Material and methods 21
2.2.1 Study sites 21
2.2.2 Field sampling and sample processing 24
2.2.3 SOC fractionation, soil respiration and radiocarbon content 25
2.2.4 Soil physical–chemical properties 26
2.2.5 Statistical analysis 29
2.3 Results 29
2.3.1 Soil properties 29
2.3.2 Relationships between SOC components and controlling factors 31
2.3.3 Radiocarbon content in colluvial soil profiles 33
2.4. Discussion 35

2.5 Conclusions 39
Acknowledgements 39
Chapter 3 41
SOC stabilization mechanisms and temperature sensitivity in old terraced soils 41
Abstract 41
3.1 Introduction 43
3.2 Material and methods 46
3.2.1 Study sites 46
3.2.2 Soil sampling 47
3.2.3 SOC fractionation 49
3.2.4 Temperature–sensitivity based on soil incubations 50
3.2.5 Soil burial–age and soil geochemical properties along the agricultural terraces 51
3.2.6 Statistical analysis 54
3.3 Results 55
3.3.1 SOC fractions composition, temperature sensitivity and soil respiration 55
3.3.2 Controls on terrace SOC stability 58
3.3.3 Terrace soil burial–age and SOC temperature sensitivity (Q_{10}) 59
3.4 Discussion 61
3.4.1 Terrace SOC stabilization: importance of carbon burial and terrace age 61
3.4.2 Main controls on temperature sensitivity 63
3.5 Conclusion 65
Acknowledgments 65
Chapter 4 67
Quantifying soil properties relevant to soil organic carbon biogeochemical cycles by infrared spectroscopy: the importance of compositional data analysis 67
Abstract 67
4.1 Introduction 69
4.2 Materials and methods 72

4.2.1 Soil sampling and calibration sample set selection....72
4.2.2 Spectroscopy measurements and pre–processing....76
4.2.3 Laboratory soil analysis....77
4.2.4 Memory–based learning model....78
4.2.5 Compositional analysis of data and log–ratio transformation....79
4.2.6 Model validation and evaluation....81
4.3 Results....82
4.3.1 Overview of the reference measurements....82
4.3.2 Comparison of three log–ratio transformation methods....84
4.3.3 Comparison of model performance between compositional data analysis and conventional methods....86
4.4 Discussion....93
4.4.1 Comparison of three log–ratio transformation methods....93
4.4.2 The advantages of log–ratio transformation methods in predicting soil properties from spectroscopy....94
4.4.3 Log–ratio transformation coupled with MBL models enable reliably predicted soil properties from spectra....95
4.5 Conclusion....97
Acknowledgements....97
Chapter 5....99
Controls on soil organic carbon stocks and dynamics in agricultural terraces along climatic and geochemical gradients....99
Abstract....99
5.1 Introduction....101
5.2 Materials and Methods....104
5.2.1 Study site and soil sampling....104
5.2.2 Soil incubation....107
5.2.3 Soil physico–chemical properties....107
5.2.4 SOC fractionation....108
5.2.5 Soil burial age....109
5.2.6 Statistical analysis....109
5.3 Results....111

5.3.1 Higher SOC stock of terracing landforms relative to non–terracing landforms....111
5.3.2 Description of SOC variables of terraced soils along climate and soil geochemistry gradients....111
5.3.3 Predicting SOC density and SPR....115
5.4 Discussion....119
5.4.1 Controls on terrace SOC stocks....119
5.4.2 Controls on soil heterotrophic respiration of terraces....121
5.5 Conclusion....123
Acknowledgements....123
Chapter 6....125
Conclusions and perspectives....125
6.1 General conclusions....125
6.2 Answers to the research questions....128
6.3 Limitations and perspectives....130
6.3.1 Re–deposited C in colluvial and alluvial settings....130
6.3.2 SOC dynamics in terraced soils....131
List of Figures....134
List of Tables....140
Appendixes....142
Supplementary discussion D1....142
How much SOC is stored in the buried soil layers in terraced landforms?....142
Supplementary tables....146
Bibliography....150

Summary

Colluvial soils consist of surface soils and/or parent materials locally transported from upper section of the slopes through water erosion, tillage erosion and construction of agricultural terraces. As a consequence of the recognition that colluvial soil stores large amounts of soil organic carbon (SOC), the SOC cycle in colluvial soils has received increasing attention. The aim of this thesis was to evaluate and understand the SOC dynamics and controlling factors in colluvial soils in the context of climate change. This was done for two specific colluvial environments: eroded and terraced agricultural systems. For the eroded colluvial soils, soil deposition rate is identified as the most important independent control on SOC stability and this is independent of climate zone. In addition, the rate of deposition also indirectly affects SOC stability by changing the average weathering status and mineral matrix of colluvial (sub)soil settings which affect mineral–dependent SOC physico-chemical protection mechanisms. The remaining part of this thesis focused on the colluvial SOC dynamics in terraced systems. Firstly, we demonstrate that the soil infrared spectroscopy, combined with compositional data analysis enables efficient and reliable 'large–scale' assessment of terracing soil properties relevant to SOC biogeochemical cycles. Furthermore, we confirm that the terraced landforms store more SOC than non-terracing landforms, mainly due to the preservation of SOC by topsoil burial in colluvial settings. Finally, we demonstrate that the terrace soil age is a key factor controlling soil heterotrophic respiration of subsoils (e.g., burial layers), likely through driving the mineral weathering and thus determining the availability of reactive mineral surfaces that stabilize SOC. In addition, the terrace soil age is also a fundamental regulator of SOC temperature sensitivity (Q_{10}) to decomposition by governing the temporal evolution of SOC fractions and soil C:N ratio (C quality). This thesis demonstrates the need to consider the specific mechanisms of SOC stabilization and temperature sensitivity to fully understand future C cycling of colluvial soils in the light of climate, land use and land management change.

List of peer–reviewed publications

Published

Zhao, P., Fallu, D.J., Cucchiaro, S., Tarolli, P., Waddington, C., Cockcroft, D., Snape, L., Lang, A., Doetterl, S., Brown, A.G. and Van Oost, K., 2021. Soil organic carbon stabilization mechanisms and temperature sensitivity in old terraced soils. *Biogeosciences*, 18(23), .6301–6312.

Brown, A. G., Fallu, D., Cucchiaro, S., Tarolli, P., **Zhao, P.,** Pears, B.R., Van Oost, K., Snape, L., Lang, A., Maria Albert, R., Alsos, I.G., & Waddington, C., 2021. Ending the Cinderella status of terraces and lynchets in Europe: The geomorphology of agricultural terraces and implications for ecosystem services and climate adaptation. *Geomorphology*, 107579.

Cucchiaro, S., Paliaga, G., Fallu, D.J., Pears, B.R., Walsh, K., **Zhao, P.,** Van Oost, K., Snape, L., Lang, A., Brown, A.G. and Tarolli, P., 2021. Volume estimation of soil stored in agricultural terrace systems: A geomorphometric approach. *Catena*, 207, 105687.

Cucchiaro, S., Fallu, D. J., **Zhao, P.,** Waddington, C., Cockcroft, D., Tarolli, P., and Brown, A. G., 2020. SfM photogrammetry for GeoArchaeology. In Developments in Earth Surface Processes (Vol. 23, pp. 183–205). Book Chapter, *Elsevier*.

Submitted

Zhao, P. Doetterl, S., Wang, Z., Hoyt, AM., Wang, E., Yu, H., Quijano, L., Fallu, J., Brown, AG., Six, J., Van Oost, K. Factors controlling SOC stability in colluvial soils under contrasting climate and soil weathering conditions. Under review in *European Journal of Soil Science*

Zhao, P. Daniel J. Fallu, Ben R., Allonsius C., Lembrechts J., Van de Vondel, S., Meysman FJR., Cucchiaro, S., Tarolli, P., van Wesemael, B., Six, J., Brown, AG., Van Oost, K. Quantifying soil properties relevant to SOC biogeochemical cycles by infrared spectroscopy: the importance of compositional data analysis. Submitted to *Geoderma*

List of abbreviations

SOC	Soil Organic Carbon
CO_2	Carbon Dioxide
CH_4	Methane
Fe	Iron
Mn	Manganese
Al	Aluminum
Ca	Calcium
K	Potassium
Mg	Magnesium
Na	Sodium
H_2O_2	Hydrogen Peroxide
MAT	Mean Annual Temperature
MAP	Mean Annual Precipitation
PET	Potential Evapotranspiration
MAP–PET	Soil Effective Water
SPR	Soil Potential Heterotrophic Respiration Rate
cPOM	Coarse Particulate OC (> 250 mm)
micro-agg	Microaggregated OC (250–53 mm)
s+c	Free Silt & Clay Associated OC (< 53 mm)
CEC	Cation Exchange Capacity
BS	Base Saturation
Fe_d/Fe_t	Ratio of Pedogenic Fe Oxides to Total Fe
TRB	Total Reserve in Bases
CIA	Chemical Alteration Index
Al_p	Pyrophosphate-extractable Al Oxyhydroxide
Fe_p	Pyrophosphate-extractable Fe Oxyhydroxide
Mn_p	Pyrophosphate-extractable Mn Oxyhydroxide
Al_o	Oxalate-extractable Al Oxyhydroxide
Fe_o	Oxalate-extractable Fe Oxyhydroxide
Mn_o	Oxalate-extractable Mn Oxyhydroxide
Al_d	DCB-extractable Al Oxyhydroxide
Fe_d	DCB-extractable Fe Oxyhydroxide
Mn_d	DCB-extractable Mn Oxyhydroxide
$Fe_{o–p}$	Poorly Crystalline Fe Oxide
$Al_{o–p}$	Poorly Crystalline Al Oxide
$Mn_{o–p}$	Poorly Crystalline Mn Oxide
Fe_{d-o}	Crystalline Fe Oxides
M_p	Sum of Pyrophosphate-Extractable Oxides

M_o	Sum of Oxalate-Extractable Oxides
M_d	Sum of DCB-Extractable Oxides
NPP	Net Primary Production
^{137}Cs	Caesium-137
pMC	Percent Modern Carbon
1:1N	1:1 Non-Expandable Clay Mineral
2:1N	2:1 Non-Expandable Clay Mineral
2:1E	2:1 Expandable Clay Mineral
Q_{10}	SOC Temperature Sensitivity to Decomposition
C:N	Carbon: Nitrogen
OSL	Optically Stimulated Luminescence
pOSL	Portable Optically Stimulated Luminescence
Rb/Sr	Ratio of Rubidium to Strontium
Vis-NIR	Visible Near Infrared Spectroscopy
MIR	Mid Infrared Spectroscopy
Texture_MIR	MIR Predicted Soil Texture
Texture_NIR	Vis-NIR Predicted Soil Texture
alr	Additive Log-ratio Transformation
clr	Centered Log-ratio Transformation
ilr	Isometric Log-ratio Transformation
SD	Standard Deviation
CV	Coefficient of Variation
MBL	Memory-Based Learning
RMSE	Standard Deviation of the Root Mean Square
R^2	The Coefficient of Determination
RPD	Ratio of Performance to Deviation
RPIQ	Ratio of Performance to Interquartile Range
EXE	The Relative Error
IQR	The Interquartile Range
Dfc	Continental Subarctic Climate
Cfb	Marine West Coast Climate
Cfa	Humid Subtropical Climate
Csa	Hot-Summer Mediterranean Climate
Bsk	Semiarid Continental Climate
WRB	World reference base for soil resources
rPCA	Rotated Principal Component Analysis
RCs	Rotated Components

Chapter 1

General Introduction

1.1 Soil organic carbon and climate change

Carbon (C) element has received a considerable attention in scientific research and news headlines over the last few decades, because of the close link between this element and global climate change. Specifically, the accumulation of C in the atmosphere in the form of carbon dioxide (CO_2) and methane (CH_4), is thought to be responsible for a large portion of the rise in global temperature since the industrial revolution. As a result of fuel combustion and land use changes, CO_2 concentrations in the atmosphere has risen from an annual average of 280 ppm in 1750 to the current 410 ppm. In the meanwhile, global surface temperature in the first two decades of the 21st century (2001–2020) is 0.99 °C higher than in 1850–1900 (IPCC, 2021). Many of the physical impacts of climate warming are already evident, including glacier retreat, extreme weather events, biodiversity loss and food insecurity (Godfray et al., 2010; Thuiller et al., 2005), necessitating the identification of strategies for mitigating CO_2 emission and global warming.

Although its significance in regulating the global climate, atmospheric C represents only a small fraction (1.8%) of the global C reservoir. The largest portion of C is distributed in ocean reservoirs (85.1%, Figure 1–1), while in the biosphere majority of C is present in soils (5.0%). It is estimated that first meter–soils globally store 1500 – 2000 Gt C, which is even larger than that of the atmosphere and surface vegetation combined. Therefore, a small disturbance to the global soil system may cause the significant transformation of soil C to atmosphere in the form of greenhouse gases (i.e., CO_2 and CH_4). For this reason, a thorough understanding of how soil systems (de)stabilize C and exchange it with atmospheric C pool has been of great interest to the soil scientist, climate modelers and politicians. The

aim of this thesis is therefore to improve our understanding of the soil organic carbon (SOC) as the largest terrestrial C reservoir.

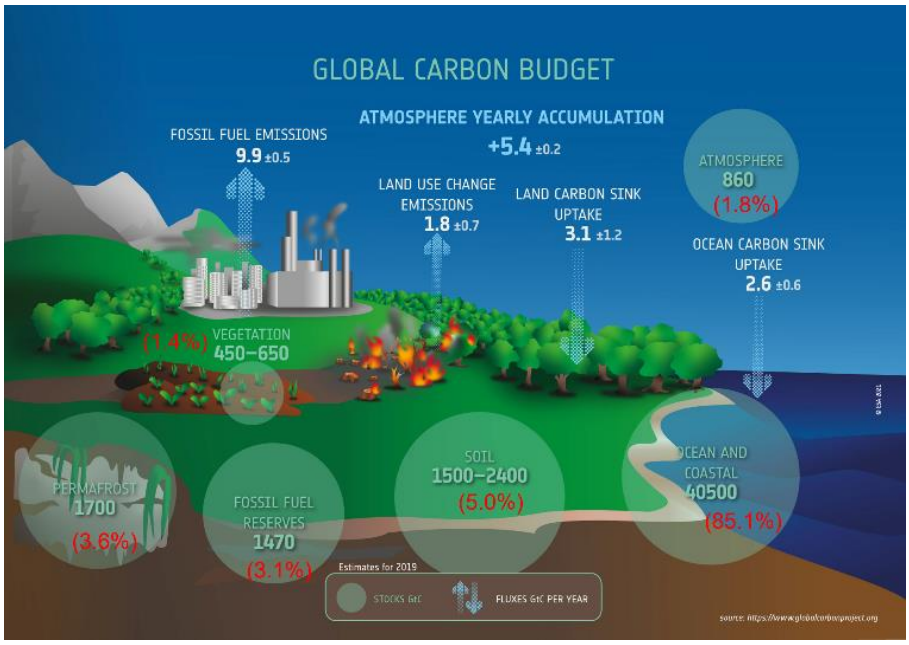

Figure 1–1 Carbon stocks (Pg C) in the major global reservoirs. Picture was produced by European Space Agency based on data from Global Carbon Project in 2019 (www.globalcarbonproject.org). The contribution of each C reservoir to the global C reservoir is shown as numbers in red.

1.2 SOC stabilization mechanisms

Three key stabilization mechanisms that can protect SOC from being mineralized and decomposed in soils have been identified: (i) Physical protection, whereby soil aggregates physically protect SOC by isolating microbes and fauna from their substrates and inhibiting the rate of diffusion of oxygen and enzymes (Six et al., 2002); (ii) Mineral protection, whereby SOC becomes chemically inaccessible to decomposers resulting from the absorption of SOC onto mineral surfaces or from complexation of dissolved organics with biochemical weathering products such as Fe–, Mn– and Al–

oxy–hydroxides (Blume et al., 2016); (iii) Biochemical stabilization, referring to inherent bio–chemical recalcitrance of SOC. Historically, it was thought that biochemical stabilization was mostly a function of molecular complexity structure of SOC (Lützow et al., 2006). However, analytical and experimental advances have questioned the selective preservation of organic structures due to recalcitrance (Kleber, 2010; Schmidt et al., 2011). For example, the plant–derived aromatic compounds, such as lignin, have been proved not as persistent as previously suggested as it can be decomposed quickly in favourable environmental conditions (Schmidt et al., 2011; Thevenot et al., 2010). In contrast, saccharides and proteins that are thought to be labile compounds persists for decades (Schmidt et al., 2011). It therefore has been proposed that the stability of SOC is determined by the interactions between three mechanisms identified above and key environmental factors related to climate, parent materials and human activities etc. (Angst et al., 2021; Hall et al., 2020).

1.3 Key environmental factors influencing SOC stabilization

1.3.1 Climatic and soil geochemical factors

Climate is widely regarded as the primary control on SOC dynamics at regional and global scales, and it often explains the largest proportion of variation in SOC turnover rates. On one hand, climate determines the C inputs into the soils through its control of net primary production. On the other hand, climate (e.g., temperature) can greatly influence the soil microbial activity and thus C turnover, resulting in a clear dependence of C turnover time on temperature (Carvalhais et al., 2014; Feng et al., 2017). These temperature–SOC relationships have been adopted by the Earth system models (ESMs) to assess soil C evolution under global climate change (Carvalhais et al., 2014; Davidson et al., 2012; McGuire and Treseder, 2010), although large uncertainty remains (Luo et al., 2016; Todd–Brown et al., 2013). Although precipitation is a relatively weaker predictor of total OC content compared to the temperature (Doetterl et al., 2015; Luo et

al., 2017), it has been suggested that soil effective moisture strongly controls the fraction of OC retained by reactive minerals across diverse parent materials and biomes (Kramer and Chadwick, 2018). This is mainly due to the soil water balance causes nonlinear changes in many soil properties, including pH, nutrient supply, weathering degree, as well as biological properties that are likely to determine C cycle (Kramer and Chadwick, 2018). Furthermore, the response of SOC mineralization rates to soil moisture is sensitive to soil water content: under dry conditions (i.e., < 25% of soil volumetric water content), soil water provides micro-organisms with energy and access to the OC substrate, and thus water content has a positive effect on soil respiration (Wiaux et al., 2014). However, the negative effect of soil water on SOC mineralization occurs when soil pores are filled with water (i.e., > 25% of soil volumetric water content), thereby limiting the O_2 concentrations soil gas diffusivity (Wiaux et al., 2014; Herbst et al., 2008).

The second key factor controlling SOC dynamics is the soil geochemical properties. Recent evidence has repeatedly shown that soil geochemical properties play an equally or even more important role than climate factors in controlling SOC dynamics (Doetterl et al., 2015a; Haaf et al., 2021; Luo et al., 2017, 2019; Reichenbach et al., 2021; Von Fromm et al., 2021) especially at the regional scale (Viscarra Rossel et al., 2019). Incorporation of soil geochemical parameters into a SOC turnover model do decrease the prediction uncertainties by 20% (Finke et al., 2019). Soil geochemical properties, resulting from the climate and vegetation controls on mineral weathering of varying soil parent materials, determine the abundance of soil reactive mineral surfaces and sorbents for forming SOC physical, chemical and bio–chemical protections (Hall et al., 2020; Doetterl et al., 2015b; Masiello et al., 2004; Denef and Six, 2005). On the one hand, soil reactive minerals are nucleus for gathering soil particles and formation of stable aggregates, thus enhancing the SOC physical protection (Berhe et al., 2012; Six et al., 2002). Specifically, soil pedogenic oxides and expandable clays have been shown to be important for aggregate formation and stability due to physical or electrostatic interactions between the 1:1 clay minerals and

oxides (Denef and Six, 2005). On the other hand, soil reactive minerals can absorb organic acid and dissolved organics to form organo–mineral associations, which can protect SOC from decomposition for decades to centuries (Kögel–Knabner et al., 2008). This SOC mineral protection is therefore widely recognized as a key mechanism for long–term C storage independent of climate zones and land use (Doetterl et al., 2015b; Fisher et al., 2018; Hemingway et al., 2019; Kögel–Knabner et al., 2008; Kopittke et al., 2020; Rakhsh et al., 2017; Wang et al., 2018). Lastly, geochemical properties are also relevant to SOC biochemical stabilization (known as biochemical recalcitrance). A recent study proposed that the lignin–derived C may largely be preserved in soils, but not because of the inherent recalcitrant. Rather, lignin may vary among ecosystems as a function of soil geochemical context. In particular, the ligand exchange by carbonylated aromatics on short–range–ordered Al phases leads to a strong bonding between lignin and Al mineral oxides, thus protecting lignin from decomposition (Hall et al., 2020). Therefore, linking the climatic and soil geochemical factors to the SOC physico–chemical and bio–chemical stabilization mechanisms is essential to understand the SOC dynamics and the role of soil in global C cycle.

1.3.2 Role of human activities

Human activities tremendously affect the SOC cycle by changing land use, resulting in the significant C fluxes at the Earth surfaces. Tracking the fate of this C fluxes is essential to understand the role of soils in global C cycle and mitigation of climate change (Van Oost et al., 2012; Wang et al., 2017). This thesis focuses on OC dynamics in the colluvial soil environment, which is a major reservoir of the redistributed C fluxes associated with land use change (Wang et al., 2017). Colluvial soils consist of surface soils and/or parent materials locally transported from the upper section of slopes through water erosion, tillage erosion and construction of agricultural terraces (Yassoglou et al., 2017). In this thesis, two major colluvial environments are studied:

eroding and terracing agriculture systems, which are described in the following sections.

1.3.2.1 Human induced erosion and colluvial soils

Erosion is a natural process that constantly shapes the landscape around us. Anthropogenic interventions such as land use change and deforestation have accelerated erosion rates up to 100 times of the geological erosion under natural forces (Sanderman and Berhe, 2017). This leads to redistribution of substantial soil fluxes and associated SOC at the Earth surfaces (Chappell et al., 2016; Borrelli et al., 2017; Quinton et al., 2010; Van Oost et al., 2012). It has been estimated that the expansion of agriculture has mobilized around 63 ± 19 Pg SOC globally after AD 1850 (Wang et al., 2017). After mobilization, eroded C is transported along the terrestrial–aquatic continuum from eroding uplands to colluvial valleys, floodplains, rivers and eventually oceans. As shown in Figure 1–2, most of the mobilized C is redeposited in colluvial (~46%) and alluvial (~31%) settings (Wang et al., 2017). This makes **colluvial soils** an important, yet underappreciated store for SOC (Zádorová et al., 2015). Colluvial soils are formed by the accumulation of surface soils that are continuously transported from upper sections of the slopes through soil erosion (Zádorová and Penízek, 2018). This makes colluvial soils characterized by a distinct environmental condition compared to their stable soil counterparts. For example, higher nutrients, available water and OC contents are observed in colluvial topsoil than stable soils (Sağlam, 2015; Wang et al., 2014). While in subsoil layers, colluvial soil shows a lower oxygen concentration and soil pore space relative to stable soils (Wiaux et al., 2015). In addition, compared to the stable soils, colluvial soils have a distinct bacterial community structure associated with the chemolithotrophic process that may slow down the decomposition of colluvial SOC (Sagova–Mareckova et al., 2016). Furthermore, water erosion can preferentially transport finer soil particles together with clay minerals and reactive mineral oxides into colluvial environments, potentially altering the weathering status and mineral matrix

of colluvial soil settings (Berhe et al., 2012; Doetterl et al., 2015b; Masiello et al., 2004). Together, the environmental conditions of colluvial soil differ from those of stable, non–eroding soils, hence the knowledge of SOC cycle gained from the studies on stable soils cannot be directly applied to assess the dynamic of colluvial SOC storage.

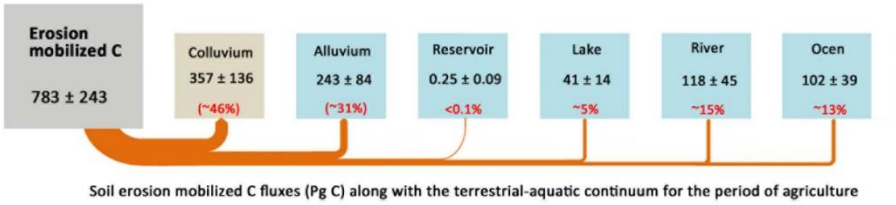

Figure 1–2 Distribution of erosion mobilized C fluxes in the major reservoirs along terrestrial–aquatic continuum. The arrows and corresponding numbers represent the modelled cumulative lateral C fluxes induced by soil erosion (Pg C) for the period of agriculture (6000 BC–AD 2015). The contribution of each C reservoir to the eroded C in percentage is shown as numbers in red. Data and figure were modified from Wang et al. (2017).

1.3.2.2 Agricultural terraces and colluvial soils

Agricultural terraces are the volumetrically largest and most common human–made landforms, which are widely distributed over the world since the ancient times. As shown in Figure 1-3, terracing practices are often found in areas where agricultural civilization firstly developed (Wei et al., 2016), ranging from Mediterranean region (e.g., Cinque Terre of Italy, French Alps), old England (e.g., ancient Lynch Mill), East Asia (e.g., Loess of N China), South Africa (e.g., Bokoni area) to Latin America (e.g., Macchu Picchu of Peru) (Brown et al., 2020). Terraces are designed as the major adaptive strategy for agricultural expansion and food production in the hilly areas (Brown et al., 2021). Construction of terraces provides a variety of ecological benefits, including erosion control, soil water recharge and soil nutrient and OC retention (De Blécourt et al., 2014; Stavi et al., 2019, 2015; Wei et al., 2016). Land–use change and the reshaping of topography during

terrace development have significantly affected the local C dynamics. The role of terracing in the C cycle has received particular attention in the last decade, and the terracing land use, age, climate, and slope gradient are recognized as the critical factors for SOC sequestration, while terracing structure and soil depth are not (Chen et al., 2020a). As reviewed in Table 1–1 (Brown et al., 2021), most studies have suggested a positive effect of terracing on SOC sequestration, despite the considerable uncertainties that are associated with these estimates. Compared to the non–terraced landforms, terracing has sequestrated C by 2.8% ~ 169.4% (Table 1–1). This is mainly because the terracing levels the slope and prevents the rainfall runoff on sloping land from accumulating, thus significantly mitigating the soil erosion and SOC losses (Nyssen et al., 2009). In the contrary, studies have shown that the terrace construction leads to a C source for the atmospheric C pool, owning to the SOC decomposition induced by topsoil removal and breakdown of soil physical structure during terracing (Table 1–1; De Blécourt et al., 2014; Gao et al., 2020). These examples highlight a critical knowledge gap, wherein the direction and magnitude of terracing–driven exchange of C between soil and atmosphere is still unclear.

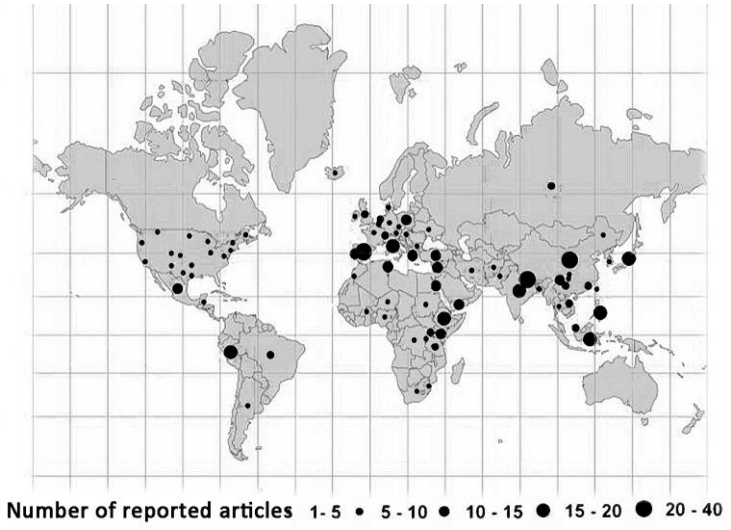

Figure 1–3 Worldwide distribution of terracing. The figure was modified from Wei et al. (2016).

Table 1–1 The studies related to the effects of terracing on SOC stocks across world.

Source	Location	Land cover	Terrace age /yr	SOC change* in %
Sandor, 1995	Andes, Peru	grass/shrub/cacti	1300-1700 B.P.	30
Walter, 2003	Brittany, France	pasture/crop	-	13 ~ 38
Kagabo, 2013	Buberuka, Rwanda	grass	20+	57
De Blécourt, 2014	Yunnan, China	rubber plantations	5-44	2.8 ~ 12.5
Xu, 2015	Shaanxi, China	crops	-	21.5
Welemariam, 2018	Mekelle, Ethiopia	grazing	20	25
Shi, 2019	Shaanxi, China	crops	27	6
Chen, 2020a	China	crop/grass/forest	1-30+	-6.4 ~ 169.4
Gao, 2020	Shaanxi, China	crops	1-2	-4.8 ~ -9.4

*Changes in SOC stock (kg m^{-2}) of terracing soils relative to non–terracing soils.

In the context of climate change, it is also important to consider the present and future stability of the large amounts of SOC stored in terraced systems (Brown et al., 2021). Terraces are commonly developed through the cut or fill processes conducted along hillslopes (Figure 1–4) or through the active erosion, deposition, and cultivation. The increased SOC stocks in terraced landforms are mainly the result of the burial of former topsoil layers (i.e., at fill section), where this SOC store has been preserved in the **colluvial settings** (Figure 1–4). However, future land use and climate change are expected to destabilize this SOC storage. Currently 69% of world terraces are either under abandonment (49%) or poor management (20%) (Figure 1–5). When abandoned, terraces are subjected to progressive failure due to

collapse of terrace walls. In the long term, such abandonments could accelerate the formation of rills, gullies, gravitational erosion, and piping (Wei et al., 2016). This will lead to an exposure of the underlying, former buried SOC storage to be re–connected with the atmosphere C pool. In addition, the collapse of terraces may lead to changes in the on–site geo–ecological properties, such as weathering status, soil texture and nutrient contents (Stavi et al., 2019), which will have a profound impact on the SOC physical and mineral stabilization mechanisms.

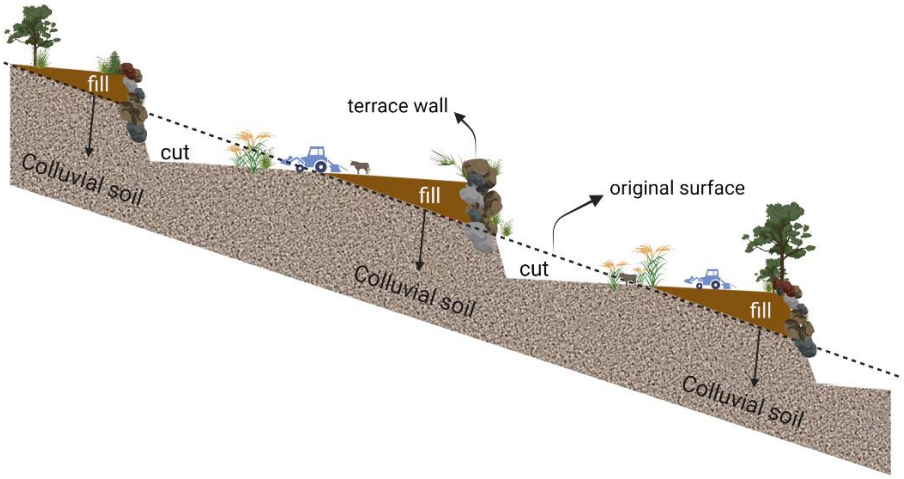

Figure 1–4 Simple idealized cut and fill terrace landforms. Soil redistribution within the terrace landforms creates the colluvial soils.

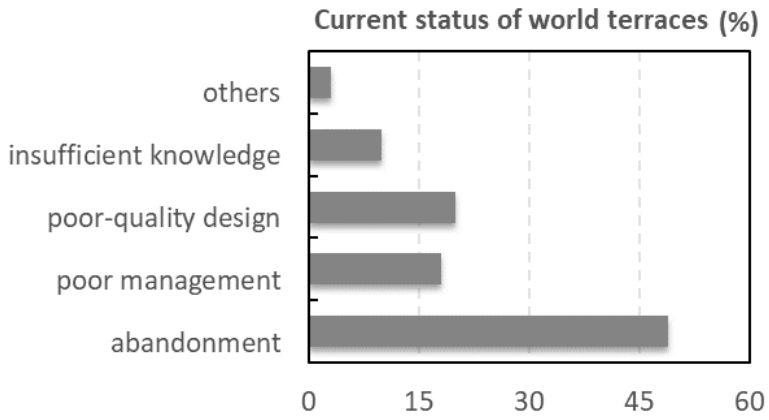

Figure 1–5 Analysis of the world terraces status based on 300 publications. Data was adopted from Wei et al. (2016).

1.3.2.3 Time

Time is one of the most fundamental factors influencing SOC dynamics, as the formation of soils and evolution of soil geochemical properties operate across temporal scales. In the early weathering stage, the original rocks and minerals are destroyed by both physical disintegration and chemical decomposition and release the nutrients as well as the primary minerals (Brady et al., 2008). At this stage, the capacity of soil to stabilize OC is very limited due to the lack of reactive mineral surfaces of primary minerals. However, as weathering continues, the primary minerals are transformed into the secondary minerals such as smectite, iron and aluminium oxyhydroxides, which have higher reactive mineral surfaces that enable soil aggregation and organo–mineral associations formation (Doetterl et al., 2018). In addition, the quality of buried SOC also evolves over time; the older and buried soils are depleted in labile components and relatively enriched in recalcitrant compositions relative to the young surface soils (Wang et al., 2014). Therefore, all three proposed SOC protection mechanisms (physical, mineral and biochemical protection as discussed in 1.2) are time dependent.

1.4 Problem statement

Organic carbon dynamics of colluvial soils in eroding landscapes

Over the past decades, significant progress has been made in understanding the mechanisms controlling SOC (de)stabilization. Climate, soil properties and human activities (e.g., cultivation) have been recognised as the dominant controls on SOC dynamics. However, most of this understanding is derived from the studies conducted on level or low-gradient, stable landscapes (Carvalhais et al., 2014; Doetterl et al., 2015b; Wang et al., 2019). Whether this knowledge can be transferred to colluvial soils in eroding environments is unclear and less studied (e.g., Wang et al., 2018). Colluvial soils, characterized by distinct environmental conditions compared to their stable soil counterparts, have been recognised as an important C reservoir. Assessing the dynamics of colluvial SOC is vital to track the fate of eroded C and its role in the global C cycle.

Organic carbon dynamics in agricultural terrace soils

Although there is no doubt that terracing is an efficient conservation practice that provides multiple ecosystem services, e.g., erosion control, soil water recharge and nutrient enhancement etc., whether terracing represents a net C sink or source is still a matter of debate (Brown et al., 2021). Both positive and negative effects of terracing on SOC stock have been reported (Table 1-1). This paradox is mainly due to the spatial variability of SOC stock is rather high across climatic and geographic zones, whereas the current studies explicitly focus on the temperature regions (Table 1-1). Therefore, more field investigations covering a wide range of climatic and geographic scales are required.

To discern the optimal strategies for managing terracing SOC storage in the context of climate change, understanding the key factors controlling the levels of SOC stock in terraced soils is important (Chaplot et al., 2010). However, knowledge on the factors influencing terracing SOC stocks and dynamics is very limited, particularly the role of soil geochemistry is not

considered. Recent studies conducted on the non-terracing soils (i.e., natural soils) have highlighted the more important role of soil geochemical properties over climate (e.g., 1.3.1) in stabilizing SOC. This indicates that the effect of future climate change on SOC dynamics in terracing systems should be assessed with the consideration of soil geochemical background. In addition, current studies explicitly focus on the relatively young terraces (< 30 years), while the use of terraces as a conservation practice can be dated back to the post-Neolithic period. As the time is one of the most fundamental factors influencing SOC dynamics (as discussed in 1.3.2.3), considering much longer time scale when assessing SOC dynamics in terraced landscapes is essential.

Global warming accelerates the rate of SOC decomposition, a major pathway for C exchange between the land surface and the atmosphere, which in turn contributes to the rise of atmospheric CO_2 and global temperature (Hopkins et al., 2012; IPCC, 2021). However, how much of the C stored in agricultural terraces is vulnerable to global warming is largely unknow. More specifically, the fundamental drivers and basic patterns of the temperature sensitivity of SOC decomposition in agricultural terraces have been poorly described so far.

1.5 Objectives and research questions

The main objective of this thesis is to understand and evaluate the SOC dynamics and controlling factors in colluvial soils in the context of climate change. In order to achieve this objective, we seek to answer the following questions:

The overall question I want to answer in this thesis is: how will the small–scale controls on SOC dynamic such as colluvial soil environment interact with the large–scale controls of climate and geochemistry, and how will such interactions evolve over time (e.g., soil age)? More specifically:

General introduction

RQ1: What are the dominant controls on colluvial SOC stability under different climate and mineral weathering settings and to what extent these controlling factors differ from those in stable, non–eroding soils?

RQ2: How can SOC be stabilized in terraced landforms?

RQ3: What are the main controls on SOC temperature sensitivity in terraced soils?

RQ4: When using infrared spectroscopy to predict terraced soil properties relevant to SOC biogeochemical cycle, can accounting for the features of compositional data significantly improve model performance?

RQ5: Will terracing play a positive or negative role in SOC sequestration?

RQ6: How do SOC stocks and respiration in terraced soils vary along the climate, soil geochemistry and terrace age gradient and which factors control the observed variation?

1.6 Outline of thesis

The structure of this thesis is shown in Figure 1–6. Chapter 1 is a general introduction of the role of soil C reservoir in global C cycle and climate change and a summary of main factors influencing SOC dynamics, such as climate, soil geochemical properties, human activities and time scale. In Chapter 2, we compared the dominant controls on SOC stability between colluvial soil and non–eroding soils to address RQ1. Using the paired soil profiles (stable versus colluvial) collected from contrasting climate and soil geochemistry conditions, relative importance of climate, deposition rate, cultivation history and weathering degree in controlling SOC stability were assessed. Chapter 3 is centred on the SOC stabilization mechanisms and temperature sensitivity in terraced soil (RQ2 and RQ3). Based on the measured optically stimulated luminescence (OSL) signal, we established a chronology of buried soil along the terrace sequence. Then the soil potential

heterotrophic respiration and temperature sensitivity were linked to the soil age to gain insight into the SOC dynamics of terraced soils. In Chapter 4, we applied soil infrared spectroscopy combining with composition data analysis to predict terraced soil properties relevant to SOC biogeochemical cycle (RQ4). This resulted in a dataset containing 117 terrace soil samples analyzed for the soil potential heterotrophic respiration, soil pedogenic oxyhydroxides, base cations, soil texture and SOC fractions. This dataset was subsequently used in Chapter 5 to address the RQ5 and RQ6. The relative importance of climate, terrace soil age, soil weathering status and pedogenic oxyhydroxides in controlling SOC stocks and soil potential heterotrophic respiration were assessed. In Chapter 6, we present the general conclusions, limitations as well as the perspectives for future research.

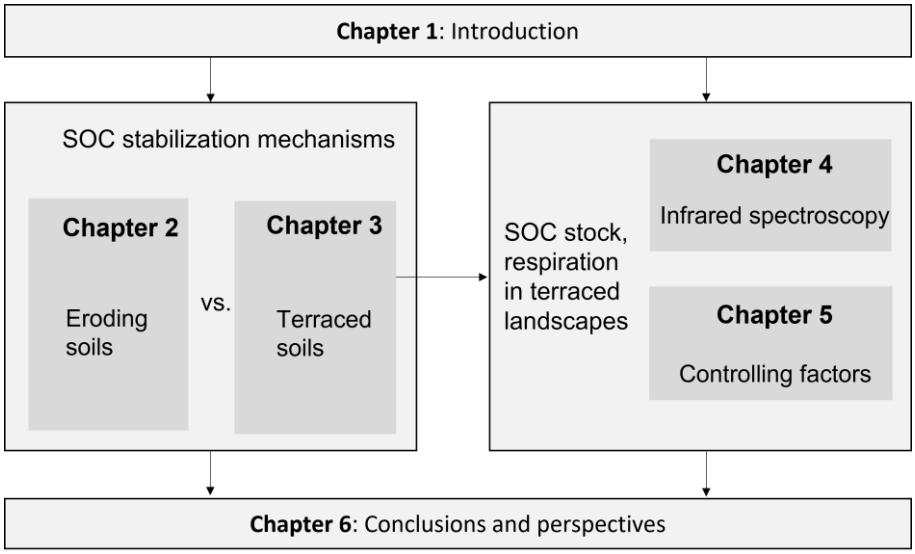

Figure 1–6 Flowchart of the outline of the thesis.

General introduction

Chapter 2

Factors controlling SOC stability in colluvial soils under contrasting climate and soil weathering conditions

The content of this chapter was submitted in:

Zhao, P. Doetterl, S., Wang, Z., Hoyt, AM., Wang, E., Yu, H., Quijano, L., Fallu, J., Brown, AG., Six, J., Van Oost, K. Factors controlling SOC stability in colluvial soils under contrasting climate and soil weathering conditions. Under review in European Journal of Soil Science.

Abstract

Although agricultural colluvial soils are an important storage for soil organic carbon (SOC), the mechanisms underlying colluvial (cumulative soils) SOC stability have received little attention so far. In this study we aim to understand to what extent the main controls on colluvial SOC stability differ from those observed in stable soils. Paired soil profiles (stable versus colluvial) were collected from five sites which differ in climate, soil geochemical background and cultivation history. Soils were analyzed for SOC fractions and mineral composition, potential soil respiration and radiocarbon content. Our analysis showed that for stable soils, climate, cultivation history and weathering degree have a significant effect on potential soil respiration. In contrast, we found that for colluvial soils, mineral weathering and the dominance of mineral related SOC stabilization mechanisms strongly influenced the relationship between climate and potential soil respiration. For colluvial soils, the most influential factor for potential soil respiration and SOC fractions (coarse particulate SOC versus free silt–and–clay–associated SOC) was the rate of deposition and this was

independent of climate zone. Furthermore, deposition rates indirectly affected potential soil respiration by interacting with the degree of weathering of deposited soil. This changed the mineral matrix of colluvial soil settings whereby may enhance soil mineral related SOC stabilization mechanisms. Together, these results suggest that the dominant controls on SOC stability in colluvial soils differ from those in stable soils and the rate of soil deposition is the most important control on colluvial SOC stability in agricultural systems.

Chapter 2

2.1 Introduction

Over past decades, substantial progress has been made in understanding the mechanisms controlling soil organic carbon (SOC) stabilization versus loss. Climate, soil geochemistry and human activities (e.g., cultivation) have been identified as dominant controls on SOC dynamics. However, most of this understanding is informed by studies conducted on level or low–gradient, stable landscapes (Carvalhais et al., 2014; Doetterl et al., 2015a; Wang et al., 2019). Whether this knowledge can be simply transferred to colluvial soils in eroding landscapes is questionable and has been less addressed (e.g., Wang et al., 2018a). Previous work has highlighted that erosion–induced changes in the soil geochemical matrix have important implications for colluvial SOC stabilization (Berhe et al., 2012; Doetterl et al., 2015b). However, to what extent this link is influenced by climatic and mineral weathering controls is rarely considered. The importance of understanding the main controls on colluvial SOC stabilization is further emphasized by the large amounts of SOC in colluvial stores. Since 1850, the expansion of agriculture has mobilized an estimated 63 ± 19 Pg C globally (Wang et al., 2017), of which 16 to 21 Pg C have been deposited in agricultural colluvial soils during the last 50 years (Van Oost et al., 2007). This makes colluvial soils an important, yet underappreciated storage for SOC.

At the continental scale, climate is generally considered to be the dominant control over SOC dynamics by governing C inputs into soils, via its control on net primary production (NPP) (Luo et al., 2017; Tang and Riley, 2015). Hence, soil carbon–climate relations have been adopted in ecosystem C cycle models and Earth system models to predict the global C budget (Carvalhais et al., 2014). At the regional scale, climate becomes less important and soil geochemical properties have a larger influence on SOC stabilization (e.g. Doetterl et al., 2015a; Viscarra Rossel et al., 2019). Soil geochemical properties, resulting from climate and vegetation controls on mineral weathering of varying soil parent material, determine the availability

of reactive mineral surfaces and sorbents for forming soil aggregates and organo–mineral associations, which can protect SOC from decomposition for decades to centuries or even millennia (Denef and Six, 2005; Masiello et al., 2004). Under similar climatic conditions, differences in the geochemistry and weathering susceptibility of parent material can result in distinct soil geochemical properties and hence SOC stabilization mechanisms (Blume et al., 2016). At the smaller plot and slope scale, geomorphic processes can have important implications for SOC stabilization. For example, erosion processes break down macroaggregates and expose formerly enclosed SOC to decomposers (Six et al., 2004). This facilitates oxidation and hydration of the previously protected SOC, enhancing its mineralization (Wang et al., 2014). In addition, erosion can preferentially transport finer soil particles together with clay minerals and reactive mineral oxides to colluvial environments (Berhe et al., 2012; Doetterl et al., 2015b), providing colluvial soils with increased potential to physico–chemically protect SOC against mineralization. Topography also exerts a control on soil hydrologic conditions via water flow and therefore interacts with mineral weathering and NPP (e.g., Metzen et al., 2019). This hydrologic mechanism is important for colluvial soils, which are typically located in valleys or concave slope positions (e.g., Wiaux et al., 2015) and can have significant horizontal components to throughflow and groundwater fluxes. However, to our knowledge, few studies have explicitly addressed the controls on colluvial SOC turnover for a range of environmental settings. In this study, we contribute to this knowledge gap by presenting a study of SOC stabilization in colluvial soils in five contrasting climatic and geochemical settings. Detailed soil geochemical properties and soil clay mineralogy composition were measured to explain the underlying mechanisms. We hypothesized that small–scale controls on colluvial C turnover such as selective deposition, aggregate breakdown and specific environmental conditions interact with large scale controls such as climate, geochemistry and the duration of cultivation. The main objectives of this study were thus (i) to identify the dominant controls on colluvial SOC stability under different

climate and mineral weathering settings and (ii) to assess to what extent these controlling factors differ from those in stable, non–eroding soils.

2.2 Material and methods

2.2.1 Study sites

We selected 20 samples from five coupled stable/colluvial sites spanning a large climatic (from arid to tropical) and soil geochemical range (Table 2–1). The deposition rates were quantified using tracer methods (see below). Site 1 (SP) is located in Northeastern Spain and is characterized by a high carbonate content (~ 5.4 ± 9.8%) and a silty texture with a relatively low sand content (29 ± 13.1%) (Calcisols). Site 1 has been cultivated since the early 20th century and the main crops are winter cereals. Site 2 (NC) is located on the Chinese Loess (Cambisols). Soils are loess derived and have a very high silt content (> 80%). The study area has a long history of cultivation dating back c. 1500 AD, with wheat and corn as the major currently planted crops (Li et al., 2015). Site 3 (BE) is located in the Belgian loam belt (Luvisols). Here, agriculture can be traced back to the Iron Age to Medieval Period (c. 2300–300 BP) and at present, the lands are cultivated for cereals, sugar beet and maize production. Site 4 (SC) is located in Yingde city of South China. Soils are Ferralsols with a high silt (~55%) and sand content (~30%). The study area has a relatively short history of agriculture (< 80 years). Finally, site 5 (SB) is located at Arvorezinha catchment in the state of Rio Grande do Sul in South Brazil. The dominant soil type is Acrisols with a high silt (~65%) and clay content (~23%). The study area has a history of agriculture dating back to around 1925, and tobacco, corn, soybean and wheat are the dominant crops. Profile–specific deposition rates were derived from published estimates based on caesium–137 (^{137}Cs) measurements (Li et al., 2015 (NC); Quijano et al., 2016 (SP); Minella et al., 2012 (SB); Wang et al., 2014 (BE); Zhang et al., 2011 (SC)). The ^{137}Cs activities were measured on the same cores used in this study, except for SC where deposition rates were inferred from an erosion study in

a nearby field with a similar topography and cultivation history (Zhang et al., 2011). The sites can be categorized into Mediterranean climate (Csa) (SP), semiarid continental climate (Bsk) (NC), temperate climate (Cfb) (BE) and subtropical climate (Cfa) (SC and SB) regions according to the Köppen climate classification (Table 2–1). Pedogenic Fe oxides (Fe_d/Fe_t) are indicative of the weathering status (Arduino et al., 1986) and we use this metric to describe the differences in weathering degree among the selected study sites.

Table 2–1 Description of the study sites

Sampling	Parent	Soil	MAT	MAP	PET	Main	Cultivation	deposition	Slope	Depth	SOC stock	Clay	Silt	CEC	pH
			℃	mm/yr	mm/yr		years	mm yr^{-1}		cm	g C m^{-2}	%	%	$cmol^{+}$	
Spain (SP)	Quaternary	Calcisols	13.4	500	1355	Winter	~120	8.33	Stable	0–10	133	27.8	67.1	7.7	8.7
										30–50	42	31.3	67.1	6.6	8.9
(42°25'28.14"N,	deposits					wheat			Colluvial	0–10	147	24.1	61.1	8.7	8.3
										30–50	231	29	61.9	9.8	8.7
NW China (NC)	Loess	Cambisols	13.2	540	1388	Wheat	>1000	4.54	Stable	0–10	104	14	82.3	8.9	8.3
										30–50	57	14	82.7	9.6	8.5
(35°3'18.45"N,						Corn			Colluvial	0–15	79	14.9	79.4	10.9	8.5
										30–45	48	13.8	82.8	11.1	8.5
Belgium (BE)	Calcareous	Luvisols	11	805	726	Maize	c. 300–2300	2.90	Stable	0–10	175	10.3	78.1	9.9	7.5
										30–50	60	12.2	79.6	12.3	7.7
(50°45'40.53"N,	loess								Colluvial	0–10	181	11.2	75.4	10.9	7.5
										30–50	54	11.7	75	10.4	7.5
S China (SC)	Granite	Ferralsols	21.5	1649	1341	Cereals	<80	4.97	Stable	0–10	135	10.4	57.8	6.5	5.0
										30–50	47	7.4	58.3	8.3	4.8
(24°18'42.16"N,									Colluvial	0–10	116	13.8	51.4	4.3	5.1
										30–45	54	18.4	55.7	5.8	5.7
S Brazil (SB)	Acidic	Acrisols	24.1	1700	1281	Corn	~95	2.01	Stable	0–10	228	15.3	63.7	25.3	6.0
										30–50	156	23.3	65.9	16.9	6.2
(28°51'36.9"S,	rhyodacite					Soybean			Colluvial	0–10	256	22.6	65.7	14.5	5.2
										30–50	202	23.6	65.3	17.2	5.2

CEC = exchangeable cation

Table 2–2 List of abbreviations.

Abbreviations	Indexes	unit
MAT	mean annual temperature	°C
MAP	mean annual precipitation	mm
SPR	soil potential respiration rate	μg C h^{-1}g SOC^{-1}
cPOM	coarse particulate SOC	kg C m^{-2} cm^{-1}_{depth}
micro–agg	microaggregated SOC	kg C m^{-2} cm^{-1}_{depth}
s+c	free silt & clay associated SOC	kg C m^{-2} cm^{-1}_{depth}
PET	potential evapotranspiration	mm
MAP–PET	soil effective water	mm
CEC	cation exchange capacity	$cmol_c$ kg^{-1} soil
BS	Base saturation	–
Fe_d/Fe_t	% of pedogenic Fe oxides to total Fe	–
Fe_p, Al_p, Mn_p	chelated organo–metal complexes	mg kg^{-1} soil
M_p	sum of Fe_p, Al_p and Mn_p	mg kg^{-1} soil
Fe_{o-p}, $Al_{o-p,}$ Mn_{o-p}	poorly crystalline oxides	mg kg^{-1} soil
Fe_{d-o}	crystalline Fe oxides	mg kg^{-1} soil
M_{o-p}	sum of Fe_{o-p}, $Al_{o-p,}$ and Mn_{o-p}	mg kg^{-1} soil
TRB	total reserve in bases	$cmole_c$ kg^{-1} soil
pMC	percent modern carbon	%
1:1N	1:1 non–expandable clay mineral	%
2:1N	2:1 non–expandable clay mineral	%
2:1E	2:1 expandable clay mineral	%

2.2.2 Field sampling and sample processing

Two replicates soil cores at each site were collected from relatively flat areas at the hilltop plateau which can be assumed to represent stable conditions where no or little erosion or deposition has taken place. Soil cores were also collected from colluvial soils in concave landscape positions at each site as two replicates. Cores were taken using a pneumatic corer and soil samples were stored in sealed PVC tubes. Compaction occurring during coring, which was in the order of 3 to 8%, was corrected for by linear extension of the length of the obtained soil column to the measured depth of the soil

core–hole. Soil cores were cut at 5 cm intervals to a depth of 50 cm, air–dried (< 30 °C), and dry–sieved at 8 mm. Replicates soil cores were combined to make a composite sample for selected soil layers (Table 2–1). Soil samples were then grouped into the following depth intervals: topsoil: 0–10 cm; subsoil: 30–50 cm, except for colluvial profiles of the NC and SC sites where the subsoil represented the 30–45 cm soil layer. Samples were collected in 2007, 2014 and 2017 (see Table S2-1).

2.2.3 SOC fractionation, soil respiration and radiocarbon content

Approximately 40 g of 2 mm sieved air–dried soils were fractionated in duplicate to obtain SOC fractions for two slope positions (stable and colluvial profile) and two depth layers (topsoil and subsoil, see field sampling and Table 2–1). We used a fractionation scheme based on the conceptual SOC model proposed by Six et al. (1998, 2002) applying a simplified version of its fractionation protocol (detailed in Doetterl et al., 2015a, b). Total SOC was fractionated into coarse particulate organic carbon (cPOM, >250 µm), microaggregate–associated SOC (micro–agg, 250–53 µm) and free silt and clay–associated SOC (s+c, < 53 µm). Ratio of cPOM to s+c fraction (cPOM/s+c) was considered as an indicator of C vulnerability to loss according to Viscarra Rossel et al. (2019). All fractions were analyzed for total C by dry combustion (CHN628 Series Leco Elemental Determinator, USA). Samples from NC and SP sites contained inorganic C that was measured using 6M HCl with 3% $FeCl_2 \cdot 4H_2O$ following Sherrod et al.(2002). SOC content was then derived from the total C by subtraction the measured inorganic C.

To determine the soil specific potential maximum heterotrophic respiration (SPR), we incubated three replicate samples of 50 g 2–mm sieved bulk soils from the selected soil layers were chosen for fractionation. A 10–day pre–incubation was carried out in order to avoid CO_2 pulses caused by soil sample preparation (i.e., sieving, drying and rewetting), and then respiration was monitored over 8 weeks keeping moisture (60% of soil water holding

capacity) and temperature (20 °C) constant to determine SPR. Samples of the gas mixture within incubation jars were taken periodically every three to seven days throughout the experiment. The gas samples were then analyzed for CO_2 concentration using a Picarro G2131–I gas analyzer (Picarro Inc., Santa Clara, USA). We followed the incubation protocol used by Doetterl et al. (2015a).

Radiocarbon content was measured for the bulk soil from five colluvial profiles. Additionally, radiocarbon analysis was conducted for the microaggregated, and free silt & clay associated SOC fractions of colluvial profiles from warm–arid (SP site), temperate (BE site) and tropical (SC site) climate regions. We further linked the depth patterns of Percent modern carbon (pMC) to weathering degree and soil geochemistry properties by calculating the ratio of subsoil to topsoil for geochemical variables. These analyses can provide insights into how soil deposition affects weathering status and soil mineral matrix and thus the colluvial SOC stability. Radiocarbon content was measured at the Max Planck Institute for Biogeochemistry (Jena, Germany). Soil samples were combusted and reduced to graphite according to Steinhof et al. (2017) prior to analysis by accelerator mass spectrometer (AMS) (MICADAS, Ionplus, Dietikon, Switzerland). Samples from SP site contained inorganic C that was separated by acid hydrolysis. Results were expressed as fraction modern ($F^{14}C$), which was the fraction with respect to the standard isotope ratio including normalization for $\delta^{13}C$. pMC was calculated from $F^{14}C$ by multiplying 100 (Stuiver and Polach, 1977). All fraction modern data and associated measurement errors were provided in Table S2–1.

2.2.4 Soil physical–chemical properties

Using 2–mm sieved bulk soils from stable and colluvial soil profiles for top– and subsoil at each study site, key soil physical–chemical properties were measured: soil texture, pH_{H2O}, cation exchange capacity (CEC), base saturation (BS), elemental composition of the soil solid phase (Fe, Mn, Al, Si,

K, Ca, Na, Mg), total reserve in bases (TRB), chelated organo–metal complexes (Fe_p, Al_p and Mn_p), poorly crystalline oxides (Fe_{o-p}, Al_{o-p} and Mn_{o-p}), crystalline Fe oxides (Fe_{d-o}), and soil clay–sized mineralogy (non–expandable 1:1 layered (1:1N), non–expandable 2:1 layered (2:1N) and expandable 2:1 layered (2:1E) minerals). These measurements provide additional support to explain the different mechanisms of SOC stability between stable and colluvial soils.

The concentration of chelated organo–metal complexes (Fe_p, Al_p and Mn_p) was measured using sodium pyrophosphate following (Bascomb, 1968). The amount of poorly crystalline oxides plus organically complexed Fe, Al and Mn were measured by extraction with ammonium oxalate–oxalic at pH = 3 following Blakemore et al. (1987); poorly crystalline oxides (Fe_{o-p}, Al_{o-p} and Mn_{o-p}) were estimated by the difference between oxalate and pyrophosphate extractable ions. The total concentration of pedogenic Fe, Al and Mn oxides were quantified through extraction with Dithonite–Citrate–Bicarbonate (DCB) following Mehra and Jackson (1958); the difference between this measurement and oxalate extractable ions provided an approximation of the crystalline Fe oxides (Fe_{d-o}) (Berhe et al., 2012; Masiello et al., 2004). Fe_d/Fe_t, representing the proportion of pedogenic iron oxides to total iron, was expected to increase with weathering and thus widely used as a weathering indicator (Arduino et al., 1986). All extracts were analyzed for their Fe, Al and Mn content using ICP–AES. Elemental contents (K, Ca, Na, Mg, Si, Al, Fe and Mn) in soils were determined by ICP–AES after alkaline fusion using Li–metaborate + Li–tetraborate at 1000 °C, followed by ash dissolution with concentrated HNO_3 (Chao and Sanzolone, 1992). The loss on ignition (LOI) was assessed at 1000 °C and the total element contents are expressed in reference to the soil dry weight at 105 °C. Total reserve in bases (TRB), a measure of four alkaline and alkaline–earth cations, was expected to decrease as cations are leached during weathering (Herbillon, 1986).

Factors controlling SOC stability in colluvial soils

Soil texture was analyzed using a laser diffraction particle size analyzer (Model LS 13 320; Beckman Coulter Inc., Fullerton, USA) after ultrasonic dispersion and removal of organic matter using H_2O_2 (35%) (Beuselinck et al., 1998). Soil pH_{H2O} was determined with a soil/solution ratio of 1:5 (w/v) with demineralized water using a pH–meter (Mettler Toledo MP220, Mettler–Toledo, Switzerland). Cation exchange capacity (CEC) was determined by quantifying exchangeable NH^{4+} displaced with KCl (10%, pH = 3) after saturating cation exchange sites with 1 M ammonium acetate buffered at pH 7.0 and measured with inductively coupled plasma–atomic emission spectrometry (ICP–AES, Jarrell Ash Iris Advantage) (Chapman, 1969).

The phyllosilicate minerals of clay fractions were determined by X–ray diffraction (XRD, Empyrean Panalytical) after removing Fe oxides from fractions by the DCB extraction method. For XRD measurements, specimens were saturated with K^+ or Mg^{2+} solution and mounted as slurries on glass slides. The air–dried Mg saturated specimens were analyzed at 25 °C and after ethylene glycol solvation overnight. The air–dried K–saturated specimens were X–rayed at 25 °C before and after heating at 105 °C, 300 °C and 550 °C for 2 h (Robert and Tessier, 1974). All XRD patterns were recorded by an Empyrean Tube X–ray equipped with a PIXcel3D detector (Malvern Panalytical Ltd, Netherlands) using Cu Kα radiation generated with 40 kV, accelerating potential and 40 mA tube current, from 2 to 30° (2θ). Clay minerals were identified according to a handbook (Moore and Reynolds, 1997). Quantification of clay minerals was performed by Pawley fit with the direct derivation method using the HighScore Plus 4.8 software. The direct derivation method is a new method that can quantify multi–component polycrystalline materials with intermediate to high accuracy (Toraya, 2016). The refinement process was carried out following the help file of HighScore Plus 4.8. Key primary minerals that can interfere with the reflection patterns and exist in clay fractions such as quartz, feldspar, calcite and mica were quantified. We then focused on secondary minerals. Note that no distinction was made between primary and secondary chlorite. Finally, we grouped

secondary minerals into non–expandable 1:1 layered (1:1N), non–expandable 2:1 layered (2:1N) and expandable 2:1 layered (2:1E) minerals.

2.2.5 Statistical analysis

Statistical analysis was performed using R 4.1.1 (http://www.R–project.org). Principle component analysis (PCA) was used to examine how SOC variables and geochemical properties differ between sampling sites. The relationship between climate, weathering, cultivation history and deposition rates were evaluated using zero–order correlation and partial correlation analysis. Partial correlation analysis is a widely applied statistical tool to isolate the relationship between two variables from the confounding effects of other correlated variables (Jukić and Denić–Jukić, 2015). Partial correlation analysis measures the strength of the linear relationship between two variables (e.g., SPR and Fe_d/Fe_t) depending on the linear effect of other (control) variable (e.g., MAT) (e.g., Jukić and Denić–Jukić, 2015). To avoid overinterpretation caused by the limited sample size (N=10 per slope position), we focus on the partial control that significantly shifted the zero–order correlations (Figure 2–3). Shapiro–Wilk tests were performed to check data normality. Pearson's correlation was used when variables were normally distributed, otherwise Spearman's correlation was chosen. We performed a Bonferroni outlier analysis on the SPR data and found that the SP colluvial topsoil observation was a significant outlier ($P < 0.05$) and therefore excluded it from the correlation analysis.

2.3 Results

2.3.1 Soil properties

In general, differences between sites were much larger than those between the stable/colluvial profiles for all selected soil properties. The PCA showed that samples from the semiarid region were similar but were distinct from samples from other climate zones (Figure 2–1a). The reactive mineral phases ($Fe_{o–p}$, $Al_{o–p}$, $Mn_{o–p}$, Fe_p, Al_p), soil fertility (CEC, BS, pH, TRB), non–

expendable clay minerals (1:1N, 2:1N) and cPOM associated SOC fraction contributed most to Dimension 1 (explaining 44% of the observed variance). Dimension 2, which explained 21% of the variance, was largely driven by soil respiration (SPR), expandable clay minerals (2:1E) and crystalline Fe oxides (Fe_{d-o}) (Figure 2–1b). Subtropical soils were abundant in Fe and Al oxides (Fe_p, Al_p, Fe_{o-p}, Al_{o-p}), while semiarid regions had higher TRB, BS and pH, as expected (Table S2–2). Soil deposition rates followed the order: SP > SC > NC > BE > SB (Figure 2–2).

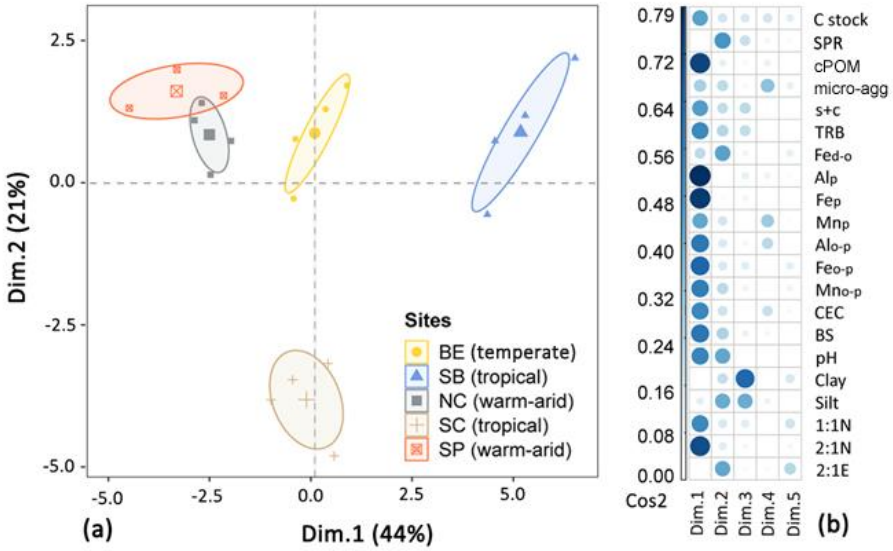

Figure 2–1 Principal components analysis (PCA) showing the differences between the sites. (a) PCA biplot. The percentage of variance explained by each PC is shown in parentheses. (b) Visualization of quality of representation of variables in top five dimensions. Cos2 is the quality of representation of the variables in the principal component maps. Abbreviations are listed in Table 2–2.

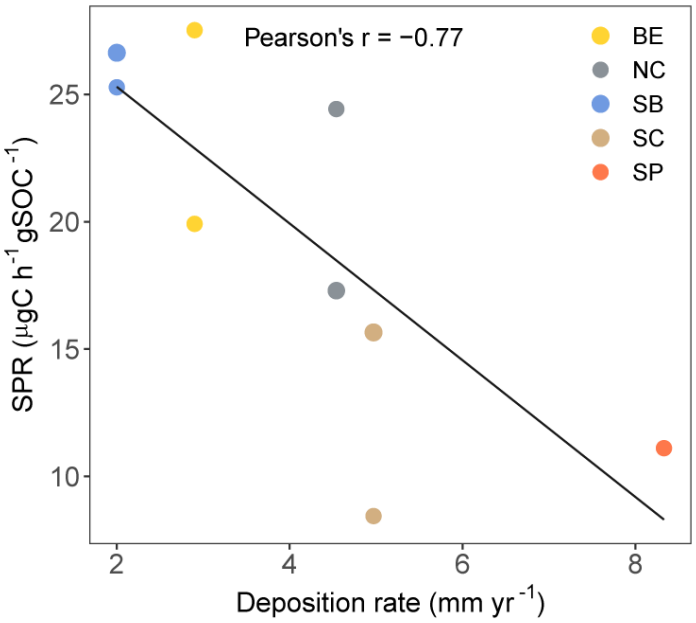

Figure 2–2 Relationship between deposition rate and soil potential heterotrophic respiration (SPR) based on colluvial soil profiles.

2.3.2 Relationships between SOC components and controlling factors

Simple correlation (zero–order) showed that in stable soils both climate factors (MAT, (MAP–PET)), cultivation history and weathering degree (Fe_d/Fe_t) were significantly correlated with SPR, while for colluvial soils, SPR was significantly correlated to the deposition rate and Fe_d/Fe_t (Figure 2–2 and Figure 2–3). Partial correlation analyses (Figure 2–3) showed that the significant correlation between deposition rate and SPR for colluvial soils remained constant when controlling for MAT, (MAP–PET), Fe_d/Fe_t and cultivation history. This result suggests that the deposition rate is the most important independent control on colluvial SOC stability. Furthermore, we found that for stable soils, controlling for cultivation history significantly decreased the zero–order correlation between Fe_d/Fe_t and SPR (r decreased from –0.65 to –0.27). While for colluvial soils, controlling for both cultivation history and deposition rate significantly altered the zero–order

correlation between Fe_d/Fe_t and SPR (Figure 2–3). These results suggest that for stable soils, the relationship between Fe_d/Fe_t and SPR depends on cultivation history, while for colluvial soils, both cultivation history and deposition rate are important. In addition, for stable soils, the correlation between climate factors (MAT, (MAP–PET)) and SPR became insignificant when controlling for cultivation history. While for colluvial soils, controlling for Fe_d/Fe_t also resulted in a sharp change in correlations between climate factors and SPR (r increased from 0.31 to 0.77). This indicates that for stable soils, the relationship between climate (MAT, (MAP–PET)) and SPR depends on cultivation history, while for colluvial soils, this depends on both cultivation history and Fe_d/Fe_t (weathering history).

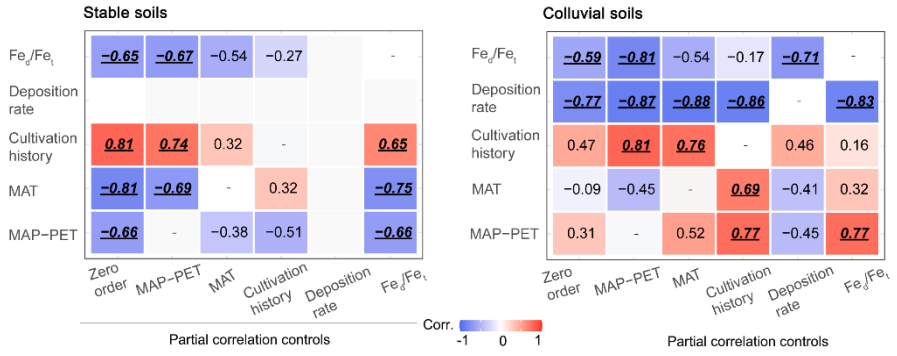

Figure 2–3 Zero–order and partial correlations between SPR and controlling factors. Difference between zero–order and partial correlations indicate the level of dependency of the correlation between a given predictor and the SOC response (see method). Colors and numbers indicate the strength (the intensity of the color) and sign (blue and red colors indicate negative and positive correlations, respectively) of correlation. No change in color between controlled variable and zero–order indicates no dependency; a decrease/increase in color intensity indicates a weaker/stronger correlation. Numbers in bold and italic indicate $P < 0.1$.

No significant correlation was found for the micro–agg fraction in both stable and colluvial soils (data not shown). For both stable and colluvial soils,

cPOM/s+c ratio was significantly related to with no change when controlling for other factors (Figure 2–4). Zero–order correlation between cPOM/s+c ratio and deposition rate in colluvial soils remained constant when controlling for other factors. These results suggest that for stable soils, climate (MAP–PET) is the most important independent control on cPOM/s+c ratio, while for colluvial soil both (MAP–PET) and depositional rate are important. Controlling for (MAP–PET) significantly increased the zero–order correlation between cPOM/s+c ratio and Fe_d/Fe_t (from –0.12 to –0.74).

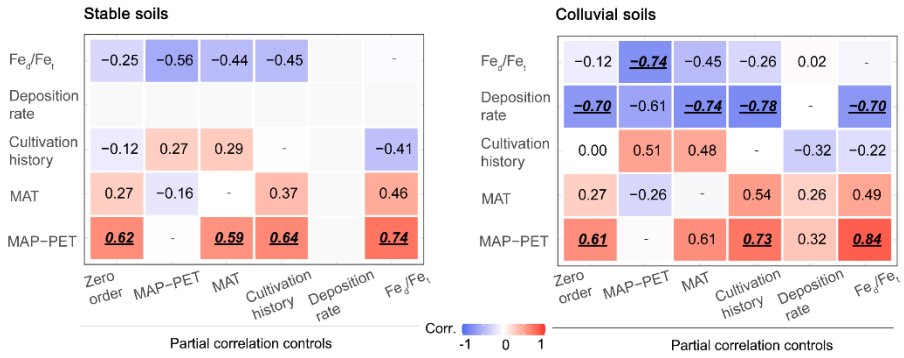

Figure 2–4 Zero–order and partial correlations between cPOM/s+c ratio and selected predictor variables. cPOM/s+c was considered as an indicator of C vulnerability to loss. Difference between zero–order and partial correlations indicate the level of dependency of the correlation between a given predictor and the SOC response (see Methods). Colors and numbers indicate the strength (the intensity of the color) and sign (blue and red colors indicate negative and positive correlations, respectively) of correlation. No change in color between controlled variable and zero–order = no dependency; decrease/increase of color intensity = loss/gain of correlation. Numbers in bold and italic means $P < 0.1$.

2.3.3 Radiocarbon content in colluvial soil profiles

The difference in pMC between topsoil and subsoil was largest for the s+c associated SOC fraction at the BE and SP sites, while the largest difference in pMC at the SC site was found for the micro–agg fraction (Figure 2–5).

Factors controlling SOC stability in colluvial soils

Further, the difference in weathering degree (i.e., TRB, Fe_d/Fe_t, Kaolinite/Illite (K/I)) between stable and colluvial soils was much larger at the SC site than the BE and SP sites (Table S2–3). Such weathering patterns between sites ultimately reflected the underlying geochemistry: 1) the colluvial subsoil at the SC site had much higher CEC and BS than the topsoil, while the inverse tendency was observed at the BE and SP sites; 2) at the SP site, subsoil had considerably higher content of organo–metal complexes (Mp = sum of Fe_p, Al_p and Mn_p) than the topsoil, and the pMC difference between soil depth layers was largest for s+c associated SOC fraction (Figure 2–6).

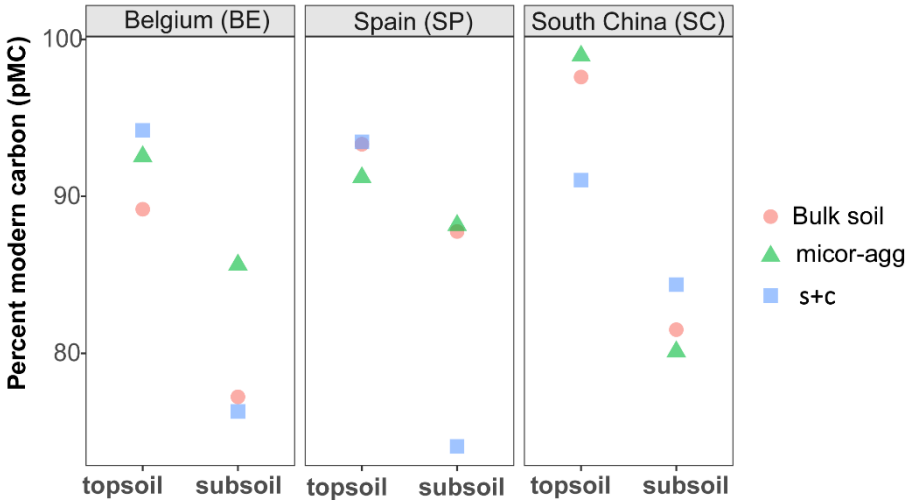

Figure 2–5 Percent modern carbon (pMC) of bulk soil and SOC fractions for selected colluvial soil profiles. micro–agg = microaggregated SOC; s+c = free silt & clay associated SOC.

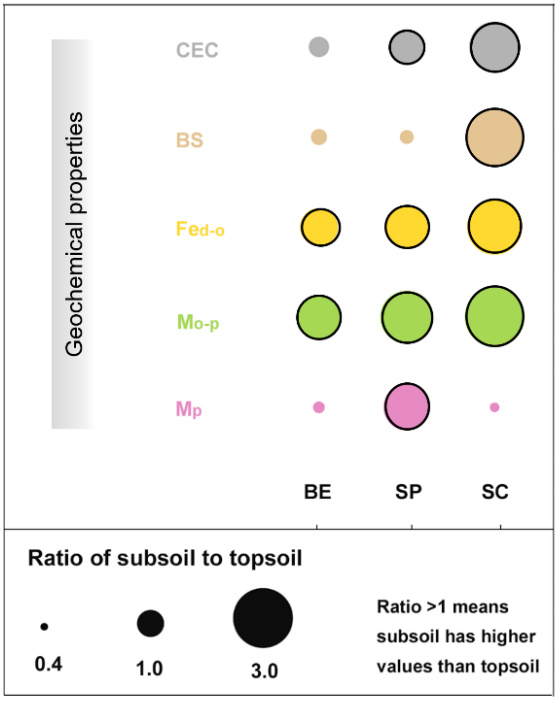

Figure 2–6 Ratio of colluvial subsoil to topsoil for key geochemical properties. Size of circle represents the ratio. Circles with a black outer ring mean the ratio > 1.0 and therefore the subsoil has higher values than topsoil. CEC = cation exchangeable capacity; BS = base saturation; Fe_{d-o}= crystalline Fe oxides; M_p = sum of chelated organo–metal complexes Fe, Al and Mn. M_{o-p} = sum of poorly crystalline Fe, Al and Mn oxides.

2.4. Discussion

Our analysis suggests that the rate of deposition is the most important independent control on colluvial SOC stability (Figure 2–2, Figure 2–3 and Figure 2–4), independent of climate zone. This is revealed by the partial correlation analysis showing that the significant correlation between deposition rate and SPR or cPOM/s+c ratio (Figure 2–3 and Figure 2–4) for colluvial soils is not influenced by controlling for other factors. Furthermore, we found that for stable soils, the relationship between Fe_d/Fe_t and SPR

depends on cultivation history, while for colluvial soils, this depends on both cultivation history and deposition rate. Lastly, for stable soils, the relationship between climate (MAT, (MAP–PET)) and SPR depends on the cultivation history, while for colluvial soils, this depends on both cultivation history and Fe_d/Fe_t. Together, these findings indicate that the dominant controls on SOC stability for colluvial soils are different than those for stable soils. Although we cannot pinpoint the underlying mechanisms given our limited sample size (N = 10 per slope position), below we outline possible causes.

Our results are corroborated by model simulation output on the role of soil deposition for SOC stability in colluvial soils for a fine–textured soil in a temperate region (Wang et al., 2015). This study reported that the deposition rate controls the time that buried soil spends at a given soil depth, thereby controlling the temporal evolution of C input and decomposition rate during the burial process. Importantly, higher deposition rates seem to increase the equilibrium SOC content of the colluvial soil profile, irrespective of climate or geochemical context. In addition, we found that deposition rate is negatively correlated with SPR, indicating that the colluvial SOC with higher rate of deposition is more recalcitrant. This is in line with the notion that the decomposition rate of colluvial SOC can be reduced by a combination of biochemical (recalcitrance of OC constituents), physical (e.g., protected with burial, aggregation) and chemical (e.g., organo–mineral associations) processes (Berhe et al., 2007). On the one hand, the deposited labile SOC in colluvial settings can be rapidly mineralized in–situ (Van Oost et al., 2012; Wang et al., 2014), resulting in more recalcitrant, remaining SOC becoming eventually buried. On the other hand, higher deposition rates are associated with more intensively weathered topsoil together with reactive minerals (e.g., smectite) within colluvial settings (Doetterl et al., 2015b). Since colluvial subsoil is buried under previous topsoil, this changes the weathering status and mineral matrix of colluvial soil settings, especially in subsoils, compared to their stable profile counterparts. The interaction effect of weathering and deposition rate on SOC stabilization is supported by the outcome of our partial correlation analysis: Fe_d/Fe_t is negatively related to SPR for both

slope positions, but for colluvial soils this relation is influenced by deposition rate (Figure 2–3). The weathering–dependent SOC stabilization has been ascribed to the facilitation of complexation and adsorption of SOC with minerals, enhancing mineral (organo–mineral associations) and/or physical SOC protection mechanisms via soil aggregation (Denef and Six, 2005; Duiker et al., 2003; Dümig et al., 2011). This is also supported by our SOC fraction data (Figure 2–4): a significant negative relation ($r = –0.74$) between cPOM/s+c ratio and Fe_d/Fe_t appeared after removing the effect of (MAP–PET), indicating that a higher weathering degree has the potential to enhance SOC physico–chemical protection (i.e., s+c).

The pronounced role of mineral protection as an important factor for colluvial SOC stability was further supported by the radiocarbon content (pMC) of SOC fractions in selected colluvial profiles. We found that the difference in pMC between topsoil and subsoil is largest for the s+c SOC fraction at the BE and SP sites, while the largest radiocarbon difference at the SC site was found for the m SOC fraction (Figure 2–5). These results suggest that at the BE and SP sites, SOC of colluvial subsoil is predominantly protected by organo–mineral associations (s+c SOC fraction), while at the SC site microaggregation protection (micro-agg SOC fraction) plays a major role in SOC stabilization. Radiocarbon data coupled with geochemical measurements further showed that less weathered colluvial subsoil (SC site as an example, Table S2–3) is concomitant with higher CEC, BS and poorly crystalline oxides than topsoil (Figure 2–6), leading to microaggregation (e.g., micro-agg SOC fraction, SC site) as the leading SOC protection mechanism for colluvial subsoils (Figure 2–5). In comparison, physico–chemical protection (e.g., s+c SOC fraction) predominately controls the colluvial subsoil SOC stabilization at the SP and BE sites (Figure 2–5). These subsoils are characterized by a slightly higher or comparable weathering status and correspondingly lower CEC and BS, along with higher organic metals (especially in SP site) compared to the topsoil (Figure 2–6 and Table S2–3). Although the sample size is small (only colluvial profiles from three sites were analyzed for ^{14}C of total SOC and three SOC

fractions), radiocarbon contents provide additional evidence for the important role of mineral weathering in controlling colluvial SOC stabilization.

In stable soils, we found that climate factors are significantly related to specific potential maximum heterotrophic respiration (SPR). In contrast, this relationship is insignificant for colluvial soil (r = –0.09~0.31). However, controlling for Fe_d/Fe_t by partial correlation significantly increased the correlation between climate and SPR (r = 0.32~0.77) (Figure 2–3). This suggests that the more pronounced role of mineralogy driven stabilization of colluvial SOC (detailed above) may obscure the direct influence of climate on colluvial SOC dynamics. This may be because, compared to stable soils, the soil physical properties (e.g., soil volumetric water content, compaction and pore space (i.e., acting as barriers for gas diffusion)), play a more important role than soil temperature in depositional SOC dynamics (Wiaux et al., 2015, 2014). In addition, colluvial soil is generally located at a valley or concave slope position, potentially receiving more water from surface runoff or ground water. On one hand, higher water availability in colluvial soils can support larger biomass and deeper mineral weathering, thus increasing C input and enhancing the mineral weathering–dependent SOC stabilization mechanisms (Masiello et al., 2004). This is also supported by the higher total reserve in bases (TRB, as a weathering indicator) in colluvial topsoil than stable topsoil (Table S2–2). On the other hand, higher water availability in colluvial soils creates an anaerobic environment, which is less favourable for decomposers to decompose OC (Wang et al., 2014; Wiaux et al., 2014). Combining our results with those of the literature, we suggest that the different hydrological regimes and physical properties of colluvial soils (Wiaux et al., 2015, 2014) together with geomorphic processes, have the potential to enhance the importance of soil geochemistry (e.g., TRB; Doetterl et al., 2015b) and may obscure the direct influence of climate on colluvial SOC dynamics.

2.5 Conclusions

Our analysis suggests that the dominant controls on SOC stability for colluvial soils are different from those for stable soils. The rate of soil deposition was identified as the most important independent control on colluvial SOC stability. The rate of deposition also indirectly affected SOC stability by interacting with the degree of weathering of deposited soils; deposition changes the average weathering status and mineral matrix of colluvial (sub)soil settings which affects mineral–dependent SOC physical and physico–chemical protection mechanisms. Our results are in line with the classical notion that climate factors are key to explain SOC stability in stable soils. However, we found no direct correlation between climate and SOC variables for a broad range of colluvial soils. This is likely due to the different hydrological regimes and physical properties of colluvial soils, that together with physical soil redistribution processes, have the potential to enhance the importance of soil geochemistry. This may therefore obscure the direct influence of climate on colluvial SOC dynamics. Finally, both in stable and colluvial soils, we found a close interrelation between cultivation history and mineral weathering in determining SOC stability. Although the sample size is relatively small but diverse, our study suggests the need to consider both the direct effect of deposition rate as well as its indirect effects (via influence on weathering status and soil mineral matrix) on colluvial SOC stabilization when evaluating the fate of eroded SOC. This conclusion should be regarded as a working hypothesis from which to design future targeted investigation

Acknowledgements

I would like to thank Marco Bravin, Anne Iserentant, Britta Jahn–Humphrey, Mario Reichenbach, Anton Jesche, Manuel Rost and Joseph Okello for their assistance with the soil geochemical and mineralogical analysis. A special thanks goes to Prof. Asmeret Asefaw Berhe and Prof. Bruno Delvaux for their patient help with the early stage of data analysis.

Chapter 3

SOC stabilization mechanisms and temperature sensitivity in old terraced soils

The content of this chapter was published in:

Zhao, P., Fallu, D. J., Cucchiaro, S., Tarolli, P., Waddington, C., Cockcroft, D., Snape, L., Lang, A., Doetterl, S., Brown, A.G. & Van Oost, K. (2021). Soil organic carbon stabilization mechanisms and temperature sensitivity in old terraced soils. *Biogeosciences*, 18(23), 6301–6312.

Abstract

Being the most common human created landforms, terrace construction has resulted in an extensive perturbation of the land surface. However, our mechanistic understanding of soil organic carbon (SOC) (de–) stabilization mechanisms and the persistence of SOC stored in terraced soils is far from complete. Here we explored the factors controlling SOC stability and the temperature sensitivity (Q_{10}) of abandoned prehistoric agricultural terrace soils in NE England, using soil fractionation and temperature sensitive incubation combined with terrace soil burial–age measurements. Results showed that although buried terrace soils contained 1.7 times more unprotected SOC (i.e., coarse particulate organic carbon) than non–terraced soils at comparable soil depths, a significantly lower potential soil respiration was observed, relative to a control (non–terraced) profile. This suggests that the burial of former topsoil due to terracing provided a mechanism for stabilizing SOC. Furthermore, we observed a shift in SOC fraction composition from particulate organic C towards mineral protected C with increasing burial–age. This clear shift to more processed recalcitrant SOC with soil burial–age also contributes to SOC stability in terraced soils. Temperature sensitivity incubations revealed that the dominant controls on

SOC stabilization and temperature sensitivity in old terraced soils

Q_{10} depend on the terrace soil burial–age. At relatively younger ages of soil burial, the reduction of substrate availability due to SOC mineral protection with ageing attenuates the intrinsic Q_{10} of SOC decomposition. However, as terrace soil becomes older, SOC stocks in deep buried horizons are characterized by a higher temperature sensitivity, potentially resulting from the poor SOC quality (i.e., soil C:N ratio). In conclusion, terracing in our study site has stabilized SOC as a result of soil burial during terrace construction. The depth–age patterns of Q_{10} and SOC fraction composition of terraced soils observed in our study site differ from those seen in non–terraced soils and this has implications when assessing the effects of climate warming and terrace abandonment on the terrestrial C cycle

Chapter 3

3.1 Introduction

Since the post–Neolithic times, the construction of terraces has played an important role in the expansion and intensification of agriculture to meet food production (Brown et al., 2021). Terracing is recognized as a major adaptive strategy for land use in hilly areas and as an efficient conservation practice that provides multiple ecosystem services, e.g., erosion control and enhanced biomass yields, soil water recharge and nutrient storage (Dunjó et al., 2003; Tarolli et al., 2015; Wei et al., 2016). At the same time the construction of terraces influences soil carbon dynamics by land–use change and the alteration of local topography and hydrological conditions (Shi et al., 2019; Stavi et al., 2019). Although the impact of terracing on soil organic carbon (SOC) stocks has been studied in diverse regions in Europe (Curtaz et al., 2015; Dunjó et al., 2003; Walter et al., 2003) Asia (Chen et al., 2020a; Shi et al., 2019), South America (Antle et al., 2007) and Africa (Kagabo et al., 2013); the mechanisms responsible for the observed C gain and loss due to terracing are unclear. For example, both positive and negative effects of terracing on SOC stock have been reported (Chen et al., 2020a; Brown et al., 2021; Gao et al., 2020). This knowledge gap limits our ability to evaluate how SOC stocks in terraced systems will respond to present and future environmental change such as terrace degradation or land use change.

Terraces are developed through active cut or fill processes conducted along hillslopes or as a consequence of erosion, deposition and cultivation (Mesfin, 2016). Soil redistribution during terrace development results in an exposure of the subsurface soil at the cut or eroding section, and burial of the original topsoil at the fill or deposition section. Thus, the impacts of terrace construction on SOC dynamics can be compared to the mechanisms proposed for erosional impacts, given the similar soil redistribution patterns, i.e., topsoil removal at erosional position (same as cut section) and soil burial at depositional position (fill section) (De Blécourt et al., 2014; Van Oost et al., 2007). Based on the knowledge from erosional studies, three

possible mechanisms that link terracing with SOC stabilization, acting together or separately, should be considered: (i) the removal of topsoil and physical breakdown of soil aggregates during terrace construction enhances the decomposition of SOC (Bailey et al., 2019; Doetterl et al., 2016; Gao et al., 2020); (ii) SOC removal at the cut or eroding section that is gradually replaced through continued SOC inputs from new photosynthate and plant litter decomposition (Berhe et al., 2012; Harden et al., 1999); (iii) burial of the original topsoil at the fill or depositional section which results in reduced SOC decomposition rates by changing the environmental context for SOC decomposition, e.g., providing a low–mineralization context by reducing oxygen availability in soil pore space and increasing soil water content (Vandenbygaart et al., 2012; Wiaux et al., 2015; Berhe et al., 2012; Wang et al., 2014)

The status of SOC stocks of terraces but also to what extent terraced soil systems will represent a net SOC loss or sink largely depends on the magnitude by which the three mechanisms identified above interact and govern SOC dynamics over time. Predicting the sensitivity of SOC decomposition to temperature change is vital to evaluate the warming–induced changes in soil SOC stock and its feedbacks to climate change (Kirschbaum, 1995; Knorr et al., 2005). However, the fundamental drivers and basic patterns of the temperature sensitivity of SOC decomposition in agricultural terraces are poorly described so far. A recent study has reported the effect of terrace construction on soil CO_2 emission and temperature sensitivity in Chinese Loess Plateau. However, the simulation of topsoil removal during terrace construction only reflected short–term (< 2 years) response and mechanisms (Gao et al., 2020). On the basis of the fundamental principles of enzyme kinetics, temperature sensitivity of SOC decomposition (Q_{10}) should be determined by the chemical complexity of SOC molecules and by the availability of SOC substrate to decomposers (Davidson and Janssens, 2006). On the one hand, chemically more complex SOC molecules (thus SOC of low quality), that is, those that require a high activation energy to degrade, should have a higher Q_{10} than SOC of higher

substrate quality (Bosatta and Ågren, 1999). On the other hand, environmental factors (e.g., SOC protection) as a constraint on substrate availability should have a negative effect on observed Q_{10} values (Gillabel et al., 2010). According to the fundamental principles mentioned above, the buried SOC stock at fill sections of a terrace is likely to be less sensitive to warming, given the high quality of this C stock. However, the labile fraction of this buried SOC stock might be gradually decomposed or transferred into protected SOC fractions as the terrace system ages (Wang et al., 2014). This changes the SOC quality and protection (and hence substrate availability) over time. We hypothesis that the terrace age is a fundamental driver of evolution of soil geochemical properties, which in turn determines the SOC protection and quality thus SOC stabilization and temperature sensitivity. These time–dependent mechanisms may have important implications for future status of terrace SOC and its feedbacks to climate change.

The overall objective of this study is to improve the mechanistic understanding of SOC dynamics in agricultural terraces and its potential feedback to climate change. To achieve this, we combined SOC fractionation experiments and temperature sensitivity incubations with measurements of relative terrace soil burial–age on a prehistoric agricultural terrace system in the Ingram Valley of NE England. The detailed objectives of this study are to investigate (i) the factors controlling SOC stabilization in old agricultural terraces and (ii) the associated patterns of SOC temperature sensitivity.

3.2 Material and methods

3.2.1 Study sites

The study area is located in the Ingram Valley (Figure 3–1a) in the Cheviot Hills of NE England within the Northumberland National Park (55° 26' 26.14" N, 1° 59'4 9.52" W). This region is characterized by Maritime temperate climate with an average monthly temperature that ranges between –1 °C (in February) and 18 °C (in July and August) and an average annual rainfall of around 650 mm (www.meteoblue.com). Umbrisols have developed from Andesite igneous bedrock of the Cheviot Volcanic Formation formed approximately 393 to 419 million years ago in the Devonian (British Geological Survey. 2018). The study site complex is one of the largest monuments in England (5.7 km^2) and is known as a multi–period archaeological landscape and currently also being investigated as part of project TerrACE (https://www.terrace.no/). Previous archaeological investigations during 1997–1999 (Frodsham and Waddington, 2004) indicate that the cultivation terraces have a prehistoric origin and date back as far as the early Bronze Age, c. 1800–1500 BC. The landscape at the time the terraces were built was likely dominated by dwarf shrubs (Ericaceae) and grasses, while during the Romano–British period cereals were identified in a pit feature cut into one of the terrace surfaces (Frodsham and Waddington, 2004). The study area is covered by terraces in a small area of c. 9000 m^2 (Figure 3–1c).

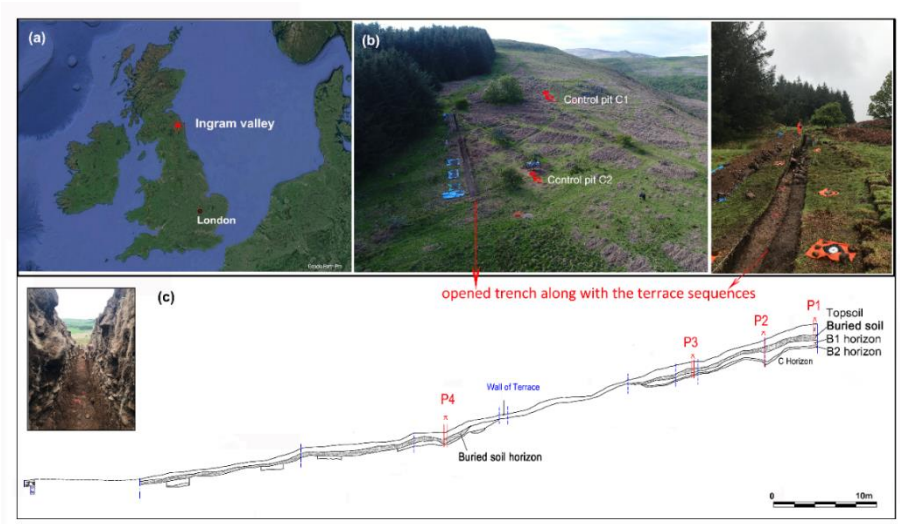

Figure 3–1 Map of (a) studying area (from © Google Maps), (b) sampling site and the (c) excavated terrace trench and sampling positions

3.2.2 Soil sampling

Topographic data in the sampling area was collected through structure–from–motion (SfM) photogrammetry technique integrating ground–based and UAV (nadir and oblique) images for a complete and detailed survey of the terrace system (Cucchiaro et al., 2020b). This technique allowed for the generation of a high–resolution digital terrain models at 0.25–0.10 m resolution, that helped identify the extent and shape of seven prehistoric agricultural terraces. Moreover, the output of the SfM workflows as point clouds allowed for the extraction of profiles and, sections of the opened trench (Cucchiaro et al., 2020a). A detailed stretch map was created (Figure 3–1c; Cockcroft and Waddington, unpublished technical report) for supporting data interpretation. In order to produce a continuous section through seven cultivation terraces, a trench measuring 63 m long by 1.5 m wide was excavated in May 2019 (Figure 3–1b). The trench was then carefully cleaned to the depth of the weathered bedrock surface in order to expose the full nature and extent of any archaeological features, structures and deposits where they survive. Four terraces (P1, P2, P3, P4) were

sampled in detail along the trench in order to cover the full range of potential burial–ages present in the sequence (Fig 3–1). Additionally, two control soil pits (C1, C2) were excavated in proximity to the terraces to provide an undisturbed soil profile, i.e., a soil profile that was not subjected to terracing. Soil samples were collected every 5 cm except for P1 where a different depth interval was used for subsoil layers (Figure 3–2; Table 3–1). Thus, whilst our sampling approach only covers one field trench, our approach is a suitable compromise between the need for spatial representativeness of soil data and the logistical criteria for detailed geo–archaeological excavations at selected sites. The number of highly depth–resolved samples collected this way does allow for the analysis of continuous trends of specific soil parameters within terraced and non–terraced profiles along a sequence of spatially and temporally clearly distinct agricultural terraces. A total of 91 depth–explicit soil samples has been collected this way along the terrace sequence and additional 23 depth–explicit samples collected from the control pits for further analysis.

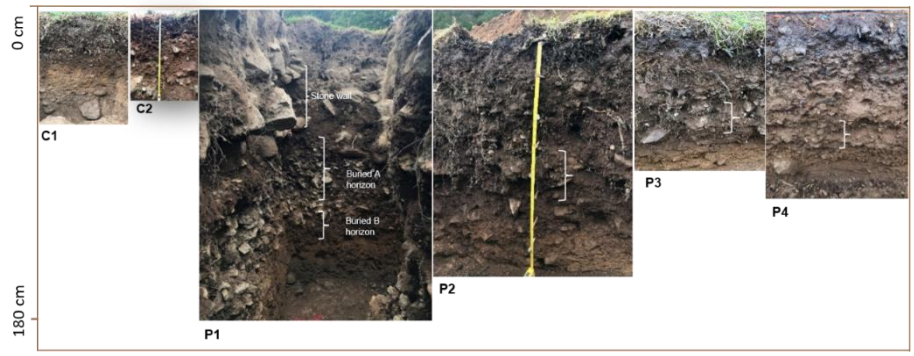

Figure 3–2 Photographs of soil profiles in the field, where soil genetic horizons can be diagnosed.

3.2.3 SOC fractionation

Forty gram of 5 mm sieved air–dried soils were fractionated in duplicate to obtain SOC fractions for selected soil layers, representing different layers within each undisturbed and terrace soil (topsoil 0–10 cm, shallow subsoil 30–45 cm, deeper subsoil ≥ 60–70 cm). These depth intervals were chosen to maximize the variation in terrace burial–age, which we will use to investigate its effect on C dynamics. We used a fractionation scheme based on the conceptual SOC model proposed by (Six et al., 2002, 1998) applying a simplified version of its fractionation protocol (Doetterl et al., 2015a, b). Total SOC was fractionated into coarse particulate organic carbon (cPOM, > 250 µm), microaggregate–associated SOC (micro–agg, 250–53 µm) and non–aggregated silt and clay SOC (s+c, < 53 µm). In brief, the microaggregate isolator was placed on a reciprocal shaker and 20 g of air–dried soils together with 50 glass beads were added on top of a sieve with 250 µm mesh size. Then, the isolator and sieve were flushed continuously with deionized water while shaking at low (= 150 rpm) speed for up to 5 minutes until water flowing out of the device onto a 53 µm mesh size sieve was clear and all aggregates on top of the 250 µm mesh size sieve were broken up. Materials left on the 250 µm mesh size sieve were interpreted as cPOM plus sand. Materials left on the 53 µm mesh size sieve were interpreted as microaggregates and all < 53 µm particles were interpreted as non–aggregated silt and clay. All fractions were analyzed for total C and N using a VarioMax CN Analyzer (Elementar GmbH, Germany). Samples showed no reaction when treated with 10% HCl and were considered free of carbonates. cPOM was interpreted as unprotected SOC and while micro–agg and s+c were interpreted as mineral–protected SOC in our analysis (Gillabel et al., 2010; Six et al., 2002).

Table 3–1 Depth layers selected for soil analysis from sampled terraces

Sampling positions	Sampling depth/cm	Bulk density /cm	SOC fractionation incubation/cm	Total SOC (Depth interval)	pXRF/pOSL (Depth interval)
Control C1	70	0–10; 30–40; 50–60	0–10; 30–45 60–70	5 cm	5 cm
Control C2	45	0–10; 30–40	0–10; 30–45	5 cm	5 cm
Terrace P1	195	0–10	0–10; 50–70; 90–100; 140–150	0–30 cm: 5 cm; 30–50 cm:	5 cm
Terrace P2	150	0–10; 30–40; 60–70	0–10; 30–45; 60–70 80–90	5 cm	10 cm
Terrace P3	80	0–10; 30–40	0–10; 30–45; 60–70	5 cm	5 cm
Terrace P4	105	0–10; 30–40 60–70	0–10; 30–45; 60–70	5 cm	5 cm

pXRF = portable energy dispersive X–ray fluorescence spectrometry; pOSL = portable optically stimulated luminescence.

3.2.4 Temperature–sensitivity based on soil incubations

Three replicate samples of 30 g 2–mm sieved bulk soils from the selected soil layers were chosen for fractionation (see Table 3–1) of each soil profile were incubated at two different temperature levels (20 and 30 °C) using 380 ml sealed jars. A 10–day pre–incubation was carried out in order to avoid CO_2 pulses caused by soil sample preparation (i.e., sieving, drying and rewetting), then respiration was monitored for 8 weeks while keeping moisture (60% of soil water holding capacity) constant during the whole experiment, by periodically adding demineralized water to the samples. The

temperature and moisture level used in the incubation were chosen to provide optimal conditions for microbe activity thus inducing the specific potential maximum heterotrophic respiration (SPR) (Paul et al., 2001). Then, respiration data were collected to calculate heterotrophic potential specific soil respiration, expressed as CO_2–C per unit mass of soil C. For this, every seven days throughout the experiment gas samples within the incubation jars were circulated through a Li–830 CO2 Gas Analyzer (LI–COR, Inc., Netherlands) for determining CO_2 concentration. CO_2 production was analyzed as the average SPR over the whole incubation period (pre–incubation excluded). To avoid CO_2 saturation effects influencing microbial decomposition processes, the incubation jars were flushed with fresh air after each measurement and left open between measurement cycles with jars covered by parafilm to allow for gas exchange while limiting water loss through evaporation. Temperature sensitivity of SPR (Q_{10}, same unit as SPR: µgC h^{-1} $gSOC^{-1}$) was calculated as the difference in SPR of the same aliquot samples at 20 °C to 30 °C incubation temperature (Paul et al., 2001; Doetterl et al., 2018). The average uncertainty for SPR measurement was 0.5 µgC h^{-1} $gSOC^{-1}$.

3.2.5 Soil burial–age and soil geochemical properties along the agricultural terraces

The main total elemental contents (Fe, Al, Mn, Sr, Rb) of the bulk soil were measured using an Olympus Vanta M series portable energy dispersive X–ray fluorescence spectrometry (pXRF) at each 5 cm depth for all terrace profiles (Table 3–1). The Rb/Sr ratio was applied as a proxy for weathering intensity since both elements fractionate during the weathering processes due to their different chemical behaviour. Because of the relative inertness of Rb compared to Sr, a higher ratio of Rb/Sr indicates a higher degree of soil weathering and a higher age (An et al., 2018) (e.g., Figure 3–3). Soil pH was determined with a soil/solution ratio of 1:2.5 (w/v) with 0.01 M $CaCl_2$ solution using a pH–meter (Mettler Toledo MP220, Mettler–Toledo, Switzerland). Soil texture was analyzed using a laser diffraction particle size analyzer (Model

LS 13 320; Beckman Coulter Inc., Fullerton, USA) after ultrasonic dispersion and removal of organic matter using H_2O_2 (35%) (Beuselinck et al., 1998).

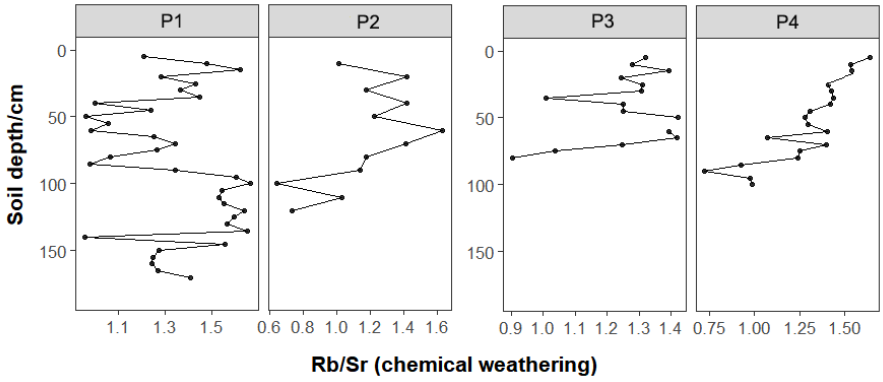

Figure 3–3 Chemical weathering degree indicated by Rb/Sr ratio. Wider ratios indicate a higher degree of chemical weathering, interpreted in this study with the burial of former topsoil (which is generally more weathered than corresponding subsoil).

Optically stimulated luminescence (OSL) has been widely applied for sediment dating (Brown et al., 2021). To establish a chronology of soil burial along the terrace sequence, OSL data was obtained using a portable OSL (pOSL) reader. pOSL was used since it has successfully and frequently been applied in similar settings (e.g., Muñoz–Salinas et al., 2011; Portenga et al., 2016; Porat et al., 2019). When compared to conventional OSL dating, pOSL is more efficient in terms of time, cost and labour and can therefore be used for large, untreated samples, especially to clarify deposition processes (Muñoz–Salinas et al., 2011; Porat et al., 2019). pOSL was recorded at 5 cm intervals throughout all terrace profiles (P1–P4). Luminescence samples were collected in bulk using blackout bags to block out the light. The bags were held against the cleaned section at the sampling location and soil scooped into them, avoiding exposure to the light. Counts were based on 60 seconds of exposure to blue light using the SUERC Meter. Here, besides others, the signal intensity is a function of mineral composition, content of moisture, and age etc. As mineral composition as well as moisture content

was relatively homogenous throughout individual profiles, age is the main discriminant for pOSL activity. The consistently low photon counts at the top of the soil profiles was therefore taken as indicator of very young ages. Thus, pOSL activity was taken as a proxy for the relative terrace soil burial–age (following Muñoz–Salinas et al., 2011) where it increased monotonically with soil depth. Note that the interpretation of relative terrace soil burial–age based on pOSL was only applied with depth within individual soil profiles rather than between profiles, to rule out batch effects caused by the drying out of the samples which could not be processed in the field. Where pOSL did not increase consistently with depth, it was considered to indicate soil heterogeneity and mixing. Lastly, soil samples were classified into relatively younger and older soils based on a (visual) change in the soil depth–age relation (see Figure 3–4). Then, the relationship of SOC fraction abundance and Q_{10} to soil burial–age was analyzed by comparing sample groups along the four investigated terraces. The pOSL signal showed that the terrace soil profiles gradually become older towards the bottom (Figure 3–4), suggesting that the terraces are most likely developed by stone lines which gradually catch soil material moving downslope, resulting in the former “topsoil” layers were buried in deep soil layers. Therefore, the soil burial–age was supposed to play a dominant role in terracing SOC dynamics.

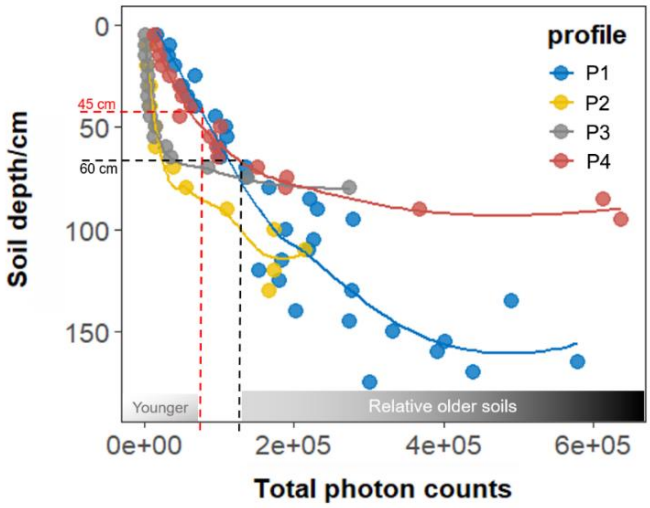

Figure 3–4 The total photon counts versus soil depth in terrace soils. The two soil burial–age categories were shown with dashed lines (i.e., above 45 cm = young, below 60 cm = old).

3.2.6 Statistical analysis

All statistical analysis was performed by R 4.1.1 (R Development Core Team, http://www.R–project.org). The differences of SOC concentration between control and terraced soil layers were analyzed with unpaired t–tests. Model fitting function of 'stat_fit_glance' from 'ggpmisc' R package was used to derive non–linear regression model between terrace soil burial–age and SOC variables (Q_{10}, SPR, SOC fractions). Linear regression and simple correlation were used to examine the relationship between SOC fractions, Q_{10}, pH and soil texture. Differences in means of SPR and Q_{10} between the buried and non–buried soil layers were tested by unpaired t–tests. The 'outlierTest' function from 'car' package was used to identify outliers ($P < 0.05$) based on a given model (i.e., cPOM% ~ Q_{10}; s+c%~ SPR; total photon counts ~ log(Q_{10}); total photon counts ~ log (SPR)). Observation for the Q_{10} from P1 topsoil (see gray point in Figure3–8a) was identified as an outlier and was therefore not included in the correlation and regression analysis.

Significance in all cases was assessed at $P < 0.05$. All figures were produced by R package ‘ggplot2’.

3.3 Results

3.3.1 SOC fractions composition, temperature sensitivity and soil respiration

For the 0–50 cm soil layers, no significant difference in SOC concentrations could be observed between the terrace and control soil layers (Figure 3–5). Below 50 cm, soil layers in control profiles showed significant lower SOC contents relative to the terrace soil layers ($P < 0.05$). The depth profile of SOC contents, soil weathering degree, and field investigation were combined to diagnose the buried soil layers. The SOC contents (Figure 3–5) of P1 for 95–125 cm, P2 for 65–85 cm, P3 for 50–65 cm and P4 for 55–70 cm depth layers were higher than at the corresponding depths of the control profiles (C). In addition, relative higher weathering degree was observed for the depth layers with higher SOC contents (except for P4) (Rb/Sr ratios, Figure 3–3). In combination with the field investigation (Figure 3–1c; Figure 3–2), we interpreted these layers as buried A horizons.

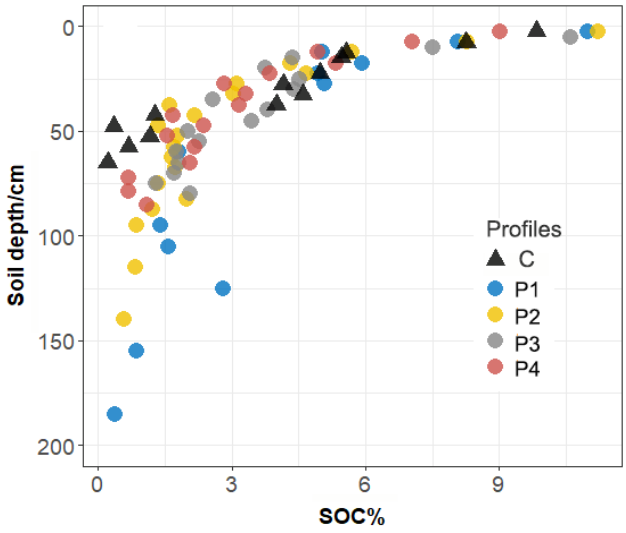

Figure 3–5 Depth profile of SOC concentration (%). C=control profiles, P1–P4 are sampled terraces from the trench. The significant difference (P < 0.05) in SOC concentration between the terraced and control soil layers can be found below 50 cm layers. No such significant difference at 0–50 cm layers.

Considering all profiles, topsoil SOC was mainly composed of SOC associated with the micro–agg fraction, followed by cPOM and s+c (Figure 3–6). For the 30–45 cm depth layer, terrace soil layers contained twice as much cPOM associated C than the corresponding soil layer in the control profiles. Below 60 cm (i.e., the buried horizons), the contribution of cPOM to total SOC in terrace soil layers was 1.7 times higher than in soil layers of the control, while a comparable proportion of physical protected SOC (micro–agg%) was found in terrace and control soil layers. Soil potential respiration (SPR) and SOC temperature sensitivity (Q_{10}) varied significantly across soil layers. On average, buried soil layers showed a significant lower SPR than the non–buried layers (P < 0.05, Figure 3–7). While for Q_{10} no significant difference between buried and non–buried soil layers could be found.

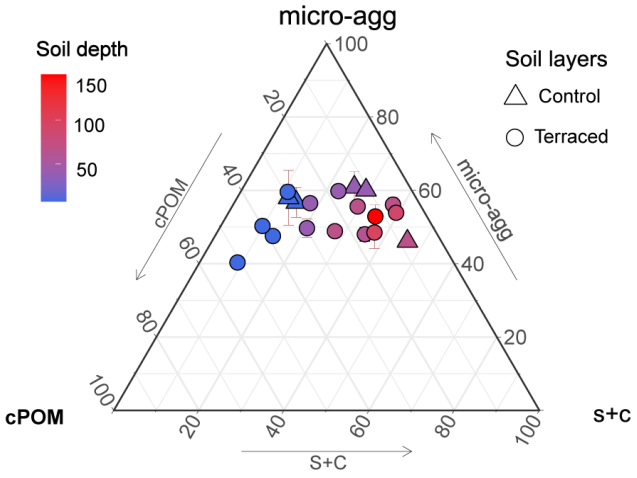

Figure 3–6 Ternary plot of SOC fractions in percentage of total SOC. micro–agg = microaggregate associated SOC; cPOM = coarse particulate SOC; s+c = silt & clay associated SOC. Color bar represents the soil depth (cm). Error bars denote one standard deviations of the micro–agg fraction measurements (N = 2).

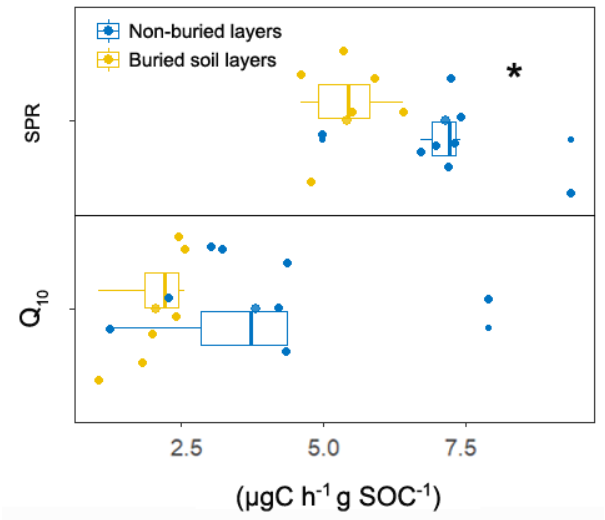

Figure 3–7 Boxplot of soil potential respiration rates (SPR) and SOC temperature sensitivity (Q_{10} = $SPR_{20℃}$ - $SPR_{20℃}$, μgC h^{-1} $gSOC^{-1}$). * = the significant differences in SPR or Q_{10} between buried and non–buried soil layers ($P < 0.05$).

3.3.2 Controls on terrace SOC stability

A non–linear regression analysis was used to identify the effect of total photon counts, which treated as a proxy for soil burial–age, on SOC fractions distributions and on SPR. We found that SPR was negatively related to total photon counts (Figure 3–8a), indicating that the terrace soil burial–age was an important control on SPR. Furthermore, cPOM and s+c fractions were significantly correlated with burial–age (Figure 3–8b), where a shift from cPOM to s+c associated SOC fractions was observed with increasing age. No significant relationship between SPR and measured soil geochemical properties (e.g., pH, soil texture and soil elements) was found (Table 3–2, $P < 0.05$).

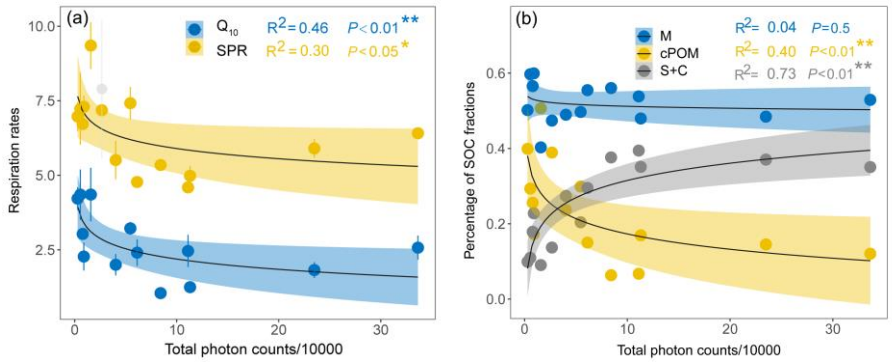

Figure 3–8 Relation between relative terrace soil burial–age (total photon counts) and (a) soil potential respiration rates (SPR) / SOC temperature sensitivity to decomposition (Q_{10}), (b) contribution of SOC fraction to total SOC. Error bars denote one standard deviation of SPR measurements (N = 3). Formula: y = log(x). cPOM = coarse particulate SOC; micro–agg = microaggregate associated SOC; s+c = silt & clay associated SOC. Datapoints are from all terrace profiles. *= $P < 0.05$; **$P < 0.01$.

Table 3–2 Relationships between soil potential respiration (SPR), SOC temperature sensitivity (Q_{10}) and measured soil geochemical properties.

	pH	Clay	Silt	Sand	Fe	Mn	Al	Rb/Sr
Relatively younger layers								
Q_{10}	–0.68	–0.90*	0.35	0.31	–0.75	–0.55	–0.56	–0.14
SPR	–0.17	–0.40	–0.15	0.43	–0.09	–0.45	–0.38	0.72
Relatively older layers								
Q_{10}	–0.44	–0.69	–0.79*	0.80*	0.66	–0.29	0.49	0.20
SPR	0.05	0.17	–0.28	0.17	–0.10	0.18	–0.32	0.66

* $P < 0.05$.

3.3.3 Terrace soil burial–age and SOC temperature sensitivity (Q_{10})

A significant relationship between Q_{10} and total photon counts was observed (Figure 3–8a). This relationship suggests that Q_{10} values decline rapidly with the increasing age for young soil horizons, while for older soil horizons Q_{10} remained relatively constant or increased in oldest soil horizons. Linear regression further showed that for relatively younger soil horizons (Figure 3–4), Q_{10} values were significantly related to the proportion of s+c associated C and cPOM associated C, while for old soil horizons no such strong relation was found (Figure 3–9).

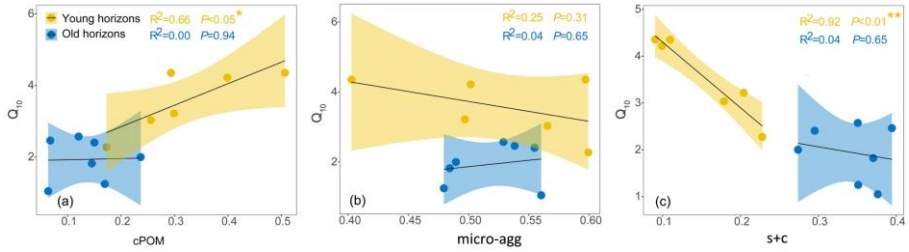

Figure 3–9 Relationship between SOC temperature sensitivity (Q_{10}) and (a) coarse particulate SOC (cPOM), (b) microaggregate associated SOC (micro–agg) and (c) silt & clay associated SOC (s+c) for relatively younger and older terrace soil horizons (Figure 3–4), respectively. *= $P < 0.05$; **$P < 0.01$.

To further identify the underlying controls, we linked the patterns of Q_{10} to soil C:N ratio and measured soil geochemical properties (e.g., pH, soil texture). We found that Q_{10} was significantly correlated to the C:N ratio of bulk soil, micro-agg and s+c fractions (Table 3–3). In addition, Figure 3–10 shows that the C:N ratio of bulk soil and SOC fractions first decreased with burial–age then significantly increased ($P < 0.05$) when the terrace soils became very old. Furthermore, the Q_{10} was significantly correlated to clay content at relatively younger burial–ages, while silt and sand contents was significantly correlated to Q_{10} at relatively older burial–ages (Table 3–2, $P < 0.05$).

Table 3–3 Relationship between SOC temperature sensitivity (Q_{10}) and C:N ratios of bulk soil and SOC fractions.

	Bulk soil	cPOM	micro–agg	s+c
Q_{10}	0.60*	0.03	0.61*	0.62*

* $P < 0.05$. N = 13. cPOM = coarse particulate C; micro–agg = microaggregate associated C and s+c = silt and clay associated C.

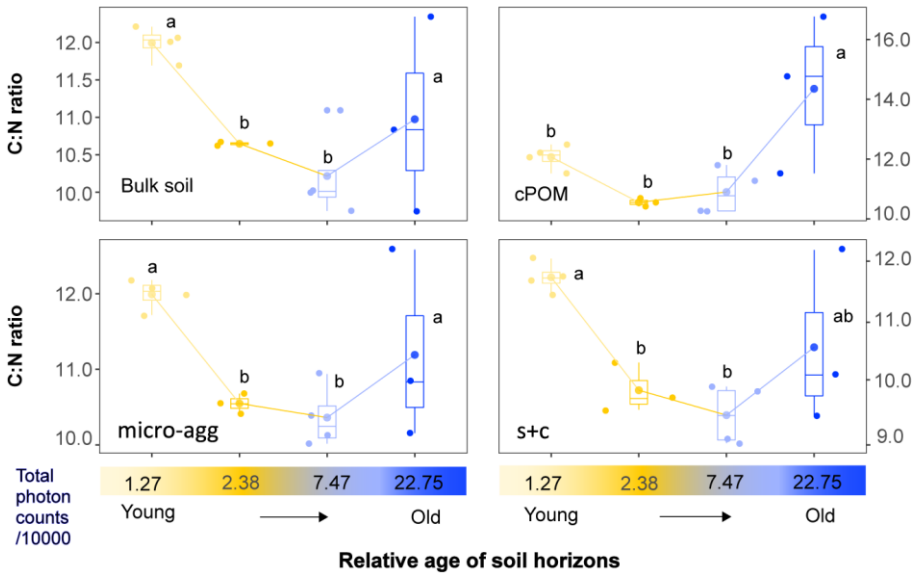

Figure 3–10 Boxplots of C:N ratios for bulk soil and SOC fractions along the gradient of terrace soil burial–age (total photon counts). cPOM = coarse particulate SOC; micro–agg = microaggregate associated SOC and s+c = silt and clay associated SOC. Significant differences in C:N ratios between soil age gradients were indicated by different lowercase letters ($P < 0.05$).

3.4 Discussion

3.4.1 Terrace SOC stabilization: importance of carbon burial and terrace age

Previous work has highlighted that carbon burial due to soil redistribution has important implications for SOC stabilization in eroding landscapes (e.g., Van Oost et al., 2012; Vandenbygaart et al., 2012; Wang et al., 2014). Our results show that the buried soil layers have a significantly lower SPR than the non–buried layers (Figure 3–7), indicating that carbon burial by terracing reduces soil potential respiration and is therefore a mechanism that contributes to SOC stabilization in agricultural terraces. Although buried A horizons in terrace profiles contain 1.7 times more unprotected SOC (cPOM, Figure 3–6) than non–terraced profiles, the less favorable environmental

conditions for microbial decomposers (e.g., mostly lack of oxygen and water saturation) are likely to constrain in–situ mineralization rates of SOC (De Blécourt et al., 2014; Vandenbygaart et al., 2012; Wang et al., 2014).This resulted in a partially–preserved but highly biologically processed SOC stock in terraced soils with a lower SPR, relative to non–terraced soils. Soil redistribution during terrace development results in an exposure of the subsurface soil at the cut or eroding section, and burial of the original topsoil at the fill or depositional section. The terraced area of study site is located in the middle and upper part of the hill. The pOSL signal showed that the terrace soil profiles gradually become older towards the bottom (Figure 3–4), suggesting that the current terraces are most likely developed by stone lines which gradually catch soil material eroded from summit. Our sampling strategy therefore mainly reflects the C stabilization mechanism of the depositional rather than the eroding part of the hill.

The significant relationship between SPR and total photon counts (Figure 3–8a) indicates that the time since terracing is a key factor controlling the stability of SOC in terrace soils. More specifically, SPR declines rapidly with increasing terrace soil burial–age until soils become relatively older, leading to an increase of SOC stock in the old terraces compared to non–terraced landscape (Chen et al., 2020a). In addition, we found that the percentage of unprotected (cPOM) and mineral protected (s+c) SOC fraction is significantly related to the terrace soil burial–age (Figure 3–8b), indicating a shift from an active SOC fractions with short residence times (higher SPR) at relatively younger burial–age to a mineral protected SOC fractions with long residence times (lower SPR) at relatively older burial–age. This clear shift to more processed recalcitrant SOC with age is the underlying process leading to SOC stabilization in terrace soils. By comparing the cPOM fraction of the topsoil layer (0–10 cm) with previous topsoil (burial horizon, >60 cm), we estimated that about 23–27% of cPOM fraction in buried horizons has been decomposed or transferred into physical protected or mineral protected SOC since the terrace were built (Figure 3–6). Given that the buried soil horizons of terrace profiles still contain 1.7 times more unprotected SOC (cPOM) than

SOC at similar soil depths in control profiles, we suggest that SOC cycling in current terrace has not yet reached a steady state and that the SOC stock is most likely to slowly decrease due to cPOM decomposition in the future.

3.4.2 Main controls on temperature sensitivity

According to the Arrhenius equation, Q_{10} of SOC decomposition is theoretically jointly determined by the molecular complexity (SOC quality) and availability of the substrates (referred to here as SOC protection) (Davidson and Janssens, 2006). In general, enzymatic decomposition of biochemically recalcitrant substrates (lower SOC quality), requires more activation energy to degrade, and should have a higher temperature sensitivity than the decomposition of more labile substrates (Bosatta and Ågren, 1999; Craine et al., 2010a). However, environmental constraints (e.g., SOC physical or chemical protection, soil acidity etc.) can reduce substrate availability, dampening the intrinsic temperature sensitivity (Gillabel et al., 2010). It has been reported that soil pH is an important control on Q_{10} at the landscape scale, by directly affecting microbial biomass, diversity and, therefore the enzyme activities, or indirectly through altering nutrient solubility, mineral matrix and therefore the substrate availability (e.g., Ali et al., 2018; Craine et al., 2010b). However, in our study soil pH was not strongly related to SPR or Q_{10} (Table 3–2), possibly due to the small variation in soil pH (pH = 3.71 ± 0.34). Instead, our results showed that at relatively younger burial–ages, Q_{10} is negatively related to s+c associated SOC fractions (Figure 3–6) and clay content (Table 3–2). This indicates that the adsorption of labile SOC (e.g., dissolved OC) by soil reactive clay minerals forms organo–mineral associations (SOC mineral protection), which reduce the substrate availability to decomposers (Kögel–Knabner et al., 2008). As a result, SOC mineral protection attenuates the intrinsic Q_{10}, resulting in the rapid decrease in Q_{10} with total photo counts at relatively young age stage. However, at relatively older soil burial stages, we could not detect any significantly correlation between Q_{10} and SOC fractions (Figure 3–8a), while C:N ratio of bulk soil, micro–agg and s+c soil fractions

were significantly related to Q_{10} (Table 3–2). More importantly, we observed a significant increase in C:N ratio for bulk soil and all SOC fractions at the oldest buried soil layers (Figure 3–10). We proposed two possible reasons as to why C:N ratios were closely linked to Q_{10}, especially in oldest buried soil layers. Both the depth profile of soil chemical weathering, SOC concentration and field investigation indicate that these oldest soil horizons (Figure 3–10, total photon counts/1000 = 22.5) are likely to originate from the former buried topsoil (detailed in 3.3.1). The former topsoil may still contain less decomposed organic litter, which is commonly reflected in a higher soil C:N ratio (Xia et al., 2021). Alternatively, unlike for fresh litter, SOC with a higher C:N ratio is usually considered as lower–quality or recalcitrant substrate, which are less bioavailable for soil microorganisms (e.g., Sollins et al., 1996; Liu et al., 2017; Wang et al., 2018). The observed increase in soil C:N ratios at greater depths in older terraces might therefore reflect a shift towards poor quality SOC substrate (Ali et al., 2018) which explains the observed increase of Q_{10} in the oldest soil horizons (i.e., Figure 3–8a, Result 3.3.3). We propose that the latter is more likely in our experiments. Together, our results suggest that the factors controlling SOC temperature sensitivity of terrace soils (SOC mineral protection or C:N ratio) changes over time. At relatively younger stages of soil burial, the reduction of substrate availability due to the increased SOC mineral protection with ageing attenuates the intrinsic Q_{10} of SOC decomposition (Figure 3–8a and Figure 3–9). Whereas at oldest terrace soil burial–age, SOC in buried layers reflects an increased Q_{10} probably due to 1) lower C–quality (higher C:N ratio, Figure 3–10) and 2) weaker SOC mineral protection (Figure 3–8b; Table 3–2).

3.5 Conclusion

Terracing currently has buried a substantial amount of former topsoil SOC (De Blécourt et al., 2014). Our results show that although buried terrace soils contained 1.7 times more unprotected SOC (i.e., coarse particulate organic carbon) than non–terraced soils at comparable soil depths, a significantly lower potential soil respiration was observed, relative to a control (non–terraced) profile. This suggests that the burial of former topsoil due to terracing provided a mechanism for enhanced C stabilization. Furthermore, we found that the evolution of SOC fractions along with terrace soil burial–age is related to the depth patterns of specific soil respiration, i.e., there is a shift from an active SOC fraction at relatively younger soil burial–ages towards more processed recalcitrant SOC fractions at older soil burial–ages.

Furthermore, our study provides empirical evidence for the drivers and basic patterns of the temperature sensitivity of SOC decomposition in agricultural terraces. We found that both the C:N ratio and SOC mineral protection regulate soil Q_{10}. However, which mechanism predominantly controls soil Q_{10} depends on the age of the buried terrace soils. At relatively younger ages of soil burial, the reduction of substrate availability due to the increased SOC mineral protection with ageing attenuates the intrinsic Q_{10} of SOC decomposition. Whereas at older terrace soil burial–age, higher C:N ratio (poor C–quality) result in an increased Q_{10} in deep horizons. It is expected that the ongoing evolution of SOC fractions and the associated changes in soil C:N ratio due to terrace ageing will slowly but steadily destabilize buried former topsoil SOC.

Acknowledgments

I would like to thank Ben R. Pears, Rosa Maria Albert, Inger Alsos, Kevin Walsh, and the volunteers who help with the field excavation in Ingram valley, UK.

Chapter 4

Quantifying soil properties relevant to soil organic carbon biogeochemical cycles by infrared spectroscopy: the importance of compositional data analysis

The content of this chapter was submitted as:

Zhao, P. Daniel J. Fallu, Ben R., Allonsius C., Lembrechts J., Van de Vondel, S., Meysman FJR., Cucchiaro, S., Tarolli, P., van Wesemael, B., Six, J., Brown, AG., Van Oost, K. Quantifying soil properties relevant to SOC biogeochemical cycles by infrared spectroscopy: the importance of compositional data analysis. Submitted to Geoderma.

Abstract

Oxyhydroxides, base cations, soil texture and soil organic carbon (SOC) fractions are key parameters determining organic carbon cycling in soils. Standard laboratory methods to determine these soil properties are however time–consuming and expensive. Visible near infrared (Vis–NIR) and mid infrared (MIR) spectroscopy have been recognized as a promising alternative, but previous studies have not explicitly considered the above–mentioned soil properties as compositional data. The fractional components in compositional data are interrelated but their sum should be unity – these features should be represented in the spectral modelling process. In this study, two unique datasets with 655 samples collected from agricultural terraces and lynchets across Europe were scanned to acquire MIR spectra and 4516 samples from private garden across Flanders, Belgium to acquire Vis–NIR spectra. Memory–based learning modelling was optimized using both raw data (conventional method) and transformed data of soil properties

by additive log–ratio (*alr*), centered log–ratio (*clr*), and isometric log–ratio (*ilr*) transformation methods. Results showed that the log–ratio transformation method produced predictions as accurate as the conventional method, yet added two significant benefits: (1) they ensured the predicted fractions added up to 100% and (2) they reduced the number of samples with extreme prediction errors. We found that for most soil properties (14 out of 22 variables) the three log–ratio transformation methods provided equivalent model performance, yet *ilr* outperformed *clr* for prediction of silt and sand content of garden soils, and for coarse particulate SOC (> 250 µm) and microaggregate–associated SOC (250–53 µm) of terrace and lynchets soils. Fair to excellent predictive models (RPD from 1.4 to 4.3; R^2 from 0.50 to 0.95) were achieved for predicting base cations (Na, K, Ca, Mg), Fe, Al, Mn oxyhydroxides, and soil texture from MIR spectra. This study demonstrates that combining soil infrared spectroscopy with a compositional data analysis is a promising technique that enables efficient and reliable large–scale quantification of soil properties relevant to the role of SOC in biogeochemical cycles.

Chapter 4

4.1 Introduction

Global soils present the largest terrestrial carbon (C) pool with the greatest potential to capture atmospheric C (Amelung et al., 2020). Significant former studies have therefore focused upon the mechanisms by which soils can stabilize C (Cui et al., 2014; Poeplau et al., 2017; Reichenbach et al., 2021; Zhao et al., 2021a). It was shown that soil pedogenic oxyhydroxides, base cations, soil texture and SOC fractions, are key soil properties necessary to answer these questions (Bukombe et al., 2021; Doetterl et al., 2015a, b; Viscarra Rossel et al., 2019; Wang et al., 2018b). Currently through standard laboratory methods for determining above soil properties are costly and time–consuming, and this hence restricts high–throughput analysis of large sample sets. For example, the determination of pedogenic oxyhydroxides requires a laborious sequential extraction procedure involving a dozen harmful chemicals and more than fifty individual manipulation steps (Stucki et al., 2012). Afterwards, the extractions need to be measured by inductively coupled plasma optical emission spectroscopy (ICP–OES). As this instrument is costly, its application is limited in many labs of developing countries (Stucki et al., 2012). Therefore, developing a fast and cost–effective method to quantify soil properties relevant to SOC cycling and stabilization (i.e., soil pedogenic oxyhydroxides, base cation extractions, soil texture and SOC fractions) would be beneficial.

Soil visible near (Vis–NIR) and mid (MIR) infrared spectroscopy and modelling can provide rapid and cost–effective analysis of certain soil properties, thus providing an alternative to traditional laboratory analyses (Baumann et al., 2021; S. Chen et al., 2020b; Nocita et al., 2014; Shi et al., 2020; Summerauer et al., 2021; Viscarra Rossel et al., 2006; Vohland et al., 2022). Features of soil mineralogy, as well as the chemical composition of soil organic matter, provide specific signatures in the spectra via reflectance at specific wavelengths. These relationships can be empirically modelled to assess soil properties qualitatively and quantitatively (Summerauer et al., 2021; Viscarra Rossel et al., 2006). This approach has been used to

adequately predict soil texture and SOC fractions (e.g., Coblinski et al., 2020; Hobley and Prater, 2019; A Jaconi et al., 2019a, b; Viscarra Rossel et al., 2006). However, it should be noted that most of soil properties involved in SOC stabilization are compositional data. The properties of compositional data are that (i) they convey relative information, as they are usually add up to a constant sum, e.g., 100% or part of total mass; (ii) the fractions in compositional data are not free to range from $-\infty$ to $+\infty$, and therefore fractions are correlated with each other (Pawlowsky–Glahn and Egozcue, 2006). By definition, soil texture (e.g., percentage clay + silt + sand = 100%), SOC fractions (e.g., particulate SOC + microaggregate associated SOC + silt & clay associated SOC = total C), soil pedogenic oxyhydroxides (e.g., extractable organically complexed Fe + extractable poorly crystalline Fe + extractable crystalline Fe + non–extractable Fe = total Fe content), and base cation extractions (e.g., base cation K + Ca + Na + Mg = total reserve in base) should be treated as compositional data. However, the compositional nature of the data was not well accounted for in previous studies where Vis–NIR–MIR spectroscopy was used to predict above soil properties. The most common method is to model all fractions separately and independently of each other (Coblinski et al., 2020; Cozzolino and Morón, 2006; Deiss et al., 2017; Hobley and Prater, 2019; Islam et al., 2003). This may cause some issues: due to the prediction uncertainties, the predicted fractions do not necessarily add up to 100% (e.g., soil texture), or predicted concentrations become negative. Although one could address this issue by calculating one fraction as the remainder to 100%, this brings on a new difficulty of error propagation (Hobley and Prater, 2019; Nussbaum et al., 2018). Moreover, when models are calibrated for each fraction separately, there is no constraint on varying of fractions when calibrating models for each fraction separately, and this may increase the number of samples with extreme prediction error (Pawlowsky–Glahn and Egozcue, 2006).

Aitchison (1982) developed a log–ratio methodology that is key to the statistical analysis of compositional data. Here, all fractions are transformed into log–ratios before further analysis. This allows the data to be

isometrically mapped into a real coordinates space on an orthonormal basis, where ordinary statistical methods then can be implemented (Palarea–Albaladejo and Martín–Fernández, 2015). Via this one–to–one transformation, the results can be transferred back to the original space (Aitchison, 1986; Palarea–Albaladejo and Martín–Fernández, 2015). Three log–ratio transformations have been proposed: (i) additive log–ratio (*alr*) transformation (Aitchison, 1986); (ii) centered log–ratio (*clr*) transformation (Aitchison, 1986); and (iii) isometric log–ratio (*ilr*) transformation (Egozcue et al., 2003). Compositional data analysis based on these log–ratio transformations has been applied in a wide range of research areas, ranging from water contamination assessment (Otero et al., 2005) over environmental pollution research (Howel, 2007), to analytical chemistry (Palarea–Albaladejo et al., 2014). In soil science, log–ratio transformation methodology is widely applied to map soil texture with digital soil mapping (Jaconi et al., 2019b; Parent et al., 2021; Wang and Shi, 2018), yet its application in predicting soil pedogenic oxyhydroxides and base cation extractions have not yet been explored. Jaconi et al. (2019a) were among the first to determine SOC fractions using Vis–NIR spectroscopy combined with a *clr* transformation. Despite this though, it is still unclear which log–ratio transformation method (*alr*, *clr, ilr*) has a clear advantage for predicting SOC fractions.

Here, we aim to evaluate and optimize the use of Vis–NIR and MIR spectroscopy in combination with compositional data analysis to predict soil properties relevant to the role of SOC in biogeochemical cycles. To this end, a large sample set was used: 655 agricultural terrace and lynchet soils and 4516 garden soils were scanned to acquire soil infrared spectroscopy. For ground truthing, 10–25% of samples were measured by standard laboratory methods for soil pedogenic oxyhydroxides, base cations, soil texture and SOC fractions. More specifically, our objectives were (i) to explore the use of log–ratio transformation methods to predict soil properties associated with the role of SOC in biogeochemical cycles; and (ii) to compare the performance of three log–ratio transformation methods (*alr*, *clr* and *ilr*).

4.2 Materials and methods

4.2.1 Soil sampling and calibration sample set selection

Agricultural terrace and lynchet landforms

48 soil profiles (45–190 cm in depth) were collected from 15 agricultural terrace and lynchet landforms in the framework of an ERC project (TerrACE, https://www.terrace.no/). The sampling regions (Figure 4–1a) span a large climatic and soil range across Europe, from a latitude of 35 °N to 62 °N and a longitude from –2 °W to 26 °E. Annual mean temperature ranges from 4 ℃ in Tafjord, Norway to 19 ℃ in Crete, Greece. Annual mean precipitation varies from 272 mm to 1696 mm (https://en.climate–data.org). Soil types are primarily Luvisols, Calcisols, and Umbrisols (World Reference Base for Soil Resources, WRB). Each soil column was cut at 5 cm or 10 cm intervals, resulting in a total of 655 bulk soil samples. Soil samples were dried at 25 °C for one week and vegetation residues and roots were removed manually using tweezers. For each of the 15 sampling sites, around 20% of the samples were selected as the reference sample set. This resulted in 151 reference samples for lab–based soil analysis. Sample selection was based on the soil depth, e.g., one reference sample was taken at around 20 cm intervals. The reference samples were prepared for measuring SOC fractions, soil pedogenic oxyhydroxides, base cation extractions and soil texture. All samples were milled as powder for MIR spectroscopy (4000 – 500 cm–1). Hereafter soils of agricultural terrace and lynchet landforms will be referred to terrace soils.

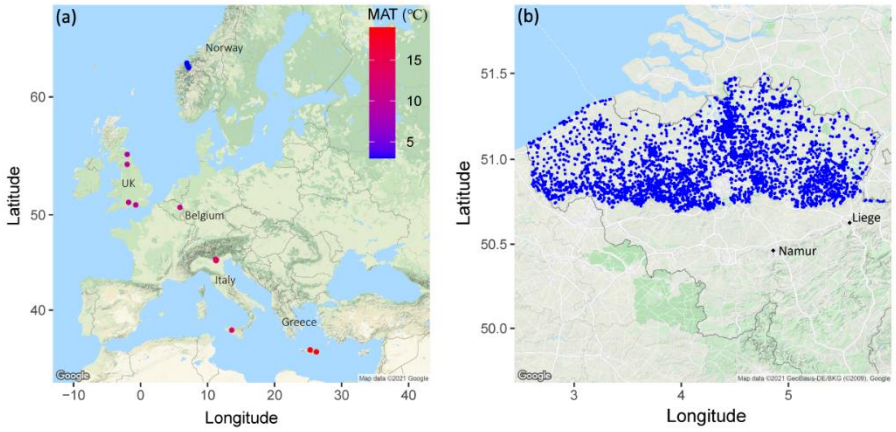

Figure 4–1 Spatial distribution of sampling sites within (a) European agricultural terrace and lynchet landforms and (b) all kinds of garden lawns sampled in the CurieuzeNeuzen citizen science project across the region of Flanders, Belgium. MAT = mean annual temperature (℃) (Figure 4–1a).

Gardens

Surface soil samples (0–10 cm) were collected by citizens in gardens in the framework of a large–scale citizen science project (www.curieuzeneuzen.be). Sample sites were dispersed across the region Flanders in Belgium, covering all types of gardens (Figure 4–1b). This region is characterized by a temperate oceanic climate, with a mean annual temperature of 10.2 °C and a mean annual precipitation of 790 mm (https://en.climate–data.org). The main soil type includes the Luvisol and Albeluvisols (WRB). Soil samples were collected in a central grass area of the garden. Three replicates of soil cores in an area of around 20 cm diameter were taken with the PVC tubes. Replicates of soil cores were subsequently combined as a composite sample. Soil samples were dried at 25 °C, vegetation residues and roots were removed, and samples were crushed to < 2 mm. We used cluster analysis to guide the selection of reference samples. The K–means algorithm was applied on spectra data as partitioning method of clustering. The Elbow method (see Kodinariya and Makwana, 2013) was used to determine the optimal number of clusters (5

clusters) that enable a coverage of the diversity of the whole dataset (4516 spectra). We then selected around 10% of the samples from each cluster. This resulted in 431 reference samples. All 4516 garden soils were scanned to obtain Vis–NIR spectroscopy (350–2500 nm), as Vis–NIR spectroscopy can be applied directly to 2 mm sieved samples. This will save time and labor in grinding soils to powder (i.e., for MIR measurement). Reference samples were only measured for soil texture. Hereafter soil texture of agricultural terrace and citizen garden samples will be referred to texture_MIR and texture_NIR, respectively.

Table 4–1 Statistical summary of the laboratory measured soil properties of agricultural terrace soil (MIR) and garden lawn soil samples (Vis_NIR).

		Minimum	Maximum	Mean	SD	CV
Terrace soil (n=151)	Clay_MIR (%)	1	42	15	9	60
	Silt_MIR (%)	23	73	53	11	21
	Sand_MIR (%)	6	76	32	16	50
	cPOM (%)	1	59	22	12	55
	micro_agg (%)	26	81	53	12	23
	s+c (%)	7	52	26	11	42
	Al_p (mg/kg)	30	42740	3017	6455	214
	Al_o (mg/kg)	352	13196	1827	1613	88
	Al_d (mg/kg)	324	20692	4983	4246	85
	Fe_p (mg/kg)	10	22185	1803	3260	181
	Fe_o (mg/kg)	480	13068	3557	2500	70
	Fe_d (mg/kg)	2168	38012	11755	8227	70
	Mn_p (mg/kg)	0	405	67	88	131
	Mn_o (mg/kg)	8	3476	605	527	87
	Mn_d (mg/kg)	12	496	107	108	101
	K (mg/kg)	272	7893	2837	1633	58
	Ca (mg/kg)	434	196071	33453	51146	153
	Na (mg/kg)	40	434	148	74	50
	Mg (mg/kg)	1510	38014	7897	6842	87
Garden soil (n=431)	Clay_NIR (%)	2	17	7	2	29
	Silt_NIR (%)	10	81	44	20	45
	Sand_NIR (%)	11	87	49	22	45

cPOM = coarse particulate SOC (> 250 µm); micro_agg = microaggregate–associated SOC (250 – 53 µm); s+c = free silt and clay–associated SOC (< 53 µm); Al_p, Fe_p and Mn_p are pyrophosphate–extractable oxyhydroxides; Al_o, Fe_o and Mn_o are oxalate–extractable oxyhydroxides; Al_d, Fe_d and Mn_d are DCB–extractable oxyhydroxides. SD = Standard deviation, CV = Coefficient of variation (%).

4.2.2 Spectroscopy measurements and pre–processing

Terrace soils were finely ground to powder using a ball mill and measured with an Alpha II FT–IR spectrometer (DRIFT module, Bruker Optik GmbH, Germany) to determine the MIR reflectance between 4000 cm^{-1} and 500 cm^{-1} at a resolution of 4 cm^{-1}. Two replicates per sample were transferred to the cups (provided by DRIFT module) and the surface was flattened without pressing using a spatula. A gold standard was used as background material to calibrate the sample spectra. Two replicates of spectral measurements were averaged to obtain one spectrum per sample.

Garden soils were scanned for Vis–NIR measurements (350 – 2500 nm) using an ASD Fieldspec 3 FR spectroradiometer (Analytical Spectral Devices Inc., USA). Soil samples were transferred to the plastic cups (a diameter of 7 cm and a height of 4 cm) and the Vis–NIR spectra were recorded. The measurements were performed using an ASD contact probe, equipped with a built–in light source (100 W halogen reflectorized lamp). Samples were measured in a dark room to avoid contamination from external light sources. Every 20 samples a white reference measurement (white panel, ASD Inc.) was added and used as background to correct the sample spectra. Every 20 samples a white sand sample was added as an internal soil standard to correct for systematic effects.

All spectra were processed using the R packages ‘prospectr’ (Stevens and Ramirez–Lopez, 2020) and ‘resemble’ (Ramirez–Lopez et al., 2020). MIR spectra were cut to the 601 – 3996 cm^{-1} region and resampled to a resolution of 4 cm^{-1}. Vis–NIR spectra were cut to the 400 – 2450 nm region and resampled to a resolution of 4 nm. Before further analysis, reflectance (R) was transformed into absorbance (A) with A = log10 (1/R). The first derivative with Savitzky–Golay third polynomial smoothing algorithms was used to pre–process both Vis–NIR and MIR spectra for eliminating the spectrum offset and scatter effects (Savitzky and Golay, 1964). Only one spectra pre–processing method was tested, as multiple studies have

suggested that the effect of pre–processing on the model performance is very limited (Baldock et al., 2013; Dotto et al., 2018; Igne et al., 2010).

4.2.3 Laboratory soil analysis

For terrace soils, the 151 reference samples (see 4.2.1) were analyzed for SOC fractions, soil pedogenic oxyhydroxides, base cation extractions and soil texture. The 431 reference samples of the private garden soils were measured for soil texture.

Soil texture was analyzed using a laser diffraction particle size analyzer (Model LS 13 320; Beckman Coulter Inc., Fullerton, USA) after ultrasonic dispersion and removal of organic matter using H_2O_2 (35%) (Beuselinck et al., 1998).

Forty gram of 2 mm sieved air–dried soils were fractionated in duplicate to obtain SOC fractions. We used a fractionation scheme based on the conceptual SOC model proposed by Six et al. (2002, 1998) applying a simplified version of its fractionation protocol (detailed in Doetterl et al., 2015a, b). Total SOC was fractionated into coarse particulate organic carbon (cPOM, > 250 µm), microaggregate–associated SOC (micro_agg, 250–53 µm) and free silt and clay–associated SOC (s+c, < 53 µm). In brief, 20 g of air–dried soils together with 50 glass beads were added onto the 250 µm mesh of a microaggregate isolator, which was then placed on a reciprocal shaker. Then the device was shaken at low speed (= 150 rpm) while the system was continuously flushed with deionized water until all aggregates on top of the 250 µm mesh were broken up and water flowing out of the device was clear. Materials left on the 250 µm sieve were interpreted as cPOM plus sand. Materials left on the 53 µm sieve were interpreted as microaggregates, and all < 53 µm materials were interpreted as free silt and clay. C concentration of all fractions was analyzed using a Vario Max CN Analyzer (Elementar GmbH, Germany). The inorganic C of sample was measured using 6M HCl with 3% $FeCl_2 \cdot 4H_2O$ following Sherrod et al (2002). SOC

content was then obtained from the total C by subtraction the inorganic C content.

A three–step sequential extraction of pedogenic oxyhydroxides was performed on milled soils in duplicate to quantify the abundance of Al–, Fe– and Mn–bearing phases (Stucki et al., 2012). First, sodium pyrophosphate ($_p$) at pH 10 was used for extracting organically complexed metals (Bascomb, 1968) (Al_p, Fe_p, Mn_p); Second, ammonium oxalate–oxalic acid ($_o$) at pH = 3 was used for extracting amorphous, short–range–order secondary oxides and poorly crystalline aluminosilicates (Dahlgren, 1994) (Al_o, Fe_o, Mn_o). Third, dithionite–citrate–bicarbonate (DCB) ($_d$) at pH = 8 was used for extracting crystalline oxyhydroxides (Mehra and Jackson, 1958) (Al_d, Fe_d, Mn_d). In addition, total elemental composition of Al, Fe, Mn, K, Ca, Na and Mg were also measured following a protocol (Doetterl et al., 2021). In brief, 1 g of powdered soil sample was digested for 90 minutes at 120 °C in aqua regia using a DigiPREP digestion system (DigiPREP MS SCP Science, Canada). All extracts including the calibration standards were filtered (41 grade Whatman filter) and diluted (dilution ratio of 1:2 for Ca, Mg, Na, K, P, and 1:1000 for Al, Fe, Mn) using a diluting system (Hamilton 100, USA) before analyzed by inductively coupled plasma optical emission spectrometry (ICP–OES) (5100 ICP–OES Agilent Technologies, USA). Total base cations (Ca + Mg + K + Na) are commonly used as an indicator of soil weathering degree (Herbillon, 1986).

4.2.4 Memory–based learning model

A memory–based learning (MBL) algorithm was applied to predict the soil properties from the spectral information. The MBL algorithm has been recognized as the most successful calibration algorithm for large soil sample sets (Hong et al., 2019; Jaconi et al., 2019b; Ng et al., 2022; Summerauer et al., 2021). For a more detailed description of the MBL approach, see Ramirez–Lopez et al. (2013). The MBL is a data–driven approach that recalls previous situations, adapts them for solving the current problem. MBL

algorithm studies the solution to solve the problem with the new explanation, and again memorizes the experience for knowledge development (Ramirez–Lopez et al., 2013). In contrast to other learning methods, the MBL method does not attempt to construct a general (global) function. Instead, for each target sample, a new and unique (local) function is developed. This new function is established using only a subset of most similar samples from a reference set, queried by a k–nearest neighbour search. Correlation dissimilarity was used here for the nearest–neighbour search. Nearest neighbour cross–validation was used to optimize the number of neighbours to retrieve (Ramirez–Lopez et al., 2013). The optimal size of nearest neighbours was tested across a range from 30 to 110, in increments of 10. Afterwards, we fitted the local models using the weighted average partial least squares regression algorithm (Shenk et al., 1997). After retrieving the nearest neighbour, a local model was fitted using the Weighted Average Partial Least Squares (WA–PLS) approach (Shenk et al., 1997). The MBL algorithm was implemented using the R packages ‘resemble’ (Ramirez–Lopez et al., 2020) and ‘prospectr’ (Stevens and Ramirez–Lopez, 2020).

4.2.5 Compositional analysis of data and log–ratio transformation

Compositional data analysis was adopted to deal with the closure effects of soil properties. The SOC fractions (cPOM, micro_agg, s+c) and soil texture (clay, silt, sand) were described as three–part compositional data of which the components should sum to 100%. Following the example given by Palarea–Albaladejo et al. (2014), we considered the pedogenic oxyhydroxides as four–part composition data: e.g., [Al_p + Al_o + Al_d + R = total Al], where R was the remaining fraction of extractable Al oxides to total Al content. A similar four–part composition was also considered for base cations [percentage K + Ca + Na + Mg = total reserve in base]. The log–ratio approach was used to carry out compositional analysis of data, thus arriving at desirable mathematical properties (Palarea–Albaladejo and Martín–Fernández, 2015). Before building the infrared spectra–soil properties

model, measured soil properties data were mathematically transformed into log–ratios with three methods (*alr*, *clr*, *ilr*).

The transformation equations (Eq.) of *alr* is defined as Eq. 4–1 (Aitchison, 1986):

$$alr(x)=\left(\ln\frac{x_1}{x_D}, \ln\frac{x_2}{x_D}, ..., \ln\frac{x_{D-1}}{x_D} \right) \quad (4–1)$$

It is defined for a D–part composition $x = [x_1, \ldots, x_D]$ considering the ratios of the components x_i to a chosen x_D.

The transformation Eq. of *clr* is defined as Eq. 4–2 (Aitchison, 1986):

$$clr(x)=\left(\ln\frac{x_1}{g(x)}, \ln\frac{x_2}{g(x)}, ..., \ln\frac{x_D}{g(x)} \right) \quad (4–2)$$

Where $g(x)$ is the geometric mean of x across component 1 through D.

The transformation equation of *ilr* is based on the *clr* transformation and defined as Eq. 4–3 (Egozcue et al., 2003):

$$ilr(x)=Vclr(x) \quad (4–3)$$

Where *clr*(x) is the centered log–ratio transformation and V is a matrix whose columns form an orthonormal basis of the *clr*–plane (Egozcue et al., 2003; van den Boogaart et al., 2021).

Here, we chose a mathematical implementation of Eqs. (4–1)–(4–3) using the R package ‘compositions’ (van den Boogaart et al., 2021). The MBL prediction model was developed using the transformed data. The results were back–transformed using inverse log–ratio transformation functions built in the R package ‘compositions’. To illustrate the advantages and disadvantages of the log–ratio transformation methods versus the non–

transformation method based on raw data (thereafter referred to as conventional method), we also fitted an MBL prediction model with the raw data of measured soil properties.

4.2.6 Model validation and evaluation

The reference sample set was randomly split into calibration and validation datasets at the 3:1 ratio. Using the calibration dataset, separate MBL model was developed for each parameter assessed (texture, SOC fraction, oxyhydroxides and base cations) as well as type for each log–ratio transformation implemented (*alr*, *clr*, *ilr* or no transformation). For each model, the model skill was evaluated against the independent validation dataset by determining four separate model performance parameters (RMSE; R^2, RPD and RPIQ). The lowest standard deviation of the root mean square error (RMSE) values was used as the criterion to choose the best prediction model. The coefficient of determination (R^2) of observed against predicted values, ratio of performance to deviation (RPD) and ratio of performance to interquartile range (RPIQ) (Bellon–Maurel et al., 2010) were calculated as additional model performance parameters. According to Chang et al. (2001), we judge the model quality by: RPD < 1.4 indicates a non–reliable model; 1.4 < RPD < 2 indicates a fair model; RPD > 2 indicates an excellent model.

To evaluate the model robustness and to statistically compare the performance of three log–ratio transformation methods, we repeated the above model development n = 100 times, where each time the reference sample set was randomly split into calibration and validation dataset. This resulted in 100 sets of predictions and model performance parameters. The same procedure was then repeated on the raw dataset (i.e., without log–ratio transformation), thus eventually resulting in four sets of model performance parameters (*alr*, *alr*, *ilr* or no transformation). One–way ANOVA with the LSD post–hoc test ($P < 0.05$) was then used to assess differences in model performance (RMSE; R^2, RPD and RPIQ) between compositional

data analysis and the conventional method, and between the three log–ratio transformation methods. To assess if the log–ratio transformation method has potential to reduce the number of samples with extreme prediction error, Eq. (4–4) was used to calculate the relative error (*EXE*):

$$EXE = ABS(x_{pre} - x_{mea}) / x_{mea} \qquad (4–4)$$

Where x_{pre} is the predicted values by log–ratio transformation or conventional method; x_{mea} is the measured values; *ABS* is the ABSOLUTE VALUE function. The interquartile range (IQR) was calculated as the region between the 75th and 25th percentile of the *EXE* dataset. Samples were considered to have extreme prediction error if *EXE* > 6 × IQR (*pEXE*).

4.3 Results

4.3.1 Overview of the reference measurements

Terrace soils represented a wide range of oxyhydroxides and base cations contents, with a CV ranging from 50% to 214% (Table 4–1). Of all oxyhydroxides, the largest CV was found for pyrophosphate–extractable oxyhydroxides (Fe_p, Al_p, Mn_p) (CV: 131 – 214%), while the variability of oxalate extractable oxyhydroxides (CV: 70–88%) and DCB–extractable oxyhydroxides (CV: 70–101%) was relatively lower. For base cations, a larger variation occurred in Ca cation with CV = 153% when compared to K, Na and Mg (CV < 87%). The ternary plot showed that SOC of terrace soils was mainly composed of micro–agg SOC fraction, accounting for 26% ~ 81% of total SOC (Figure 4–2a, Table 4–1). Both terrace soils and garden soils were classified primarily as silt loam, loam and sandy loam soils according to the USDA classification system. (Figure 4–2b, c). Garden soils presented high contents of either sand (mean = 49%) or silt (mean = 44%), while clay content was very low (mean = 7%). The range of clay content for terrace soils (1–42%) was higher than garden soils (2–17%). Moreover, CV

of soil texture for terrace soils (21–60%) was higher than garden soils (CV: 29–45%).

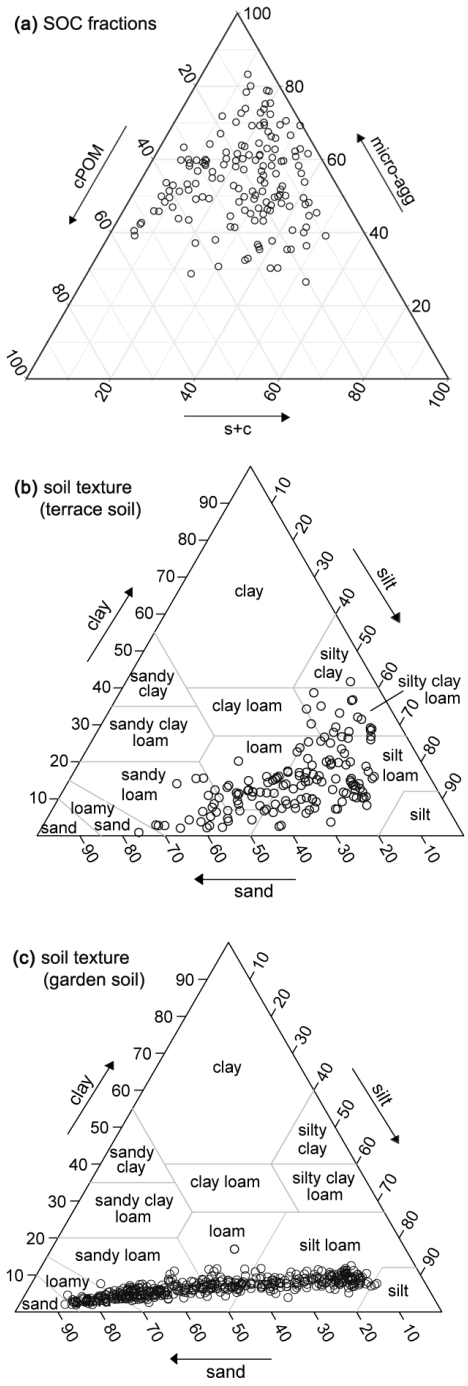

Figure 4–2 Ternary plot of SOC fractions in percentage of total SOC for terrace soils (a), soil texture triangle based on the USDA textural soil classification for (b) terrace soil and (c) garden soil.

4.3.2 Comparison of three log–ratio transformation methods

Overall, the model performance of the three log–ratio transformation methods was rather similar (Figure 4–3). For 14 out of the 22 soil parameters assessed, there were no significant difference between three log–ratio transformation methods (*alr*, *clr*, *ilr*) for any of the 4 model performance parameters (R^2, RMSE, RPD, RPIQ). These included Fe oxides (Fe_p, Fe_o, Fe_d), Mn oxides (Mn_p, Mn_o, Mn_d), base cations (K, Ca, Na, Mg) and texture (Clay_MIR, Silt _MIR, sand_MIR, Clay_NIR, Clay_NIR) ($P > 0.05$; Figure 4–3). For the other 8 soil parameters, there was a significant difference in at least one of 4 model performance indicators ($P < 0.05$; Figure 4–3). For Al oxides (Al_p, Al_o, Al_d), the *alr* method showed significantly higher model performance (higher R^2 and RPD) than the *ilr* method. For cPOM and micro_agg SOC fractions, the model performance of the *alr* and *ilr* methods was better than that of *clr* method, as indicated by significantly higher R^2, RPD and lower RMSE. For Silt_NIR and Sand_NIR, *ilr* gave a better model performance than *clr*, while no significant difference was found between the *alr* and *clr* methods.

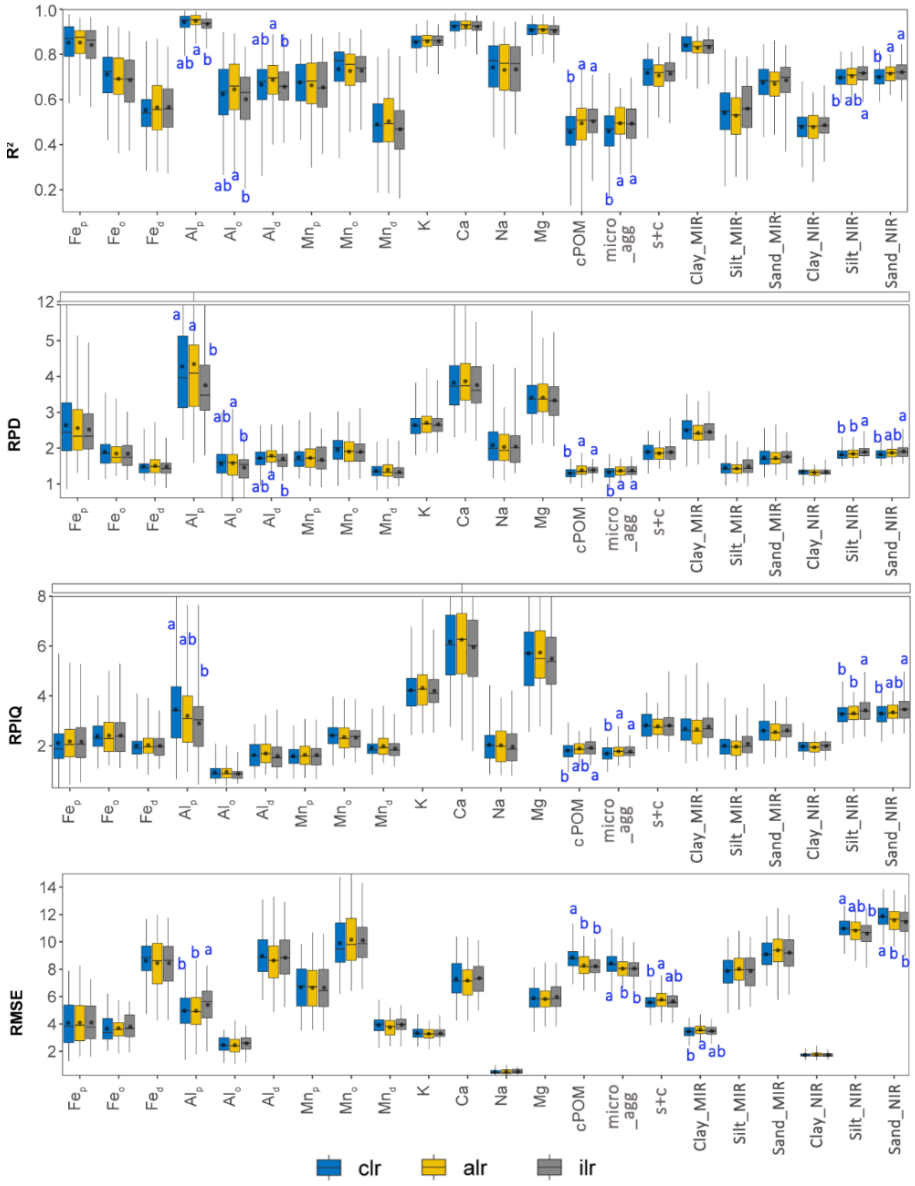

Figure 4–3 Comparison of model performance between three log–ratio transformation methods. For each soil parameter and model performance indicator, the boxplot shows the mean (dot), median (line) and interquartile of N = 100 separate model trials (see 5.2.6). *alr* = additive log–ratio; *clr* = centered log–ratio; *ilr* = isometric log–ratio. R^2, coefficient of determination; RMSE, root mean square error; RPD, ratio of performance to deviation; RPIQ, ratio of performance to interquartile range. Blue letters indicate significant differences in mean values (a > b > c) of model performance parameters between log–ratio transformation methods ($P < 0.05$).

4.3.3 Comparison of model performance between compositional data analysis and conventional methods

4.3.3.1 Model performance parameters

For soil texture, no significant differences in model performance were found between the log–ratio transformation–based method (the one with best model performance) and the conventional method (without transformation) (Table 4–2). Similarly, there was no significant differences in model performance between two methods when predicting Al_p, Al_o, Al_d, Fe_p, Fe_o, Mn_p and s+c ($P > 0.05$). The log–ratio transformation method showed a higher accuracy in predicting Na, K, Ca and Mg ($P < 0.05$), while the conventional method gave a higher accuracy (e.g., higher R^2, RPD and RPIQ) in predicting Fe_d, Mn_o, Mn_d, and micro_agg.

Table 4–2 Comparison of model performance parameters between the log–ratio transformation and conventional (raw data) methods.

	R^2		RPD		RPIQ		RMSE	
	Log ratio	Raw data	Log ratio	Raw data	Log ratio	Raw data	Log ratio	Raw data
Al_p	0.95	0.95	4.3	4.2	3.2	3.6	4.96	4.83
Al_o	0.65	0.68	1.6	1.7	1.0	1.1	2.45	2.25
Al_d	0.69	0.69	1.8	1.8	1.7	1.7	8.64	8.67
Fe_p	0.85	0.85	2.6	2.6	2.1	2.2	4.07	3.79
Fe_o	0.71	0.74	1.9	2.0	2.4	2.6	3.65	3.48
Fe_d	0.55	**0.64**	1.5	**1.8**	2.0	**2.4**	**8.63**	7.32
Mn_p	0.68	0.64	1.7	1.6	1.6	1.4	6.67	6.96
Mn_o	0.73	**0.77**	2.0	**2.1**	2.4	2.5	9.90	9.47
Mn_d	0.50	**0.59**	1.4	**1.6**	2.0	**2.3**	3.95	**3.30**
Na	**0.74**	0.69	**2.1**	1.8	**2.0**	1.7	0.50	**0.56**
K	**0.86**	0.84	**2.7**	2.5	4.3	4.1	3.28	**3.52**
Ca	0.92	0.92	**3.9**	3.6	6.3	5.8	7.17	**7.59**
Mg	0.91	0.90	**3.4**	3.2	5.7	5.3	5.83	**6.18**
cPOM	0.50	**0.55**	1.4	**1.5**	1.9	**2.1**	**8.23**	7.68
micro_agg	0.49	**0.51**	1.4	1.4	1.8	1.8	**8.04**	7.75
s+c	0.72	0.71	1.9	1.9	2.8	2.8	5.57	5.68
Clay_MIR	0.84	0.84	2.5	2.5	2.7	2.8	3.45	3.41
Silt_MIR	0.56	0.56	1.5	1.5	2.1	2.1	7.87	7.66
Sand_MIR	0.69	0.69	1.8	1.8	2.6	2.7	9.21	8.89
Clay_NIR	0.49	0.47	1.3	1.3	2.0	2.0	1.73	1.71
Silt_NIR	0.72	0.70	1.9	1.8	3.4	3.2	10.60	10.89
Sand_NIR	0.72	0.70	1.9	1.8	3.5	3.3	11.45	11.79

Note that the log–ratio transformation method with the best model performance is selected as comparison with conventional method. R^2, coefficient of determination; RPD, ratio of performance to deviation; RPIQ, ratio of performance to interquartile range; RMSE, root mean square error. Numbers in bold and underlined indicate a significantly higher performance of that model parameters comparted with its counterpart ($P < 0.05$, N = 100).

4.3.3.2 Sum of predicted fractions based on conventional method

The use of a log–ratio transformation method introduces a constraint that forces the predicted fractions to sum to 100% (Pawlowsky–Glahn and Egozcue, 2006). Verification of the model output showed that the sum of predicted fractions equal to 100% (data do not show), so this constraint was indeed met. When building spectral models using the conventional method, the predicted fractions do not necessarily add up to 100%. This effect was shown in Figure 4. Although the sum of predicted fractions was close to 100% for most of soil samples, a small proportion of samples showed a rather large bias. For example, the sum of SOC fractions ranged from 86% to 133%. Similarly, the sum of clay, silt, and sand fractions of the garden soils (texture_NIR) ranged from 80% to 123%. Overall, the sum of fractions of soil mineral extractions (Al, Mn, Fe and base cations) were closer to 100% than that of SOC fractions and soil texture.

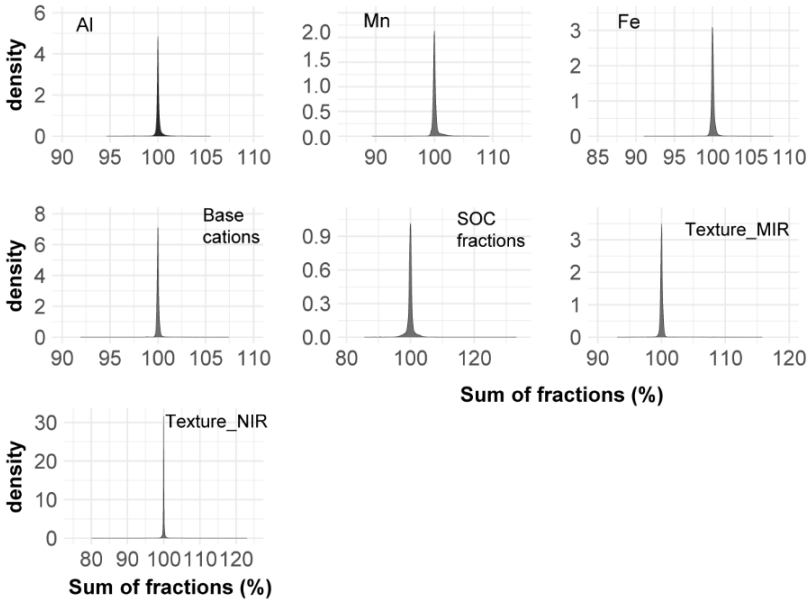

Figure 4–4 Distribution of the sums for predicted fractions derived with conventional method. The plots were based on 504 predictions for terrace soils and 4085 predictions for garden soils.

4.3.3.3 Number of samples with extreme prediction error

Using Eq. 4–4, we determined the percentage of samples with extreme prediction error (*pEXE*, Figure 4–5). Overall, the log–ratio transformation method showed lower *pEXE* than the conventional method. In particular, the log–ratio transformation–based method reduced *pEXE* at least 2 times for 6 out 22 soil parameters (i.e., from 8.4 to 0.2 for Al_p, from 2.8 to 1.2 for Al_d, from 8.9 to 0.5 for Fe_p, from 4.1 to 0.1 for Na, from 1.9 to 0.7 for Mg, from 6.2 to 3.9 for cPOM), when compared to conventional method. For the remaining soil properties, the differences in *pEXE* between two methods were rather small (*pEXE* < 2).

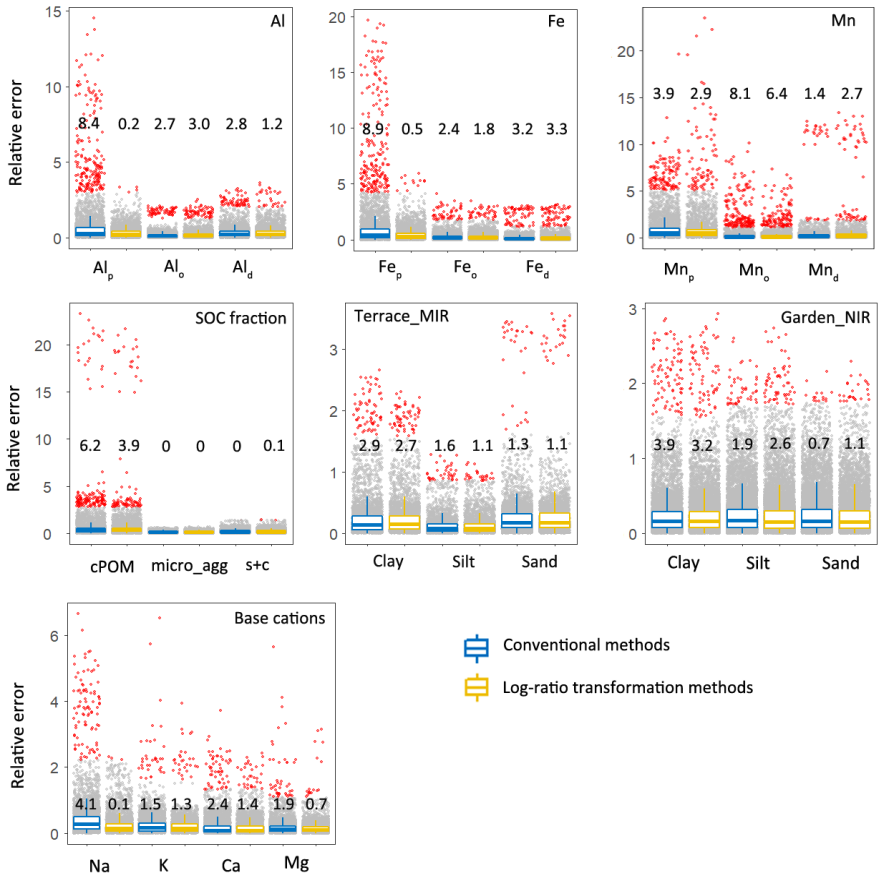

Figure 4–5 Comparison of the prediction error (y–axis) based on the conventional method and log–ratio transformation methods. The prediction error was calculated by Eq. (4) using the data from 100 model runs after randomly splitting the calibration and validation dataset each time. Samples with extreme prediction error (see Eq. 4) were indicated by red dot. The percentage (‰) of samples with extreme prediction error (*pEXE*, red dots) was given as the numbers above the bar.

4.3.3.4 Prediction of soil properties

Vis–NIR and MIR spectra coupled with the log–ratio transformation approach provided reliable models to predict measured soil properties (Figure 4–6). Excellent models were achieved for predicting 8 out of 22 soil

properties: Al_p, Fe_p, Mn_o, Clay_MIR, and base cations (RPD > 2). This was also indicated by high values of R^2 (0.73 – 0.92), RPIQ (2 – 6.3) and low values of RMSE (0.51 – 7.2%). Fair models were obtained for predicting 13 out of 22 soil properties: Al_o, Al_d, Fe_o, Fe_d, Mn_p, Mn_d, Silt_MIR, Sand_MIR, Silt_NIR, Sand_NIR, and SOC fractions, with RPD ranging from 1.4 to 1.9. The model performance for the Clay_NIR was the lowest and considered marginally unreliable (R^2 = 0.49; RPD = 1.3).

All base cations (K, Ca, Na, Mg) could be predicted with high accuracy by our MBL spectra models (RPD > 2.1, R^2 > 0.74). The model accuracy for organically complexed Fe, Al metals (Al_p, Fe_p) was consistently better than that for poorly crystalline aluminosilicates (Al_o, Fe_o) and crystalline oxyhydroxides (Al_d, Fe_d). The model performance for soil texture and SOC fractions was lower than that of soil mineral extractions (mineral oxides and base cations). The predictive performance for s+c SOC fraction (RPD = 1.9) was higher than that for cPOM and micro_agg SOC fractions (RPD = 1.4). For texture of terrace soils, the best model was obtained for predicting clay fraction (PRD = 2.5, Clay_MIR), while for garden soils the spectra model was unreliable when predicting clay fraction (Clay_NIR).

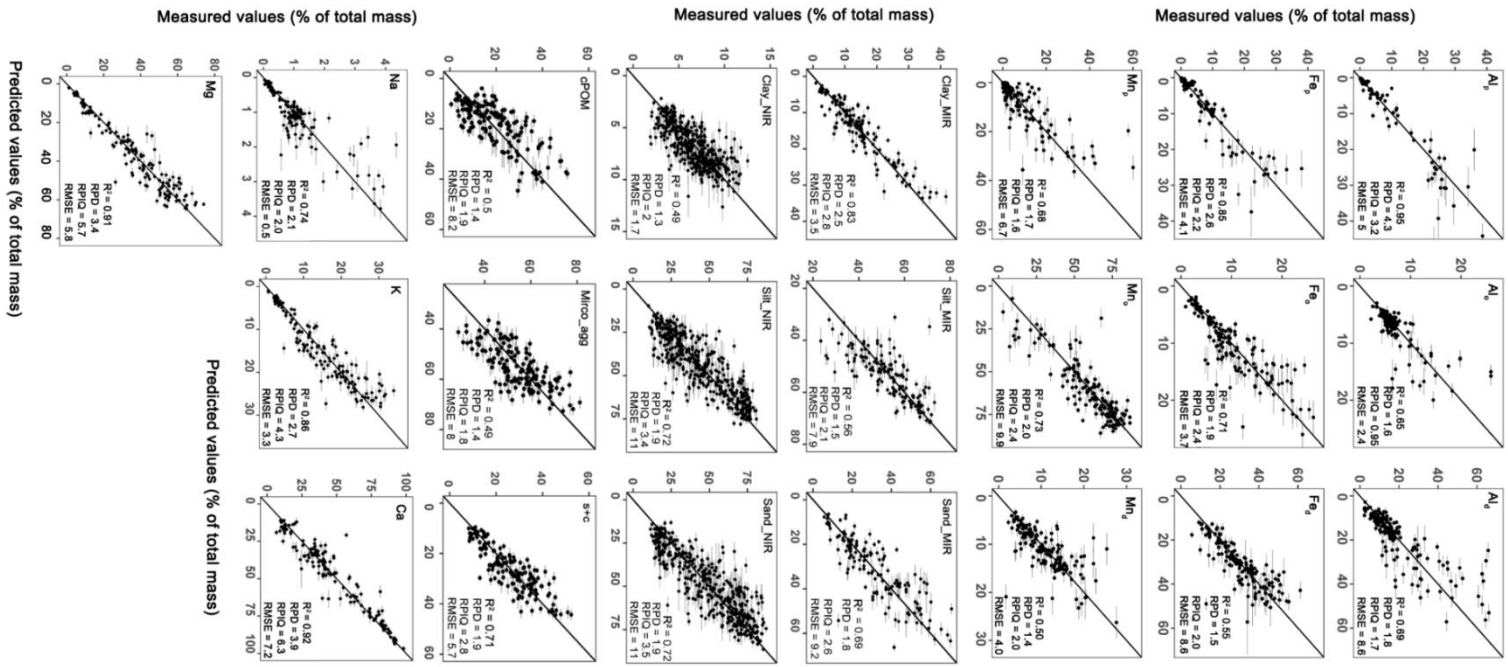

Figure 4–6 Modelled versus measured soil properties expressed as percentage to total mass. Predicted values are the mean ± SD based on 100 replicate model runs after randomly splitting the calibration and validation dataset each time. Results were based on log–ratio method that gave the best model performance. R^2, coefficient of determination; RMSE, root mean square error; RPD, ratio of performance to deviation; RPIQ, ratio of performance to interquartile range. Solid line is the 1:1 line.

4.4 Discussion

4.4.1 Comparison of three log–ratio transformation methods

The *clr*, *alr* and *ilr* transformation methods have been widely applied to compositional data within a diverse range of research fields (Jaconi et al., 2019b; Otero et al., 2005; Palarea–Albaladejo et al., 2014; Shenk et al., 1997; Zhang et al., 2020). Among them, the *ilr* approach is particularly interesting because it theoretically overcomes the main drawbacks of the *clr* method (Egozcue et al., 2003; Palarea–Albaladejo et al., 2014). For example, *ilr* avoids the issue of data collinearity caused by the *clr* transformation and represents the information in the real Euclidean space. In this geometry, classical correlation analysis can be more reliable (Reimann et al., 2017). Previous studies have shown that the *ilr* method combined with ordinary kriging can indeed outperform *clr* and *alr* when mapping soil texture (Wang et al., 2021; Wang and Shi, 2018; Zhang et al., 2020). These results are partly consistent with our findings showing that *ilr* gives significantly higher model performance than *clr* in predicting silt_NIR, sand_NIR texture fractions, cPOM and micro–agg SOC fractions ($P < 0.05$), while *alr* provides equivalent results as *ilr*. For remaining soil properties (Fe oxides, Mn oxides, base cations, texture_MIR and s+c SOC fraction), however, we did not find the significant difference in model performance between the three log–ratio transformation methods (Figure 4–3). Muzzamal et al. (2018) has also reported that *ilr* does not produce significantly better results than *alr* in predicting soil texture using ancillary data collected by proximally sensed gamma–ray spectrometry. Similarly, when log–ratio transformation methods are combined with different predictive models (e.g., Cubist, random forest model) to map soil texture, the best log–ratio transformation method is not necessarily *ilr* (Li et al., 2020). Together, these results suggest that none of three transformation methods performs intrinsically better. The choice of the best log–ratio transformation method depends on which soil properties are targeted as well as which predictive models are chosen.

4.4.2 The advantages of log–ratio transformation methods in predicting soil properties from spectroscopy

For the majority of soil properties (13 out of 22 variables), we found no difference in RPD between log–ratio transformation based and conventional methods. Only when predicting base cations (Na, K, Ca, Mg), the log–ratio transformation method (mean RPD = 3.0) slightly outperformed the conventional method (mean RPD = 2.8) (Table 4–2). These results suggest that using the log–ratio transformation method does not necessarily improve the model performance.

However, the use of log–ratio transformation methods does improve the consistency of the predicted soil properties. As shown by our results, the predicted fractions by the conventional method do not necessarily add up to 100% (Figure 4–4). The conventional method minimizes the prediction error for each fraction separately and independently in the predictive process, and so there is no guarantee that the sum of fractions will add up to 100% (Wang and Shi, 2017). However, such internal data consistency is however a necessary requirement for utilizing the predicted results, e.g., to classify soils based on soil texture (Hobley and Prater, 2019). With compositional data analysis using log–ratio transformations, a hard constraint is introduced that ensures that all fractions will add up to 100% (Aitchison, 1986). Thus, one of the advantages of the log–ratio transformation approach is to ensure that predicted fractions sum up to a constant value (i.e., = 100%), while attaining a model accuracy that is as good as that of conventional methods (Table 4–2, Figure 4–4).

Our analysis also shows that log–ratio transformation method has the potential to reduce the number of samples with extreme prediction errors compared to the conventional method. This is more pronounced for predicting Al_p, Al_d, Fe_p, Na, Mg and cPOM (Figure 4–5). In the conventional method, each fraction is modelled independently and allowed to vary freely when optimizing the spectral model (Ramirez–Lopez et al., 2013). However,

with the compositional data analysis approach, fractions are transformed as log–ratios, so that a link is added between these fractions, forcing the fractions to be interrelated so they no longer are free to vary (Palarea–Albaladejo et al., 2014). In this way, the predicted values always remain positive with relatively lower possibility to produce extreme errors.

4.4.3 Log–ratio transformation coupled with MBL models enable reliably predicted soil properties from spectra

Soil texture, SOC fractions, pedogenic oxyhydroxides and base cation extractions are among the most important geochemical properties for understanding SOC biogeochemical cycles in the context of human perturbation and climate change (Bukombe et al., 2021; Doetterl et al., 2015a; Viscarra Rossel et al., 2019; Wang et al., 2018b). In the underlying study, infrared spectroscopy coupled with a compositional data analysis provides an efficient (i.e., rapid and cost–effective) and reliable (i.e., accurate and internally consistent) solution for estimating the above–mentioned soil properties (Figure 4–6). We obtained excellent MIR spectra models for predicting Na (RPD = 2.1), K (RPD = 2.7), Ca (RPD = 3.9) and Mg (RPD = 3.4) cations. Excellent models (RPD ranged from 2.2 to 3.2) have also been developed by Reda et al. (2021) and Mayrink et al. (2019) for predicting K, Ca and Mg cations. However, most previous studies have reported a lower model quality (as summarized in Mayrink et al., 2019) compared to the current study. Infrared spectroscopy has been used to predict Fe oxyhydroxides (Chakraborty et al., 2017; Zheng et al., 2019), but its application to Al and Mn oxyhydroxides has been rarely reported. In current study, models with higher accuracy were developed for predicting Fe oxyhydroxides (RPD: 1.5 – 2.6) (Figure 4–6) compared to previous studies using Vis–NIR or MIR spectroscopy (RPD < 1.4) (Chakraborty et al., 2017; Zheng et al., 2019). We also obtained reliable models for predicting Al and Mn oxyhydroxides. Overall, the MBL model technique combined with the log–ratio transformation approach provides better models for predicting soil extractable minerals (base cations and pedogenic oxyhydroxides) than other

methods using large–scale datasets (Mayrink et al. 2019). The higher performance of our approach could be attributed to 1) the MBL model is more suitable to handle complex large–scale datasets compared to other regression models such as partial least–squares regression (Jaconi et al., 2019b; Ramirez–Lopez et al., 2013) and 2) the benefit of applying log–ratio transformation to mineral fractions in spectroscopic models.

Soil Vis–NIR and MIR spectra have already been successfully used for predicting SOC fractions and soil texture (Cozzolino and Morón, 2006; Henaka Arachchi et al., 2016; Hobley and Prater, 2019; Jaconi et al., 2019a, b). Our approach also provides reliable models to estimate SOC fractions and soil texture, while ensuring that fractions sum up to 100% of grain size content or total C content (Figure 4–6). For SOC fractions, our approach provided a comparable model performance as other studies using the same SOC fractionation scheme (i.e., aggregate fractionation; (Henaka Arachchi et al., 2016)), but lower than those using a chemical fractionation scheme (Briedis et al., 2020; Knox et al., 2015).A chemical fractionation scheme using oxidants (e.g., NaOCl) or acids (e.g., HCl) as treatments is more effective than aggregate fractionation in isolating stable SOC fractions from labile SOC fractions. As a result, chemically isolated SOC fractions are more distinct from each other in term of their turnover time, chemical composition, and mineralogical characteristics than those obtained by aggregate fractionation (von Lützow et al., 2007). Therefore, with a chemical fractionation scheme, the chemical composition and mineralogical characteristics of SOC can be more easily captured by the MIR spectra, thus exhibiting better prediction accuracy than with the aggregate fractionation scheme.

4.5 Conclusion

In the underlying study, soil infrared spectroscopy was combined with three log–ratio transformation approaches to predict soil pedogenic oxyhydroxides, base cations, soil texture and SOC fractions, which are considered as composition data. Fair to excellent MIR spectra models (RPD from 1.4 to 4.3; R^2 from 0.50 to 0.95) were obtained for predicting base cations (Na, K, Ca, Mg), Fe, Al, Mn oxyhydroxides, and soil texture of terrace soils. Reliable models were also achieved for predicting silt and sand contents of garden soils using Vis–NIR spectra (RPD = 1.9; R^2 = 0.72), whereas accuracy for clay was relatively lower (RPD = 1.3; R^2 = 0.49). Regarding the three log–ratio transformation methods, *ilr* outperformed *clr* when predicting silt_NIR, sand_NIR, cPOM and micro–agg SOC, whereas for remaining soil properties three log–ratio transformation methods provided equivalent results. Our results suggest that using log–ratio transformation method provides predictive models that are as accurate as the conventional method, yet with two significant advantages: (1) it ensures the predicted fractions summing to 100% and (2) it reduces the number of samples with extreme relative prediction error. Additionally, we demonstrate that soil Vis–NIR and MIR spectroscopy, combined with compositional data analysis is a promising technique that enables efficient and reliable 'large–scale' assessment of soil properties relevant to SOC biogeochemical cycles.

Acknowledgements

I would like to thank the colleagues at TECLIM, UCLouvain (Marco Bravin, Klara Dvorakova, He Zhang, Yue Zhou, Sebastian Paez–Bimos, François Clapuyt) who helped with the Vis–NIR measurements, and Lore Fondu (KU Leuven) for grain size analysis. Special thanks go to the citizens of Flanders region, Belgium, who helped collect the garden soil samples (Figure 4–1b)

Chapter 5

Controls on soil organic carbon stocks and dynamics in agricultural terraces along climatic and geochemical gradients

Abstract

Although agricultural terraces are considered to be effective systems for soil organic carbon (SOC) sequestration, the factors controlling SOC stocks and dynamics are not well understood, particularly the role of terrace age and soil geochemistry are not considered. Using samples collected from 13 agricultural terrace landforms across Europe, we assessed the relative importance of climate, terrace soil burial age, soil mineral weathering and pedogenic oxyhydroxides in controlling SOC stock and soil potential heterotrophic respiration (SPR). Results showed that terracing landforms had a higher SOC stock (89 ± 122 %) compared to the non–terracing landforms. Multiple regression models indicated that for topsoil layers (0–10 cm) of terraces, climate was the most important factor explaining variability of SOC density, while for subsoil layers (> 10 cm), the strongest predictor was the reactive mineral oxides (organically complexed metals and poorly crystalline oxides). Although climate is generally considered as a primary or secondary control on SPR in non–terracing soils, our results suggest that across soil depth, the primary controls on SPR in terracing systems were the degree of mineral weathering and soil pedogenic oxyhydroxides. Interestingly, for subsoil layers (> 10 cm), the terrace soil burial age was selected as the key predictor of SPR. Partial correlation analysis further showed that controlling for terrace soil burial age significantly altered the correlations between SPR and weathering degree, soil texture and clay & silt associated SOC fraction. These results suggest that for terraced subsoils (e.g., buried layers), soil age is a key factor in controlling soil heterotrophic

respiration, most likely through driving mineral weathering and thus determining the availability of reactive mineral surfaces that stabilize SOC.

Chapter 5

5.1 Introduction

As the consequence of recognition that soils have the potential to store large amounts of organic carbon (OC) and offset greenhouse gas emissions, there is an increasing interest in the capacity of soils to sequestration OC in different ecosystems (Contreras–Cisneros et al., 2022; Scharlemann et al., 2014; Toma et al., 2013; Van De Broek et al., 2016). As the volumetrically largest and most common human–made landforms, agricultural terrace ecosystems have shown its potential to sequester OC in diverse regions, such as Europe (Curtaz et al., 2015; Dunjó et al., 2003; Walter et al., 2003), South America (Antle et al., 2007), Asia (Chen et al., 2020a; Shi et al., 2019), and Africa (Kagabo et al., 2013). Terrace construction involves cutting of the soil from the upper slope and filling the downslope part of the terraces. This introduces extensive disturbances to local topography, soil redistribution and land use, and thus affects the C dynamics and its exchange with the atmosphere C pool (Brown et al., 2021; Wei et al., 2016; Zhao et al., 2021a).

The first step to evaluate the C sequestration potential of soils is to investigate the inventory of SOC stocks. By comparing the SOC stocks of terracing landform with an non–terracing landform, there seems to be consensus that in most cases, construction of terraces has a positive effect on SOC sequestration (Walter et al., 2003; Antle et al., 2007; Kagabo et al., 2013; Xu et al., 2015; Welemariam et al., 2018; Shi et al., 2019). For example, a meta analysis (Chen et al., 2020a) reported that terracing on average increases SOC sequestration by 32.4%, mainly arising from the accumulation of SOC due to soil deposition and soil burial in the fill section of terraces (De Blécourt et al., 2014). However, negative effects of terracing on SOC sequestration have been also reported (Gao et al., 2020; Hamdan et al., 2000). These examples indicate that although construction of terraces undoubtedly triggers a significant impact on SOC dynamics (De Blécourt et al., 2014; Wei et al., 2016; Zhao et al., 2021a), uncertainties remain in the

direction and capacity of terraced soils to sequestrate OC (Brown et al., 2021).

Moreover, it is of utmost importance to study the key factors controlling the levels of SOC stock in terrace soils in order to identify optimal strategies for terrace management (Chaplot et al., 2010). Meta–analysis has shown that current land use, climate, topography, and terrace age are the critical factors controlling SOC sequestration in terrace soils. However, there are still lack of investigations on terracing SOC stock from a broad range of climatic and geographic range (Chen et al., 2020a). In particular, the role of soil geochemistry background is not considered. This is a significant knowledge gap considering that the recent studies have highlighted the more importance of soil geochemical properties in stabilizing OC than climate factors (Doetterl et al., 2015a; Haaf et al., 2021; Luo et al., 2019). Soil clay minerals and Fe–, Mn– and Al–oxy–hydroxides, characterized by large specific surface area, can absorb organic acid and form strong organo–mineral associations thus protecting SOC against mineralization (Blume et al., 2016). Therefore, soil geochemical properties, inherited from the weathering of parent material, may play a crucial role in determining the capacity of terrace soils to sequester OC.

Field investigations have clarified two major competing processes involved in SOC dynamics in terrace systems: (i) SOC depletion due to C–rich topsoil removal and soil structure breakdown at cut section when constructing terraces; (ii) SOC accumulation due to dynamic replacement of lost SOC at the cut section and topsoil burial at the fill section of terraces. The overall effect of terracing on SOC sequestration thus depends on which process is dominant. Exposed subsoil due to terrace construction typically has more reactive sites on mineral surface that are not saturated with C compounds (Doetterl et al., 2016). Fresh C from photosynthate can form organo–mineral complexes with these reactive mineral surfaces thus capturing new C at the cut section of terraces (known as “dynamic replacement”; De Blécourt et al., 2014; Harden et al., 1999). The available evidence indicates that it takes at

least 5–29 years to replace the lost SOC due to topsoil removal after terracing (Chen et al., 2020a; De Blécourt et al., 2014; Stavi et al., 2019). Hence, dynamic replacement of lost SOC in terrace system is significantly age–related. Moreover, burial of SOC at the fill section of terrace provides a long–term mechanism to preserve SOC in terraced systems (De Blécourt et al., 2014; Zhao et al., 2021a). For example, deep burial environments provide a less favorable context for SOC mineralization by reducing available oxygen in soil pore space and increasing soil water content (Vandenbygaart et al., 2012; Wiaux et al., 2015). However, the buried SOC could be gradually mineralized over time. Hence, SOC burial at fill section of terraces is also significantly age–related. Current studies are exclusively focused on relatively young terraces (< 30 years), pointing out the need for considering much longer time scales when assessing SOC dynamics in terracing landforms.

Dating agricultural terraces has been a challenge until recent development of direct sediment–dating techniques particularly optically stimulated luminescence (OSL) (Lang et al., 2003). Although the OSL dating have been successfully applied to a wide range of terraces and lynchets (Davidovich et al., 2012; Kinnaird et al., 2017), this technique is costly and time consuming and not suitable for analyzing a large number of samples for a large-scale study (Brown et al., 2021). The portable OSL (pOSL) reader developed by SUERC (Glasgow, UK) is now widely used in geoarchaeological and geomorphological studies as it is more efficient and can be used for large, untreated samples (Porat et al., 2019; Portenga et al., 2016). The pOSL reader records the bulk OSL signal intensity, which can be used as a proxy for the relative soil burial age (e.g., Muñoz–Salinas et al., 2011; Zhao et al., 2021a).

The overall objective of this study is to improve our understanding of SOC dynamics and its influencing factors in agricultural terrace systems. To achieve this, we collected terraced soils from a broad climatic and geographic range across Europe. Measurements of SOC stock and soil

potential heterotrophic respiration were linked to the climate, soil burial age and soil geochemistry properties. The detailed objectives of this study are to (i) evaluate the SOC stock of terraced landforms relative to non–terracing landforms; (ii) assess the relative importance of climate, terrace soil burial age, soil mineral weathering and pedogenic oxyhydroxides in controlling terrace SOC stock and soil heterotrophic respiration.

5.2 Materials and Methods

5.2.1 Study site and soil sampling

We selected 13 agricultural terrace landforms spanning a large climatic and soil geochemical range of Europe, from a latitude of 35 °N to 62 °N (Norway) to a longitude of –2 °W to 26 °E (Greece) (Figure 5–1a). Annual mean temperature (MAT) ranges from 3 ℃ in Homlong, Norway to 19 ℃ in Crete, Greece. Annual mean precipitation (MAP) varies from 303 mm to 1696 mm (https://en.climate–data.org). Climate types include continental subarctic climate (Dfc), marine west coast climate (Cfb), humid subtropical climate (Cfa) and hot–summer Mediterranean climate (Csa) according to the Köppen climate classification (Table 5–1). Soil types are primarily Luvisols, Calcisols and Umbrisols (World Reference Base for Soil Resources, WRB). Current land use includes grassland and woodland. Terraces can be dated back to early Bronze Age, e.g., the terrace in Ingram site (Frodsham and Waddington, 2004).

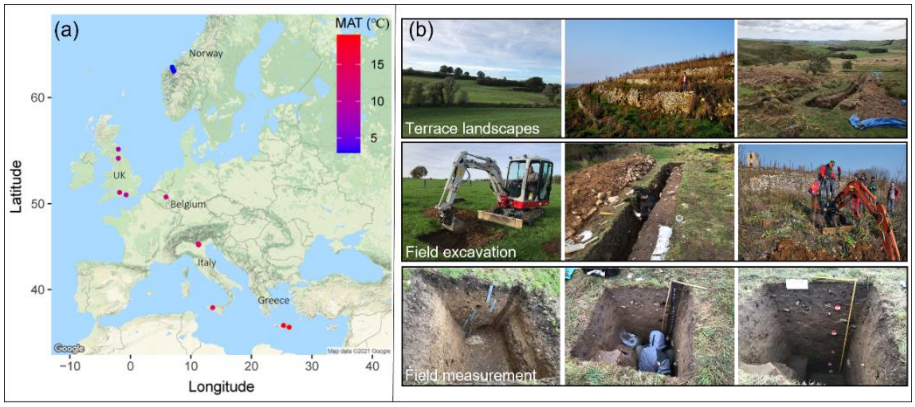

Figure 5–1 (**a**) Distribution of study sites and (**b**) photo of terrace landforms and field excavation. MAT = annual mean temperature (℃).

In total 38 terrace soil profiles were excavated to the depth of weathered bedrock surfaces (down to 190 cm) in order to estimate the SOC stock in terraced landforms (Figure 5–1b). Additionally, undisturbed soil profiles (non–terracing) in proximity to the terraced landforms were also excavated as the control profiles. It is very difficult to identify undisturbed soils nearby the terraced landforms because the undisturbed sites are non-existent or are difficult to access. However, we obtained 7 control profiles at 5 sites (Table 5–1). To provide additional estimation of SOC stock for non–terraced soils, we extracted SOC stock data from the publications for Martelberg site of Belgium and Blick site of UK (Table 5–1). For Blick site, we extracted SOC stock of 12 soil profiles (reach to bedrock) from 12 non–terracing, arable landforms (Thuiller et al., 2005). The sampling sites are located within a 12 km radius of the Blick terrace site. Meersmans et al. (2011) published a dataset containing SOC stock data of over six hundred soil profiles (1–1.5 m in depth) from grassland and cropland in Belgium. We extracted the SOC stock data of grassland, which is under the same land use as our terrace landforms (Martelberg). Extracted SOC stock data from publications will be a complement to the control profiles we have excavated. Soil columns were cut at 5 cm or 10 cm depth interval and the vegetation residues and roots were removed manually using tweezers to be prepared for further analysis.

Table 5–1 Information of sampling sites

Site code	Latitude	longitude	Koppen climate	MAT ℃	MAP mm	Soil type (WRB)	Parent material	No. of terrace profiles	No. of control profiles
Homlong	62°06'N	7°10'E	Continental subarctic climate (Dfc)	3	1696	Podzols		1	-
Skotet	62°24'N	6°54'E		3	1696	Podzols	Granites	3	-
Smoge	62°14'N	7°02'E		3	1696	Podzols		2	1
Ingram	55°26'N	1°59'W	Marine west coast climate (Cfb)	8	650	Umbrisols	Andesite rock	4	2
Blick	51°10'N	1°47'W		10	772	Umbrisols		2	1
Charlton	50°55'N	0°43'W		9	778	Luvisols	Loess	2	-
Gueswick	54°35'N	1°59'W		10	719	Luvisols	Chalk	4	-
Martelberg	50°42'N	5°52'E		11	886	Luvisols		4	1
Belloca	45°32'N	11°12'E	Humid Subtropical Climate (Cfa)	14	803	Calcic Grumic Vertisols	Volcanic or limestone	4	-
Fornace	50°42’N	11°15'E		14	803	Calcic Vertisols		3	-
Terroca	45°28'N	11°19'E		14	803	Calcic Grumic Vertisols		2	-
Castronovo	37°40'N	13°36'E	Hot-summer Mediterranean climate (Csa)	17	500	Calcic vertisols	Limestone	2	-
Crete	35°18'N	25°18'E		19	303	Cambisols		5	2

5.2.2 Soil incubation

For each soil column, 2–4 sub-layers (topsoil 0–10 cm, shallow subsoil 30–45 cm, deeper subsoil ≥ 60–70 cm) were chosen for soil incubation. This resulted in 117 samples. These depth intervals were chosen to maximize the variation in terrace burial–age, which we will use to investigate its effect on C dynamics. Three replicate samples of 30 g of 2 mm sieved bulk soils (in total 117 × 3 repeats = 351 samples) were incubated in laboratory over 9 weeks. Optimal conditions for microbe activity were established by keeping temperature (20 ℃) and moisture (60 % of soil water holding capacity) constant throughout the experiment, in order to derive specific potential maximum heterotrophic respiration (SPR) (Paul et al., 2001). A technical description of soil incubation experiment has been given in Chapter 2.2.4.

5.2.3 Soil physico–chemical properties

Using 2–mm sieved bulk soils (same samples as incubation experiments), key soil physico–chemical properties were measured: soil texture, pH_{CaCl2}, elemental composition of the soil solid phase (Fe, Mn, Al, K, Ca, Na, Mg), total reserve in bases (TRB), chemical alteration index (CIA), pyrophosphate–extractable oxides (Fe_p, Al_p and Mn_p), oxalate–extractable oxides (Fe_o, Al_o and Mn_o) and DCB–extractable oxides (Fe_d, Al_d and Mn_d).

For Ingram, Martelberg, Belloca, Fornace, Terroca and Gueswick sites, soil bulk density (BD) was measured from an undisturbed soil sample taken from a Kubiena tin (10 cm × 10 cm × 5 cm) and dried at 105℃ before weighting. BD values for deep soil layers (>100 cm) were approximated using the 90–100 cm observations considering (i) soil horizons > 100 cm are difficult to retrieve the intact soil columns and (ii) the variation of soil BD below 100 cm is quite small. The weight and volume of gravels (> 2 mm, if > 3% in weight) were also determined to derive the BD for the fine earth (BD_{fine}). SOC concentration for each horizon (5 cm or 10 cm depth interval) was measured along with soil profile until reach the bedrock.

For Charlton, Crete and Castronovo sites, BD was indirectly estimated from the measured soil properties using pedotransfer functions proposed by Souza et al. (2016)

$$BD = a \times SOC + b \times Clay + c \times Silt + d \quad (5\text{–}1)$$

Where SOC is the soil organic carbon content (%), *Clay* is the clay content (%), *Silt* is the clay content (%). Coefficient parameters of *a*, *b*, *c* and *d* were estimated by fitting the equation (5–1) using the measured BD data of Martelberg site (R^2 = 0.61), because the soil properties of these sites are more close to Martelberg site (e.g., hiher pH at 6–7, lower SOC content). Similarly, for Homlong, Skotet, Smoge and Blick sites, BD was estimated by calibrating equation 5–1 with the measured BD data of Ingram site (R^2 = 0.70), where the soil properties were close to these sites (e.g., lower pH at 3–5, higher SOC content).

SOC density for each soil horizon was estimated using the equation (5–2):

$$\text{SOC density} = \frac{SOC}{100} \times BD_{fine} \quad (5\text{–}2)$$

Where SOC density is in kg C m^{-2} cm^{-1}, *SOC* is in %, BD_{fine} is the bulk density for the fine earth (kg m^{-3}). SOC stock of each soil horizon was calculated as SOC density multiplying the thickness of horizon. We applied soil infrared spectroscopy technique to reduce the cost on determining above soil properties (e.g., pH, CN, texture, mineral oxides etc.). The implementation of soil infrared spectroscopy technique was described in detail in Chapter 4.2.

5.2.4 SOC fractionation

40 g of 5 mm sieved air–dried soils was fractionated in duplicate to obtain SOC fractions (same samples as incubation experiments). Following the fractionation scheme proposed by Six et al. (2002, 1998) and simplified by

Doetterl et al. (2015a, b), total SOC was fractionated into coarse particulate organic carbon (cPOM, > 250 µm), microaggregate–associated SOC (micro–agg, 250–53 µm), and non–aggregated silt & clay associated SOC (s+c, < 53 µm). A detailed description of SOC fractionation experiment was given in Chapter 3.2.3.

5.2.5 Soil burial age

Optically stimulated luminescence (OSL) has been widely used to date the last time sediments is exposed to light (Brown, et al., 2021). As sediment (e.g., quartz, feldspar minerals) is transported by water, tillage, or wind, it will be exposed to sunlight and zeroed of any previous luminescence signal. Once these sediments (i.e., quartz, feldspar) are deposited and subsequently buried, they absorb ionizing energy and accumulate luminescence signal from the surrounding environment. The amount of absorbed energy per mass of mineral is a function of geologic time (Preusser et al., 2008). In this study, instead of dating sediment, a portable optically stimulated luminescence (pOSL) reader was used to record the bulk OSL signal intensity, which has been widely used as a proxy for relative soil burial age (Muñoz–Salinas et al., 2011). When compared to conventional OSL dating, pOSL is more efficient in terms of time, cost, and labor and can therefore be used for large, untreated samples (Muñoz-Salinas et al., 2011; Porat et al.,2019). The pOSL was recorded at 5 cm or 10 cm intervals throughout all terrace profiles. For control profiles, we did not measure pOSL because most of control soil profiles are too shallow (e.g., only 15 cm in depth for Smoge) to have a reliable pOSL measurement, which requires strict working conditions (e.g., block out the light contamination). A detailed description of the pOSL sample collection and OSL signal measurement are given in Chapter 3.2.5.

5.2.6 Statistical analysis

Statistical analysis was performed using R 4.1.1 (R Development Core Team, http://www.R–project.org). Principle component analysis (PCA) was

used to examine how climate and soil geochemical properties differ between sampling sites. The model fitting function of “stat_fit_glance” from the “ggpmisc” R package was used to derive the relationship between SOC variables (SPR, SOC density), climate and soil properties. To identify the variables (climate, soil properties) that have the greatest predictive power for SOC response variables (SPR, SOC density), we used stepwise regression. The best regression model was selected via forward–backward stepwise regression with the ‘olsrr’ package in R, which defines model fitness as low Akaike information criterion (AIC) and high coefficient of determination (R^2) values ($P < 0.05$). The relative importance of the variables determined by stepwise regression model for predicting SOC response variables was calculated as the standardized regression coefficient. Overall, the dataset for regression analysis consisted of 22 independent variables and 117 observations. To reduce the data dimensionality, we performed rotated principal component analysis (rPCA) (no. of considered components = 15) before conducting the stepwise regression analysis. The rotated components (RCs) were used as new input variables to regression models, with a selection criterion being eigenvalue >1 and explained proportion of variance > 5% (Gareth et al., 2013; Jolliffe, 1995). We then named all RCs according to the loadings of original variables. A threshold of $r > 0.5$ was used to decide whether an independent variable loaded into RC was used for mechanistic interpretation of the RC or not (Bukombe et al., 2021). To further explore the importance of soil burial age in explaining terrace SOC density and SPR, we performed partial correlation analysis while controlling for RC represented by soil burial age (pOSL) (i.e., Table 5–2). Partial correlation analysis is a widely applied statistical tool to isolate the relationship between two variables from the confounding effects of other correlated variables (Jukić and Denić–Jukić, 2015)

5.3 Results

5.3.1 Higher SOC stock of terracing landforms relative to non–terracing landforms

SOC stocks of terrace profiles down to the bedrock (max. 190 cm) were compared with the non–terracing profiles (Table 5–2). On average, terracing landforms had a higher SOC stock (89 ± 122 %) than the non–terracing landforms. Positive effects of terracing on SOC stock were observed, except for Crete site, where terracing landforms showed a slightly lower SOC stock than the non–terracing landforms (-3%). When compared to the reference papers (detailed in 5.2.1), terracing landforms of Blick and Martelberg sites stored 10–64% more SOC than the non–terracing landforms. The positive effect of terracing on SOC stock was more pronounced in Smoge (Dfc climate, Podzols), Ingram (Cfb climate, Umbrisols) than Crete site (Csa climate, Cambisols).

Table 5–2 SOC stock of terracing profiles compared to the non–terracing profiles

Sites code	Compared to non-terracing profiles (%)	Compared to ref. papers (%)[1]
Smoge	302	-
Ingram	59	-
Blick	53	10
Martelberg	33	64
Crete	-3	-

[1] detailed in 5.2.1.

5.3.2 Description of SOC variables of terraced soils along climate and soil geochemistry gradients

PCA showed that climate significantly impacted soil properties (Figure 5–2). Soil properties of continental subarctic climate regions (Dfc, e.g., Skotet, Homlong, Smoge) were distinct from the humid subtropical climate (Cfa, e.g., Terroca, Fornace etc.) and hot–summer Mediterranean climate (Csa,

e.g., Castronovo, Crete) regions. Specifically, contents of pyrophosphate–extractable oxides (Fe_p, Al_p, Mn_p) and oxalate–extractable oxides (Fe_o, Al_o) decreased from Dfc to Csa climate regions, whereas the opposite tendency was observed for DCB–extractable oxides (Fe_d, Al_d, Mn_d), pH, TRB, and clay content. The climate (MAT, MAP), pH, soil texture (clay, sand) and Fe_p provided the greatest contribution to Dim 1 (r > 0.5). Dim 2, which explained 16.8% of the variance, was largely driven by the Fe_o and Mn_d (Figure 5–2).

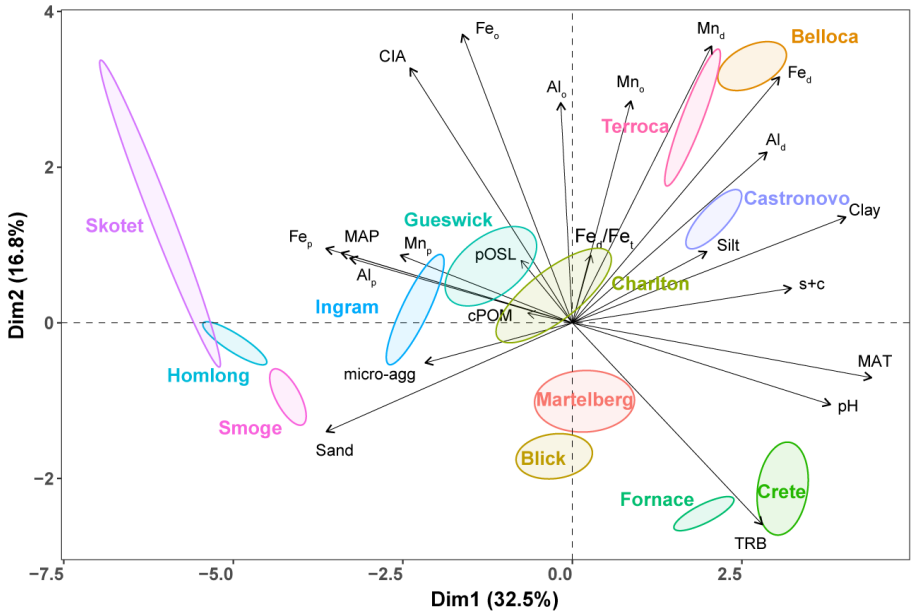

Figure 5–2 Principal component analysis (PCA) showing the distribution of sites along with climate gradient. Percentage of variance explained by each PC is shown in parentheses. MAT = annual mean temperature (℃); MAP = annual mean precipitation (mm); TRB = total reserve in bases; CIA= chemical alteration index; pOSL = total photon counts measured by pOSL reader. Fe_o, Al_o, Mn_o = oxalate–extractable oxides; Fe_d, Al_d, Mn_d = DCB–extractable oxides; Fe_p, Al_p and Mn_p = pyrophosphate–extractable oxides; cPOM = coarse particulate SOC; micro–agg = microaggregate–associated SOC; s+c= silt & clay associated SOC. Climate types are based on Köppen climate classification.

Along with the climate gradient, SOC density generally increased from Csa to Dfc climate regions (Figure 5–3a), with Dfc regions stored ~five times more SOC than Csa regions. For soil specific potential respiration (SPR), no clear tendency along with the climate gradient could be observed (Figure 5–3b). While SPR was more associated with the soil type, e.g., Podzols with high SOC density generally respired CO_2 at lower rates per unit C than Luvisols and Cambisols soils with low SOC density (Table 5–1; Figure 5–3b).

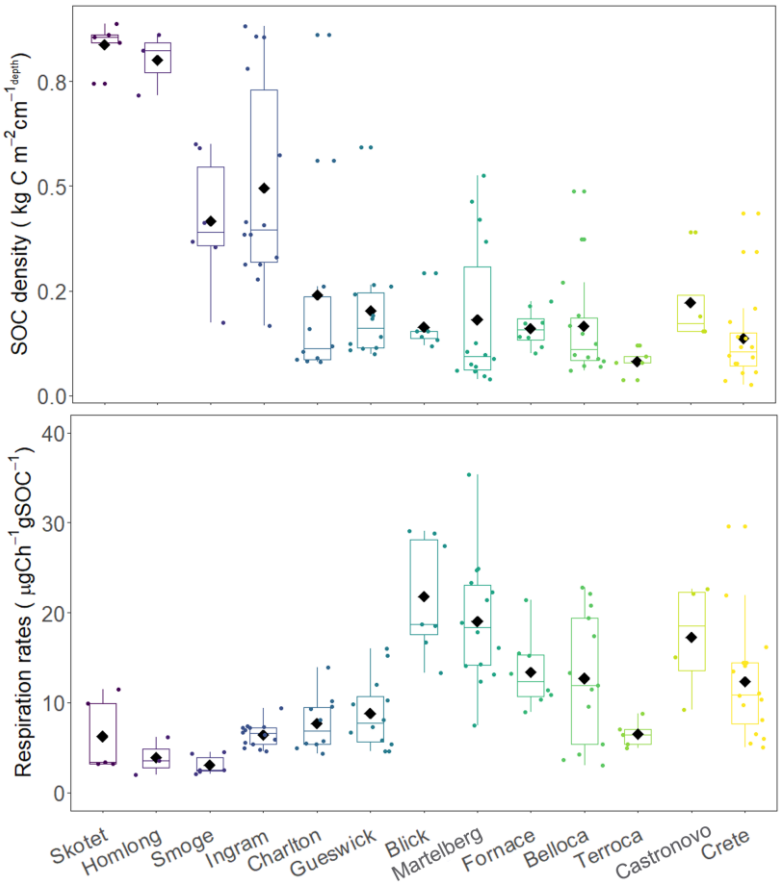

Figure 5–3 (a) SOC density and **(b)** soil specific potential respiration (SPR) along with climate gradient. Dfc = continental subarctic climate, Cfb = marine west coast climate, Cfa = humid subtropical climate, Csa = hot–summer Mediterranean climate (Köppen climate classification).

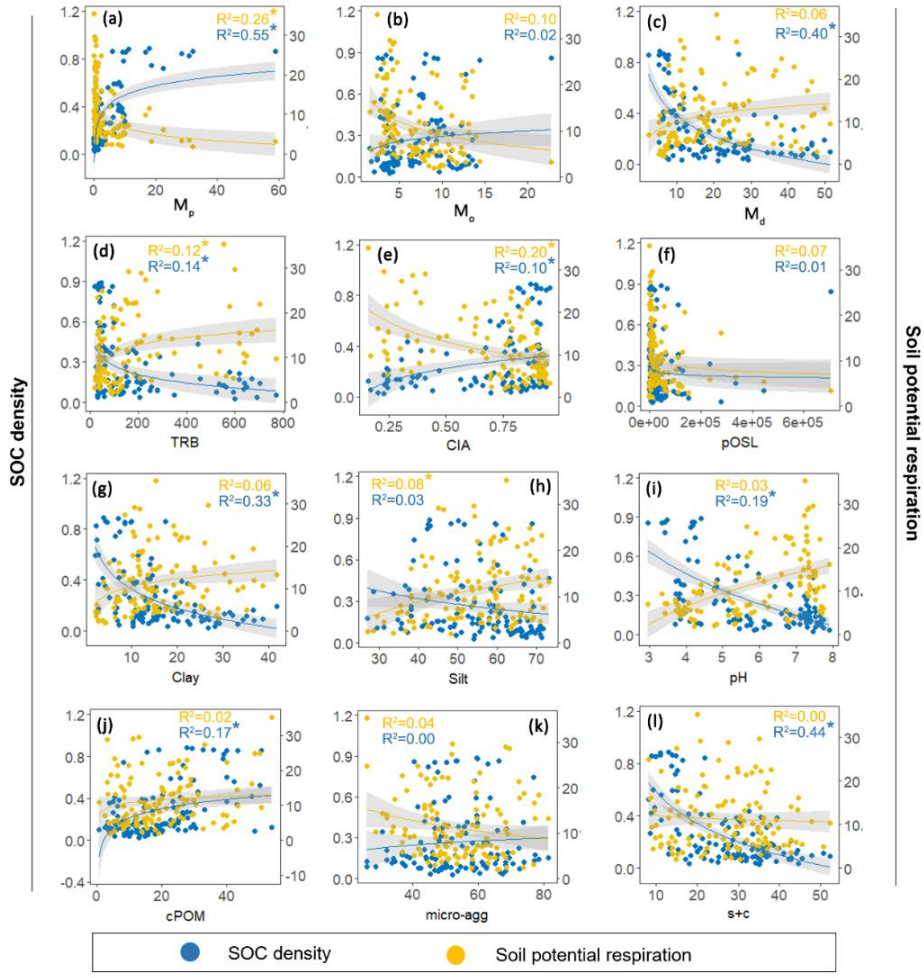

Figure 5–4 Relationships between SOC density (right y axis), soil potential respiration (left y axis) and soil physico–chemical properties. * = significant correlation at the 0.01 level (n = 117). M_d = sum of DCB–extractable oxides; M_p = sum of pyrophosphate–extractable oxides; M_o = = sum of oxalate–extractable oxides; cPOM = coarse particulate organic carbon; micro–agg = microaggregate–associated SOC; s+c= silt & clay associated SOC. TRB = total reserve in bases; CIA= chemical alteration index; pOSL = total photon counts measured by pOSL reader.

Our results showed that the soil properties played an important role in determining terrace SOC density and SPR. Specifically, increasing in M_p, weathering degree (TRB, CIA) and cPOM raised the SOC density (Figure 5–4). Conversely, M_d, clay content and pH were negatively correlated with SOC density (P < 0.01). Moreover, increasing in M_p, silt contents and weathering degree (TRB, CIA) resulted in a decrease in SPR (P < 0.01).

5.3.3 Predicting SOC density and SPR

5.3.3.1 Mechanistic interpretation of rotated principal components (RCs)

rPCA showed that eight retained RCs (eigenvalue >1; explained variance > 5%) together explained 79% of variance (Table 5–3). RC1 (eigenvalue 3.1, explaining 15% of variance) represents the mineral weathering degree, in which CIA had strong positive loadings (r > 0.94), while TRB and pH had strong negative loadings (r < –0.70). RC2 (eigenvalue 2.8, explaining 13% of variance) represents the DCB extractable Fe, Mn oxides, with loadings > 0.89. RC3 (eigenvalue 2.4, explaining 11% of variance) represents the pyrophosphate–extractable Fe, Al oxides and oxalate–extractable Al oxides (r > 0.71). RC4 (eigenvalue 2.1, explaining 10% of variance) represents the soil texture (silt and sand). Proportion variance explained by the remaining RCs ranged from 8% to 5%, representing the climate (RC5), silt & clay associated SOC (RC6), aggregation (RC7) and soil burial age (RC8), respectively.

Table 5–3 (*next page*). Eight rotated principal components (RCs) retained with a threshold of eigenvalues > 1 and proportional variance > 5% (n = 117). The upper part of the table shows eigenvalues, individual and cumulative variance and mechanistic interpretation of specific RCs. Variable loadings of Pearson's r > 0.5 and < −0.5 are highlighted with bold font type.

Rotated component		**RC1**	**RC2**	**RC3**	**RC4**	**RC5**	**RC6**	**RC7**	**RC8**
Eigenvalue		3.1	2.8	2.4	2.1	1.8	1.7	1.7	1.1
Proportion variance explained (%)		15	13	11	10	8	8	8	5
Cumulative variance (%)		15	28	39	49	57	66	74	79
Mechanistic Interpretation		weathering degree	DCB extractable Fe, Mn	pyro-extrac. Fe, Al; oxa-extrac. Al	soil texture	climate	silt & clay associated SOC	aggre-gation	soil burial age
Variables	Units								
pOSL	-	0.08	-0.01	0.09	-0.11	0.00	0.09	-0.04	**0.98**
MAT	℃	-0.47	0.26	-0.23	0.25	**-0.65**	0.31	0.09	-0.03
MAP	ppm	0.19	-0.07	0.36	-0.12	**0.84**	-0.20	-0.08	-0.01
pH	-	**-0.70**	0.24	-0.17	0.09	-0.16	0.18	0.00	-0.07
TRB	cmol/kg	**-0.94**	-0.01	-0.04	0.05	-0.18	0.16	0.05	0.00
Clay	%	-0.29	0.46	0.01	0.22	-0.38	0.41	0.14	0.04
Silt	%	-0.01	0.08	-0.04	**0.98**	-0.04	-0.04	0.08	-0.09
Sand	%	0.17	-0.31	0.03	**-0.82**	0.24	-0.20	-0.13	0.04
Al_p	mg/kg	0.20	-0.24	**0.86**	-0.15	0.25	-0.10	0.05	0.08
Al_o	mg/kg	-0.01	0.30	**0.89**	0.11	0.09	0.12	0.02	-0.03
Al_d	mg/kg	-0.01	0.36	-0.04	0.40	-0.03	0.18	0.02	-0.07
Fe_p	mg/kg	0.27	-0.21	**0.71**	-0.12	0.17	-0.24	0.09	0.22
Fe_o	mg/kg	0.38	0.38	0.30	-0.11	0.36	0.05	-0.12	0.18
Fe_d	mg/kg	-0.01	**0.89**	-0.05	0.14	-0.11	0.18	0.09	-0.02
Mn_p	mg/kg	0.30	-0.13	0.07	-0.08	0.09	-0.21	0.23	-0.02
Mn_o	mg/kg	0.19	0.31	-0.03	0.01	-0.12	0.08	-0.05	0.05
Mn_d	mg/kg	0.07	**0.94**	0.01	0.17	-0.05	0.01	-0.02	-0.01
cPOM	%	0.03	-0.03	0.07	0.08	0.04	-0.36	**0.90**	-0.08
micro-agg	%	0.13	-0.11	-0.02	-0.13	0.18	-0.43	**-0.85**	-0.03
s+c	%	-0.18	0.15	-0.06	0.06	-0.25	**0.89**	-0.05	0.12
CIA	-	**0.94**	0.15	0.14	-0.04	0.07	0.01	-0.03	0.09

Table 5–4 Results of three stepwise regression models (topsoil only, subsoil only and all data) using RC scores to predict terrace SOC density and potential soil respiration (SPR), including standardized coefficients and model performance indicators. Blank cells indicate non–significant predictors ($P < 0.05$) that were not selected by the stepwise regression model.

		R^2	(RC1) weathering degree	(RC2) DCB extractable Fe, Mn	(RC3) pyrophosphate, oxalate-extractable Al, Fe	(RC4) soil texture	(RC5) climate	(RC6) silt&clay associated SOC	(RC7) aggregation	(RC8) soil burial age
SOC density	All data	0.78			0.54	-0.22	-0.45	-0.74	0.31	
	Topsoil	0.81			1.23		-1.63	-1.34		
	Subsoil	0.81		-0.30	0.77					
SPR	All data	0.35	-0.77	0.51	-0.21			-.091		
	Topsoil	0.29		0.54						
	Subsoil	0.24	-0.32							-0.24

5.3.3.2 Relative importance of RCs for predicting SOC density and SPR

Using the rotated components identified in 3.3.1 as predictor variables (Table 5–3), significant regression models ($P < 0.05$) were developed for predicting SOC density and SPR (Table 5–4). For SOC density using all data, RC6 (silt & clay associated SOC), RC3 (pyrophosphate–extractable Fe, Al and oxalate–extractable Al) and RC5 (climate) were the most important predictors, followed by RC4 (soil texture) and RC7 (aggregation). When using topsoil only, RC4 (soil texture) was excluded from the SOC density model based on all data. For subsoil, only RC2 (DCB extractable Fe, Mn) and RC3 (pyrophosphate–extractable Fe, Al and oxalate–extractable Al) were important.

For SPR using all data, RC1 (weathering degree), RC2 (DCB extractable Fe, Mn), RC3 (pyrophosphate–extractable Fe, Al and oxalate–extractable Al) and RC6 (silt & clay associated SOC) were the most important predictors. While for topsoil, only RC2 (DCB extractable Fe, Mn) was selected as a predictor for SPR. Interestingly, only RC8 (soil burial age) was selected for predicting SPR of subsoil.

The role of terrace soil burial age in SOC density and SPR of subsoil was further explored by the partial correlation analysis (Figure 5–5). Significant relationships between SOC density and RCs ($P < 0.01$) were not influenced by controlling for soil burial age (RC8). However, controlling for soil burial age (RC8) significantly decreased the correlations between SPR and RC1 (weathering degree), RC4 (soil texture), RC6 (silt & clay associated SOC) (P value changed from 0.01 to 0.05)

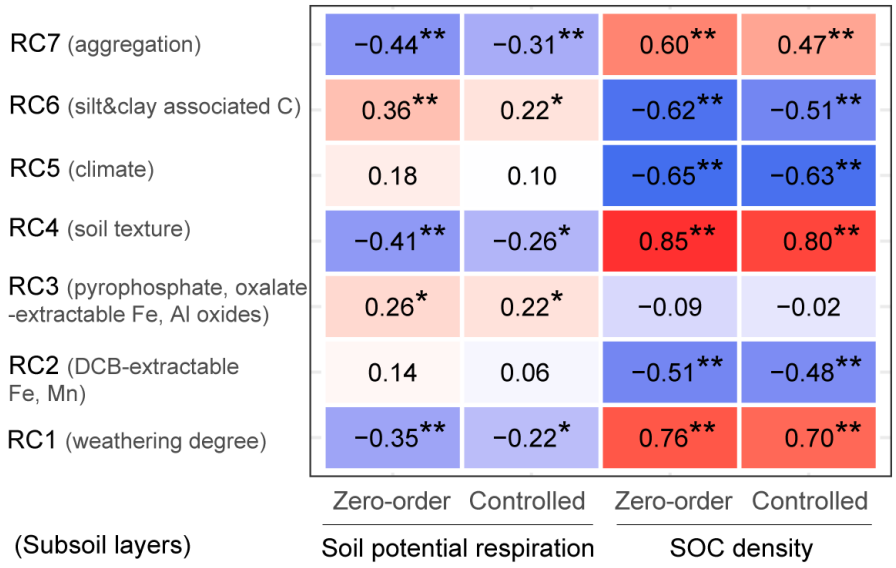

Figure 5–5 Zero–order and partial correlation between subsoil SOC variables (SOC density, SPR) and retained RCs, controlling for soil burial age (RC8). The colors and numbers indicate the strength (the intensity of the color) and sign (blue and red colors indicate negative and positive correlations, respectively) of correlation. No change in color between controlled variable and zero–order = no dependency; decrease/increase of color intensity = loss/gain of correlation. *= $P < 0.05$; ** = $P < 0.01$.

5.4 Discussion

5.4.1 Controls on terrace SOC stocks

As summarized in Table 1–1 (Chapter 1), there seems to be consensus that in most cases, terracing has a positive effect on SOC stock. The terracing–landforms in this study on average had a higher SOC stock (89 ± 122 %), relative to the non–terracing landforms (Table 5–2). The positive effect of terracing on SOC storage has been attributed to (Brown et al., 2021) (i) terracing protects soil from erosion thus reducing the SOC loss (Nyssen et al., 2009); (ii) terracing increases the SOC input into soils by creating fertile

soils (soil water, nutrients) that supports plant growth (Wei et al., 2016); (iii) soil deposition and burial at the fill section of terraces results in a accumulation of SOC contents (De Blécourt et al., 2014).

Previous studies have shown that climate and terrace age are the dominate controls on SOC stock of terrace landforms (Chen et al., 2020a; De Blécourt et al., 2014). Using the terraced soils collected from a large climatic and soil geochemical range of Europe, our results show that the strongest predictors for terracing SOC stocks are the soil reactive mineral phases (RC3), climate (RC5) and mineral related SOC stabilization mechanisms (aggregation, silt & clay associated SOC) (Table 5–4). Consistent with a meta–analysis (Chen et al., 2020a), current study shows that the positive effect of terracing on SOC stock is more pronounced in areas with lower temperature (e.g., Smoge, Ingram and Blick sites). While in a hot–summer Mediterranean climate (i.e., Crete), SOC stock does not benefit from terracing (Table 5–2). Moreover, a clear trend towards increasing SOC stocks in the lower temperature regions was observed (Figure 5–3a). This is particularly relevant to topsoil, where climate is the most powerful predictor of SOC density (Table 5–4). Previous studies suggest that the terracing driven SOC sequestration is significantly age–related: very young terraces (< 5 years) tend to be a C source (Gao et al., 2020) while the old terraces (5–30 years) drive a C sink for the atmospheric C pool (De Blécourt et al., 2014). In the current study, terrace soil burial age (RC8) was not selected as predictor for SOC density. Furthermore, no significant relationship between pOSL and SOC density could be found (Figure 5–4f). Preliminary OSL dating results of TerrACE project (not published; led by Lang et al.) indicate that terraces in current study are at least 190 years old. This is much older than the terraces investigated by previous studies (< 44 years; Table 1–1). Thus, when the terraces become very old (> ~50 years), the effect of terrace age on SOC stock may not be apparent. The very old terrace systems are likely to suffer from the terrace failures, e.g., collapse of terrace wall, which in the long run can accelerate the formation of rills, gullies, piping and landslides on

marginal slopes. This will lead to a partial loss of terraces' function in retain SOC.

However, our results suggest that the soil pedogenic oxyhydroxides, particularly the pyrophosphate–oxalate–extractable Fe and Al oxides (RC3), are the most important predictor of SOC density for all soil layers (Table 5–4). This is also supported by the significant relationship between M_p and SOC density (P < 0. 01, R^2 = 0.55; Figure 5–4a). The pyrophosphate–oxalate–extractable oxides consist mainly of organically complexed metals, amorphous secondary and poorly crystalline oxides (Bascomb, 1968; Dahlgren, 1994). These mineral phases provide the most reactive mineral surfaces in soils, which can absorb organic acids and form organo–mineral complexes (Blume et al., 2016; Masiello et al., 2004). Studies have shown that the reactive mineral phases can promote the formation of soil aggregates, thus providing a SOC aggregation protection mechanism in soils of grassland or eroding landscapes (Berhe et al., 2012; Six et al., 2002). Our results suggest that this mechanism is also relevant to the terraced soils, as both RC3 (pyrophosphate–oxalate–extractable Fe and Al oxides) and RC7 (aggregation) are selected as the significant predictors for SOC density (Table 5–4).

5.4.2 Controls on soil heterotrophic respiration of terraces

Climate is generally considered as a primary or secondary control over SOC dynamics in non–terracing soils (Carvalhais et al., 2014; Doetterl et al., 2015a; Luo et al., 2017). Our results suggest that in terrace systems, SOC dynamics (SPR) are primarily controlled by soil physico–chemical properties rather than climate. Specifically, no clear trend in SPR with climate gradient could be found (Figure 5–3b). While across soil depth, mineral weathering degree (RC1) was the most important variable to explain SPR, followed by DCB extractable Fe, Mn oxides (RC2), pyrophosphate–oxalate–extractable Fe and Al oxides (RC3) (Table 5–4). Additionally, correlation analysis showed that the SPR was significantly related to weathering indicators (TRB,

CIA) and pyrophosphate–extractable oxides (M_p) ($P < 0.01$). These results suggest that the soil mineral weathering and pedogenic oxyhydroxides play crucial role in regulating SOC dynamics of terrace systems.

Interestingly, we found that in addition to mineral weathering degree (RC1), soil burial age (RC8) is also a key factor in explaining SPR of subsoils (Table 5–4). Partial correlation analysis further revealed that removing the effect of soil burial age (RC8) significantly altered the correlations between SPR and RC1 (weathering degree), RC4 (soil texture), RC6 (silt & clay associated SOC) (Figure 5–5). These results indicate that for terraced subsoils, soil burial age is a key factor controlling soil respiration, most likely through driving mineral weathering. A case study on Ingram terraces (Chapter 3) suggests that these old subsoil horizons originate from the topsoil previously buried due to terracing (Zhao et al., 2021a). For younger buried soils (low pOSL count), mineral weathering continues to provide reactive mineral surfaces to stabilize OC, e.g., via SOC mineral protection or aggregation (Blume et al., 2016). As a result, C availability to decomposers decreases with the increase of terrace soil burial age (Zhao et al., 2021a). However, once the buried soils become very old, their ability to provide reactive mineral surfaces could be diminished. This is because as the soil ages and weathers, highly reactive minerals, i.e., poorly crystalline oxides, continue to be transformed into the well crystalline oxides, which significantly reduce the mineral specific surface area for OC absorption (Lair et al., 2009; Thompson et al., 2006). Therefore, the SOC cycling in buried layers of terraced soils is age–dependent. As terrace age, the capacity of buried soils to stabilize SOC may be diminished due to the loss of reactive mineral surfaces as continuing of weathering. When considering that half of the additional SOC stock due to terracing was buried in the subsoil horizons (Supplementary discussion D1), findings of this study demonstrate the need to consider the specific SOC stabilization mechanisms to fully understand future C cycling of terrace systems in the light of climate, land use and land management change.

5.5 Conclusion

In this study, we evaluated the relative importance of climate, terrace soil burial age, soil mineral weathering and pedogenic oxyhydroxides in controlling SOC density and soil potential heterotrophic respiration (SPR) of agricultural terraces. Results showed that for the topsoil layers (0–10 cm), climate was the most important factor to explain the variability of SOC density, while for subsoil layers (> 10 cm), the strongest predictor for SOC density was the reactive mineral oxides (organically complexed metals, amorphous secondary and poorly crystalline oxides). Although climate is generally considered as a primary or secondary control on SPR in non–terracing soils, our results suggest that across soil depth, the primary controls on SPR in terracing systems are the soil mineral weathering and pedogenic oxyhydroxides. For buried soil horizons, terrace soil age is a key factor regulating soil heterotrophic respiration, through driving mineral weathering and thus determining the availability of reactive mineral surfaces that stabilize SOC. We suggest that the studies on C dynamics of terrace systems and their exchange with the atmosphere C pool should pay particular attention to the older terraces developed on the soils containing less pedogenic oxyhydroxides.

Acknowledgements

I would like to thank the members of TerrACE project team, who helped collect the soil samples. A special thank goes to Benjamin Bukombe from Augsburg University for his support on rPCA analysis.

Chapter 6

Conclusions and perspectives

The objective of this thesis was to improve our understanding of SOC dynamics of colluvial soils in the context of climate change. For this, two majors anthropogenic colluvial soil settings were studied: (i) re–deposited soils from agricultural erosion and (ii) terraced soils from human–made agricultural terraces. SOC stability and its controlling factors were assessed at the soil profile and regional scales. The main findings, limitations and perspectives will be summarised, and the answers to the research questions posted in Chapter 1 will be given.

6.1 General conclusions

Main findings

The thesis started by comparing the dominant control on SOC stability between the colluvial soil and non–eroding, stable soils (Chapter 2). The main finding was that for stable soils, climate, cultivation history and weathering degree significantly affected the soil potential respiration. In contrast, for colluvial soils, the most influential factor was the deposition rate and this was independent of climate zone. Deposition rates also indirectly affected soil potential respiration by interacting with the degree of weathering of deposited soil. This changed the mineral matrix of colluvial soil settings whereby may enhance soil mineral related SOC stabilization mechanisms. This research highlights the need to consider both the direct effect of deposition rate as well as its indirect effects (via influence on weathering status and soil mineral matrix) on colluvial SOC stabilization when evaluating the fate of eroded SOC.

Conclusions and perspectives

The remaining part of this thesis focused on the colluvial SOC dynamics in terrace systems. In the Chapter 3, the factors controlling SOC stabilization mechanisms and temperature sensitivity to decomposition (Q_{10}) in terraced soils were investigated. The results showed that the soil burial due to terracing provided a significant mechanism for stabilizing SOC. This is mainly because the buried soils settings have a less favourable environmental condition for microbial decomposers (e.g., lack of oxygen and water saturation), thus constraining in situ mineralization rates of SOC. This study also provided empirical evidence for the drivers and basic patterns of the Q_{10} in agricultural terraces. We found that the patterns of Q_{10} were regulated by terrace soil burial age: at relatively younger ages of soil burial, the reduction in substrate availability due to the increased SOC mineral protection with aging attenuates the intrinsic Q_{10} of SOC decomposition, whereas at the older terrace soil burial ages, higher C:N ratios (poor C quality) result in an increased Q_{10} in deep horizons. It is expected that the ongoing evolution of SOC fractions and the associated changes in soil C:N ratio due to terrace aging will slowly but steadily destabilize buried topsoil SOC.

As terrace landscapes can be found in all climate zones, different soil geochemical background, and are characterized by a wide range of terrace ages, a large number of samples has to be analysed in order to reliably assess the factors controlling SOC stock and dynamics in terrace systems. Therefore, in the Chapter 4, the infrared spectroscopy technique was applied to predict the soil properties relevant to SOC biogeochemical cycle, including soil oxyhydroxides, base cations, soil texture and SOC fractions. In contrast to previous studies, we considered the above-mentioned soil properties as the composition data: the fractional components in compositional data are interrelated and their sum should be unity (e.g., percentage clay + sand + silt = 100%), and these features are represented in our spectra–soil models. The results demonstrate that soil infrared spectroscopy, combined with the compositional data analysis is a powerful technique that enables efficient

and reliable ‘large–scale’ assessment of soil properties relevant to SOC biogeochemical cycles.

Chapter 5 focused on the understanding of SOC dynamics in terrace systems from a large range of climatic and geochemical conditions. The basis of this study was an intensive filed sampling across Europe and a laboratory analysis combined with the outputs of Chapter 4. The obtained dataset allowed to gain insights into the mechanisms controlling terracing SOC stock and soil potential respiration. Results showed that the most important factor explaining the observed variability in terraced topsoil layers SOC stocks, was climate while for subsoil layers (> 10 cm) it was the reactive mineral oxides. We found that terrace soil burial age is a key factor in controlling soil heterotrophic respiration of subsoils, likely through driving mineral weathering and thus determining the availability of reactive mineral surfaces that stabilize SOC.

This thesis confirmed that the terracing has created an additional SOC stock than non-terracing landforms, due to the accumulation of redistributed soil material on top of the original soil surface combined with the preservation of SOC in the burial soil settings. Considering that agricultural terraces are volumetrically the largest and most common landforms that humans have ever produced (Brown et al., 2021), dynamics of SOC storage in terraced landforms will have important implications for regional C cycle. Overall, terrace age was identified as the key factor controlling for not only SOC stability but also its response to future warming. Ongoing evolution of soil geochemical properties and the associated shift in SOC pool composition as terrace aging, coupled with the massive terrace abandonment (e.g., wall collapse) and climate warming, may slowly destabilize the current terracing SOC stock over time. To mitigate this risk of C emission and maintain the role of terraces in providing ecosystem services (e.g., erosion control), sustainable practice of terrace maintenance needs to be designed.

6.2 Answers to the research questions

RQ1: *What are the dominant controls on colluvial SOC stability under different climate and mineral weathering settings and to what extent do these controlling factors differ from those in stable, non–eroding soils?*

The results suggest that the dominant controls on SOC stability for colluvial soils are different from those for stable, non–eroding soils: for colluvial soils the most important independent control on SOC stability is the soil deposition rate, while for stable soils it is jointly controlled by climate, weathering degree and cultivation history.

RQ2: *How can SOC be stabilized in terraced landforms?*

Our analysis identified two major mechanisms for SOC stabilization in terraced soils: (i) The burial of former topsoil due to terracing provides a SOC stabilization mechanism; (ii) there is a clear shift in SOC fraction composition from particulate organic C towards mineral–protected C with increasing terrace soil burial age. This clear shift to more processed recalcitrant SOC with soil burial age contributes to SOC stability in terraced soils.

RQ3: *What are the main controls on SOC temperature sensitivity (Q_{10} in terraced soils?*

We found that both the C:N ratio and SOC mineral protection regulate Q_{10}. However, which mechanism predominantly controls Q_{10} depends on the age of the buried terrace soils. At relatively younger ages of soil burial, the reduction in substrate availability due to the increased SOC mineral protection with aging attenuates the intrinsic Q_{10} of SOC decomposition, whereas at older terrace soil burial ages, higher C:N ratios (poor C quality) result in an increased Q_{10} in deep horizons.

Chapter 6

RQ4: *When using infrared spectroscopy to predict soil properties relevant to SOC biogeochemical cycle, can accounting for the features of compositional data significantly improve model performance?*

Our results suggest that accounting for the features of compositional data provides predictions as accurate as the conventional method, yet adds two significant advantages: (1) it ensures the predicted fractions summing to 100% and (2) it reduces the number of samples with extreme relative prediction error.

RQ5: *does terracing play a positive or negative role in SOC sequestration?*

Using 22 soil profiles (15 terraced versus 7 non–terraced profiles) collected from 5 agricultural terrace landforms, I showed that on average terraced landforms have a higher SOC stock (89 ±122 %), relative to the non–terracing landforms. Together with the synthesis from previous studies (as summarized in Table 1–1), we conclude that in general terracing has a positive effect on SOC stocks.

RQ6: *How do SOC stocks and respiration in terraced soils vary along the climate, soil geochemistry and terrace age gradients and which factors control the observed variation?*

Along with the climate gradient, SOC stock generally increases from the hot–summer Mediterranean climate (Csa) to the continental subarctic climate regions (Dfc). For soil specific potential respiration (SPR), no clear tendency along with the climate gradient could be observed. While the variation of SPR is more related to soil types, e.g., SPR of Podzols is generally lower than Luvisols and Cambisols.

Although climate is considered as a primary or secondary control on SPR in non–terracing soils, this thesis suggested that across soil depth in terraced soils, the primary controls on SPR are weathering degree and pedogenic

oxyhydroxides. For buried soil horizons, terrace soil age is a key factor regulating SPR, through driving mineral weathering.

For topsoil layers (0–10 cm) of terraces, climate is the most important factor predicting variability of SOC stock, while for subsoil layers (> 10 cm), the strongest predictor is the reactive mineral oxides (organically complexed metals, amorphous secondary and poorly crystalline oxides).

6.3 Limitations and perspectives

6.3.1 Re–deposited C in colluvial and alluvial settings

This thesis contributed to a mechanistic understanding of the SOC stability in colluvial soils from agricultural erosion. Both the small–scale controls (e.g., deposition, aggregate breakdown) and the large–scale controls (e.g., climate, geochemistry and the duration of cultivation) were addressed. However, we encourage further investigations under variety of environmental conditions to reduce the uncertainties arising from the relatively small sample size of the current work. (Chapter 2). As with the majority studies on SOC dynamics, all experimental analyses in this thesis were conducted under controlled laboratory conditions in order to vary the factor of interest (e.g., temperature, soil age) while eliminating the interfering factors (e.g., soil heterogeneity). Therefore, analysis of soil properties was based on the air-dried and sieved (2 mm or 5 mm) samples using the standard protocols. Nonetheless, in situ monitoring experiments are encouraged to reveal the full picture of the SOC cycle in colluvial soils. In addition, current studies on colluvial SOC dynamics are explicitly focused on the physico–chemical processes such as selective deposition and mineral weathering, while the further insights should be also gained from a biological perspective. For example, how will the microbial structure and functional potential respond to colluvial settings and what are the implications for colluvial SOC storage at the long–term scale?

As shown in Figure 1–2, most (~77%) of the erosion–mobilized C is redeposited in colluvial (~46%) and alluvial (~31%) settings (Wang et al.,

2017), making both colluvial and alluvial soils as a significant storage for SOC. This thesis focused on the colluvial SOC storage and attention should be also given to the alluvial SOC storage (i.e., floodplains) considering that: (i) floodplains store the largest amount of eroded C (Wang et al., 2017); (ii) floodplains act as a transition zone between the terrestrial and aquatic environments; (iii) when the eroded soil C is entered into aquatic system, the aquatic microbial community and hydrological conditions can significantly enhance the SOC decomposition (Zhao et al., 2021b). Therefore, one further research direction could be to understand the controls and dynamics of the alluvial SOC storage, with a particular focus on formulating the measures to retain erode C in the alluvium and minimize its export to the aquatic systems. This is essential for assessing the role of human–induced erosion in the global C cycle and climate change.

Beyond the C storage, colluvium also reserves the information of burial history, which could be used to reconstruct the chronology of erosion and land use and to historically track the human disturbance of nature. For example, the dating techniques such as radiocarbon and optically stimulated luminescence can be combined with the numerical modelling to construct a chronology for the ancient colluvial soil cores. Obtained information can be linked to the land use history (remote sensing), archaeological or climatic records, supporting the research in ecology, archaeology and paleoclimate science.

6.3.2 SOC dynamics in terraced soils

To estimate the effect of terracing on SOC sequestration, a common approach is to compare the SOC stocks in terraced landforms with a nearby non-terraced landform (reference site). Reliability of approach thus depends on the quality of reference site: on the one hand, reference sites should avoid terracing or anthropogenic disturbance; on the other hand, reference site should have a similar climatic and geochemical background as to the terraced landforms. This is a considerable challenge as terracing practices

are often implemented in the highly agricultural and urbanized areas, where it is difficult to find natural soil profiles around terraced landforms. In this thesis, reference sites were only obtained for 5 out of 15 terrace sites, and therefore large uncertainty still remains in assessing the impact of terracing on SOC stocks.

Understanding the drivers of the temperature sensitivity of SOC decomposition is critical for assessing warming–induced changes in SOC stocks of terraced landscapes and its feedbacks to future climate change. In this thesis, a clear shift in SOC pool composition and SOC quality along with terrace soil burial age are identified as the key mechanisms regulating SOC response to warming. However, the processes leading to this shift could not be explained by the current study. We hypothesise that this shift might be a result of the temporal evolution in soil geochemical and biological properties, such as mineral composition and microbial community structure. This hypothesis needs to be tested in the future studies.

In order to predict how SOC stocks of terraced landscapes will react to future environmental change such as climate warming, developing numeric models is required. The empirically derived understanding of SOC dynamics in terraced soils in this thesis can be used to calibrate one of the SOC models, such as the Introductory Carbon Balance Model (ICBM) or Rothamsted Carbon Model (RothC). For example, the following directions can be proposed: upgrading the current SOC model (e.g., ICBM) to account for the role of soil geochemical and biological processes in SOC turnover. The upgraded SOC model can then be applied to simulate how the terrace age will drive the evolution of soil geochemical and biological properties, thereby influencing SOC dynamics.

I conclude with a perspective on SOC losses under abandonment and poor management. Currently 69% of the world terraces are either under abandonment (49%) or poor management (20%) (Figure 1–4, Chapter 1). However, current knowledge on the effect of terrace abandonment on SOC

dynamics is very limited (Stavi et al., 2019). Progressive failure of terraces may lead to the exposure of former buried SOC storage to be re–connected with the atmosphere C pool, but the involved mechanisms and magnitude are unknow. A comprehensive investigation on the magnitude of SOC loss associated with the terrace abandonment is urgently required.

List of Figures

Figure 1–1 Carbon stocks (Pg C) in the major global reservoirs. Picture was produced by European Space Agency based on data from Global Carbon Project in 2019 (www.globalcarbonproject.org). The contribution of each C reservoir to the global C reservoir is shown in numbers in red.

Figure 1–2 Distribution of erosion mobilized C fluxes in the major reservoirs across terrestrial–aquatic continuum. The arrows and corresponding numbers represent the modelled cumulative lateral C fluxes induced by agricultural soil erosion (Pg C) from the onset of agriculture (6000 BC) to the present day. The contribution of each C reservoir to the eroded C in percentage is shown in numbers in red. Data and figure were modified from Wang et al. (2017).

Figure 1–3 Simple idealized cut and fill terrace landforms. Soil redistribution within the terrace landforms creates the colluvial soils.

Figure 1–4 Analysis of the world terraces status based on 300 publications. Data was adopted from Wei et al. (2016).

Figure 1–5 Flowchart of the outline of the thesis.

Figure 2–1 Principal components analysis (PCA) showing the differences between the sites. (a) PCA biplot. The percentage of variance explained by each PC is shown in parentheses. (b) Visualization of quality of representation of variables in top five dimensions. Cos2 is the quality of representation of the variables in the principal component maps. Abbreviations are listed in Table 2–2.

Figure 2–2 Relationship between deposition rate and soil potential heterotrophic respiration (SPR) based on colluvial soil profiles.

List of Figures

Figure 2–3 Zero–order and partial correlations between SPR and controlling factors. Difference between zero–order and partial correlations indicate the level of dependency of the correlation between a given predictor and the SOC response (see method). Colors and numbers indicate the strength (the intensity of the color) and sign (blue and red colors indicate negative and positive correlations, respectively) of correlation. No change in color between controlled variable and zero–order indicates no dependency; a decrease/increase in color intensity indicates a weaker/stronger correlation. Numbers in bold and italic indicate $P < 0.1$.

Figure 2–4 Zero–order and partial correlations between cPOM/s+c ratio and selected predictor variables. cPOM/s+c was considered as an indicator of C vulnerability to loss. Difference between zero–order and partial correlations indicate the level of dependency of the correlation between a given predictor and the SOC response (see Methods). Colors and numbers indicate the strength (the intensity of the color) and sign (blue and red colors indicate negative and positive correlations, respectively) of correlation. No change in color between controlled variable and zero–order = no dependency; decrease/increase of color intensity = loss/gain of correlation. Numbers in bold and italic means $P < 0.1$.

Figure 2–5 Percent modern carbon (pMC) of bulk soil and SOC fractions for selected colluvial soil profiles. micro–agg = microaggregated SOC; s+c = free silt & clay associated SOC.

Figure 2–6 Ratio of colluvial subsoil to topsoil for key geochemical properties. Size of circle represents the ratio. Circles with a black outer ring mean the ratio > 1.0 and therefore the subsoil has higher values than topsoil. CEC = cation exchangeable capacity; BS = base saturation; Fe_{d-o}= crystalline Fe oxides; M_p = sum of chelated organo–metal complexes Fe, Al and Mn. M_{o-p} = sum of poorly crystalline Fe, Al and Mn oxides

Figure 3–1 Map of (a) studying area (from © Google Maps), (b) sampling site and the (c) excavated terrace trench and sampling positions

List of Figures

Figure 3–2 Photographs of soil profiles in the field, where soil genetic horizons can be diagnosed.

Figure 3–3 Chemical weathering degree indicated by Rb/Sr ratio. Wider ratios indicate a higher degree of chemical weathering, interpreted in this study with the burial of former topsoil (which is generally more weathered than corresponding subsoil).

Figure 3–4 The total photon counts versus soil depth in terrace soils. The two soil burial–age categories were shown with dashed lines (i.e., above 45 cm = young, below 60 cm = old).

Figure 3–5 Depth profile of SOC concentration (%). C=control profiles, P1–P4 are sampled terraces from the trench. The significant difference ($P < 0.05$) in SOC concentration between the terraced and control soil layers can be found below 50 cm layers. No such significant difference at 0–50 cm layers.

Figure 3–6 Ternary plot of SOC fractions in percentage of total SOC. micro–agg = microaggregate associated SOC; cPOM = coarse particulate SOC; s+c = silt & clay associated SOC. Color bar represents the soil depth (cm). Error bars denote one standard deviations of the micro–agg fraction measurements (N = 2).

Figure 3–7 Boxplot of soil potential respiration rates (SPR) and SOC temperature sensitivity (Q_{10}). * the significant differences in SPR or Q_{10} between buried and non–buried soil layers ($P < 0.05$).

Figure 3–8 Relation between relative terrace soil burial–age (total photon counts) and (a) soil potential respiration rates (SPR) / SOC temperature sensitivity to decomposition (Q_{10}), (b) contribution of SOC fraction to total SOC. Error bars denote one standard deviation of SPR measurements (N = 3). Formula: y = log(x). cPOM = coarse particulate SOC; micro–agg =

microaggregate associated SOC; s+c = silt & clay associated SOC. Datapoints are from all terrace profiles. *= $P < 0.05$; **$P < 0.01$.

Figure 3–9 Relationship between SOC temperature sensitivity (Q_{10}) and (a) coarse particulate SOC (cPOM), (b) microaggregate associated SOC (micro–agg) and (c) silt & clay associated SOC (s+c) for relatively younger and older terrace soil horizons (Fig. 3–4), respectively. *= $P < 0.05$; **$P < 0.01$.

Figure 3–10 Boxplots of C:N ratios for bulk soil and SOC fractions along the gradient of terrace soil burial–age (total photon counts). cPOM = coarse particulate SOC; micro–agg = microaggregate associated SOC and s+c = silt and clay associated SOC. Significant differences in C:N ratios between soil age gradients were indicated by different lowercase letters ($P < 0.05$).

Figure 4–1 Spatial distribution of sampling sites within (a) European agricultural terrace and lynchet landforms and (b) all kinds of garden lawns sampled in the CurieuzeNeuzen citizen science project across the region of Flanders, Belgium. MAT = mean annual temperature (℃) (Fig. 4–1a).

Figure 4–2 Ternary plot of SOC fractions in percentage of total SOC for terrace soils (a), soil texture triangle based on the USDA textural soil classification for (b) terrace soil and (c) garden soil.

Figure 4–3 Comparison of model performance between three log–ratio transformation methods. For each soil parameter and model performance indicator, the boxplot shows the mean (dot), median (line), interquartile and range of N = 100 separate model trials (see 5.2.6). *alr* = additive log–ratio; *clr* = centered log–ratio; *ilr* = isometric log–ratio. R^2, coefficient of determination; RMSE, root mean square error; RPD, ratio of performance to deviation; RPIQ, ratio of performance to interquartile range. Blue letters indicate significant differences in mean values (a > b > c) of model performance parameters between log–ratio transformation methods ($P < 0.05$).

List of Figures

Figure 4–4 Distribution of the sums for predicted fractions derived with conventional method. The plots were based on 504 predictions for terrace soils and 4085 predictions for garden soils.

Figure 4–5 Comparison of the prediction error (y–axis) based on the conventional method and log–ratio transformation methods. The prediction error was calculated by Eq. (4) using the data from 100 model runs after randomly splitting the calibration and validation dataset each time. Samples with extreme prediction error (see Eq. 4) were indicated by red dot. The percentage (‰) of samples with extreme prediction error (*pEXE*, red dots) was given as the numbers above the bar.

Figure 4–6 Modelled versus measured soil properties expressed as percentage to total mass. Predicted values are the mean ± SD based on 100 replicate model runs after randomly splitting the calibration and validation dataset each time. Results were based on log–ratio transformation method that gave the best model performance. R^2, coefficient of determination; RMSE, root mean square error; RPD, ratio of performance to deviation; RPIQ, ratio of performance to interquartile range. Solid line is the 1:1 line.

Figure 5–1 (a) Distribution of study sites and (b) photo of terrace landforms, field excavation. MAT **=** annual mean temperature (℃).

Figure 5–2 Principal component analysis (PCA) showing the distribution of site along with climate gradient. Percentage of variance explained by each PC is shown in parentheses. MAT **=** annual mean temperature (℃); MAP = annual mean precipitation (mm); TRB = total reserve in bases; CIA= chemical alteration index; pOSL = total photon counts measured by pOSL reader. Fe_o, Al_o, Mn_o = oxalate–extractable oxides; Fe_d, Al_d, Mn_d = DCB–extractable oxides; Fe_p, Al_p and Mn_p = pyrophosphate–extractable oxides; cPOM = coarse particulate SOC; micro–agg = microaggregate–associated SOC; s+c= silt & clay associated SOC. Climate types are based on Köppen climate classification.

List of Figures

Figure 5–3 (a) SOC density and **(b)** soil specific potential respiration (SPR) along with climate gradient. Dfc = continental subarctic climate, Cfb = marine west coast climate, Cfa = humid subtropical climate, Csa = hot–summer Mediterranean climate (Köppen climate classification).

Figure 5–4 Relationships between SOC density (right y axis), soil potential respiration (left y axis) and soil physico–chemical properties. * = significant correlation at the 0.01 level (n= 117). M_d = sum of DCB–extractable oxides; M_p = sum of pyrophosphate–extractable oxides; M_o = = sum of oxalate–extractable oxides; cPOM = coarse particulate organic carbon; micro–agg = microaggregate–associated SOC; s+c= silt & clay associated SOC. TRB = total reserve in bases; CIA= chemical alteration index; pOSL = total photon counts measured by pOSL reader.

Figure 5–5 Zero–order and partial correlation between subsoil SOC variables (SOC density, SPR) and retained RCs, controlling for soil burial age (RC8). The colors and numbers indicate the strength (the intensity of the color) and sign (blue and red colors indicate negative and positive correlations, respectively) of correlation. No change in color between controlled variable and zero–order = no dependency; decrease/increase of color intensity = loss/gain of correlation. *= $P < 0.05$; ** = $P < 0.01$.

List of Tables

Table 1–1 The studies related to the effects of terracing on SOC stocks across world.

Table 2–1 Description of the study sites

Table 2–2 List of abbreviations.

Table 3–1 Depth layers selected for soil analysis from sampled terraces

Table 3–2 Relationships between soil potential respiration (SPR), SOC temperature sensitivity (Q_{10}) and measured soil geochemical properties.

Table 3–3 Relationship between SOC temperature sensitivity (Q_{10}) and C:N ratios of bulk soil and SOC fractions.

Table 4–1 Statistical summary of the laboratory measured soil properties of agricultural terrace soil (MIR) and garden lawn soil samples (Vis_NIR).

Table 4–2 Comparison of model performance parameters between the log–ratio transformation and conventional (raw data) methods.

Table 5–1 Information of sampling sites

Table 5–2 SOC stock of terracing profiles compared to non–terracing profiles

Table 5–3 Eight rotated principal components (RCs) retained with a threshold of eigenvalues > 1 and proportional variance > 5% (n = 117). The upper part of the table shows eigenvalues, individual and cumulative variance and mechanistic interpretation of specific RCs. Variable loadings of Pearson's $r > 0.5$ and < -0.5 are highlighted with bold font type.

List of Tables

Table 5–4 Results of three stepwise regression models (topsoil only, subsoil only and all data) using RC scores to predict terrace SOC density and potential soil respiration (SPR), including standardized coefficients and model performance indicators. Blank cells indicate non–significant predictors ($P < 0.05$) that were not selected by the stepwise regression model.

Appendixes

Supplementary discussion D1

—Extended discussion based on the Chapter 3.

How much SOC is stored in the buried soil layers in terraced landforms?

In conclusion, the terraced hillslope had a higher SOC stock (64.9 ± 31.5%) than the non–terraced landscape. Half of (43.5 ± 5.5%) this additional SOC storage was found within the buried soil horizons. The following is a detailed description of the methods and results.

Sampling

At the Ingram site of UK, we excavated a trench (63 m long by 1.5 m wide) to the depth of weathered rocks in order to estimate the SOC stock of terraces. We sampled four high resolution (5 cm or 10 cm depth interval) depth profiles (T1, T2, T3, T4) on the terraced catena and two additional undisturbed soil profile profiles (C1, C2) in proximity to the terraces as a control (Figure S1–1). A detailed stretch map was created for supporting SOC stock assessment for the whole terraced hillslope. A detailed description of sampling was given in the Chapter 3.2.2.

Appendixes

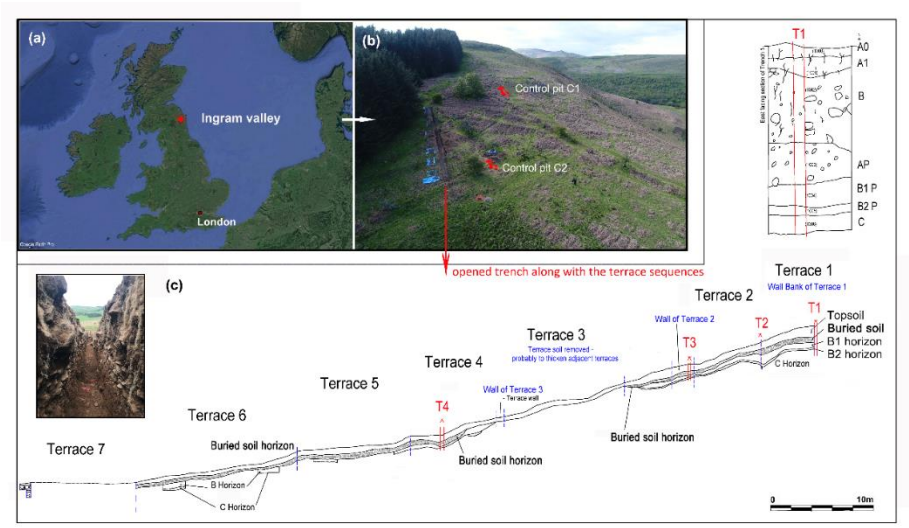

Figure S1–1. Map of (a) studying area, (b) sampling site and the (c) excavated terrace trench and sampling profiles.

Bulk density and SOC stock

Bulk density (BD) for the selected soil layers (Table 3–1) were measured from an undisturbed soil sample taken with a Kubiena tin (10 cm × 10 cm × 5 cm) and dried at 105℃ before weighting. T1 is a very deep profile (c. 2 m) and tends to collapse, making intact soil retrieval difficult. We therefore assumed that the BD of T1 is similar to T2. BD values for deep soil layers (> 70 cm) were approximated using the 60–70 cm observations. The weight and volume of gravels (> 2 mm, if > 3% in weight) were also determined to derive the BD for the fine earth (BD_{fine}). SOC concentration for each horizon was measured along with soil profile until the bedrock was reached. SOC stock for each horizon was estimated using the following equation (Eq. S1–1):

$$\mathrm{SOC}_{\mathrm{stock}} = \frac{SOC}{100} \times BD_{fine} \times z \qquad \text{(Eq. S1-1)}$$

Supplementary discussion D1

Where SOC_{stock} is in kg m^{-2}, SOC is in wt.%, BD_{fine} is in kg m^{-3} and *z* is the soil horizon thickness in meters. We extrapolated the SOC stock to the whole terraced hillslope by combining the detailed soil profile catena map (Fig S1–1c) with SOC stock estimates derived from the four high resolution depth profiles (T1–T4). For this, we used a linear regression to model the relation between soil horizon thickness and SOC stock for each horizon (i.e., topsoil, buried soil layer, B horizon, Figure. S1–1c). using the "lm" function in R software. The regression models had R^2 between 85% and 95% (*p*-values between 0.0013 and 0.009); The detailed soil profile catena was then used to estimate the thickness of each horizon along the catena (Figure. S1–1c; detailed in Chapter 3.2.2). Finally, the SOC stock of the whole hillslope was predicted by applying the regression model. The Uncertainty associated with this stock estimate was evaluated by considering the standard error on the regression parameters.

Identification of the buried soil layers

Diagnosis of the buried soil horizons in terraces was supported by the stretch map combined with weathering patters and SOC concentration depth profiles. A detailed description was given in Chapter 3.3.1.

Results

When applying the SOC stock extrapolation model to the entire slope, the terraced hillslope had a higher SOC stock (64.9 ± 31.5%) than the non-terraced landscape. 43.5 ± 5.5% of this additional SOC storage was found within the buried soil horizons (Figure. S1–1c). The direct comparison of two control profiles with the four terrace profiles confirmed that majority of the additional SOC storage was stored in the buried soil horizons (below 50 cm). Especially in T1, soils below 70 cm stored as much SOC as the whole control profile (Figure S1–2).

Appendixes

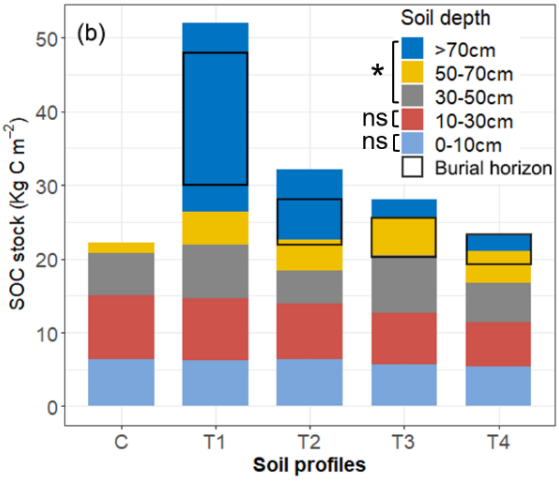

Figure S1–2. Depth profile of SOC stock. * means the significant difference in means of SOC stock at topsoil (0–10 cm) and subsoil (> 30 cm) between the terrace profile and control profile. $P < 0.1$. ns means no significant difference. T1–T4 are terrace profiles; C is the control profile (average of C1 and C2, Fig. 2–1b)

Supplementary tables

Table S2–1. Radiocarbon contents are expressed as fraction modern ($F^{14}C$)

Study sites	Soil*	depth	Bulk soil		Micro–agg		s+c	
	year	cm	$F^{14}C$	error	$F^{14}C$	error	$F^{14}C$	error
Spain (42°25'28.14"N, 1°13'36.09"W)	2017	0-10	0.9332	0.0017	0.912	0.0019	0.9347	0.0019
		30-50	0.8776	0.0017	0.8816	0.002	0.7407	0.0016
Belgium (50°45'40.53"N, 4°44'8.91"E)	2017	0-10	0.8918	0.002	0.9254	0.0018	0.942	0.0016
		30-50	0.7723	0.0015	0.8564	0.0014	0.763	0.0016
S China (24°18'42.16"N, 113°46'7.84"E)	2017	0-10	0.976	0.0015	0.9894	0.0017	0.9103	0.0019
		30-45	0.8151	0.0014	0.8011	0.0013	0.8438	0.0016
Brazil (28°51'36.9"S, 52°04'59.4"W)	2014	0-10	0.9375	0.0018				
		30-50	0.9399	0.0015				
NW China (35°3'18.45"N, 109°38'25.34"E)	2007	0-15	0.702	0.0016				
		30-45	0.5488	0.0013				

*Soil samples were collected in different years but all radiocarbon analyses were done in November 2019 at the Max Planck Institute for Biogeochemistry (Jena, Germany). Results were expressed as fraction modern ($F^{14}C$), which was the fraction with respect to the standard isotope ratio including normalization for $\delta^{13}C$. Abbreviations are listed in Table 2–2.

Supplementary tables

Table S2–2. Measurements of soil chemical properties.

Sites	Slope position	Soil depth	Al_p	Fe_p	Mn_p	Al_{o-p}	Fe_{o-p}	Mn_{o-p}	Fe_{d-o}	Fe_d/Fe_t	CEC	pH	TRB	Clay	Silt
SP	Stable	top	127	135	29.9	201	73	34.2	8166	0.41	7.7	8.7	1045	27.8	67.1
		sub	76	123	27.3	67	76	27.1	7626	0.37	6.6	8.9	1058	31.3	67.1
	Colluvial	top	126	111	51.8	275	222	38.2	7245	0.42	8.7	8.3	975	24.1	61.1
		sub	182	132	46.1	365	313	62.9	8428	0.42	9.8	8.7	925	29.0	61.9
NC	Stable	top	103	40	11.4	531	504	138.7	6757	0.24	8.9	8.3	606	14.0	82.3
		sub	96	36	4.9	642	540	197.8	6928	0.25	9.6	8.5	590	13.6	82.7
	Colluvial	top	104	40	5.1	628	598	168.7	6749	0.25	10.9	8.5	605	17.0	79.4
		sub	102	36	3.9	633	466	161.6	6809	0.26	11.1	8.5	630	13.8	82.8
BE	Stable	top	228	553	145.6	617	2237	235.6	3569	0.29	9.9	7.5	132	10.3	78.1
		sub	230	332	28.5	905	2429	270.7	7152	0.36	12.3	7.7	137	12.2	79.6
	Colluvial	top	167	359	133.0	473	1381	204.1	5548	0.36	10.9	7.5	126	11.2	75.4
		sub	175	226	35.7	641	1607	297.2	6294	0.37	10.4	7.5	124	11.7	75.0
SC	Stable	top	734	1220	11.8	255	391	3.8	15089	0.73	6.5	5.0	58	10.4	57.8
		sub	591	623	38.7	393	415	81.4	31634	0.68	8.3	4.8	101	7.4	58.3
	Colluvial	top	553	1222	8.3	90	156	0.0	9966	0.69	4.3	5.1	48	13.8	51.4
		sub	314	296	26.8	328	389	29.2	19067	0.75	5.8	5.7	65	18.4	55.7
SB	Stable	top	2270	1260	33.0	1386	1143	231.2	10889	0.29	25.3	6.0	133	15.3	63.7
		sub	1539	2393	40.6	1148	2435	291.7	17766	0.46	16.9	6.2	87	23.3	65.9
	Colluvial	top	1477	1562	167.5	914	3044	470.1	16898	0.43	14.5	5.2	92	22.6	65.7
		sub	1614	184	162.8	1176	3503	702.9	16820	0.41	17.2	5.2	91	23.6	65.3

Abbreviations are listed in Table 2–2.

Supplementary tables

Table S2–3. Depth patterns of weathering indices (TRB, K/I, Fe_d/Fe_t)* in selected sites for ^{14}C measurements.

Sampling sites	Slope position	Soil depth	TRB	K/I	Fe_d/Fe_t
SP (Arid)	Stable	Top	1045	0.29	0.41
		Sub	1058	0.13	0.37
	Colluvial	Top	975	0.40	0.42
		Sub	925	0.22	0.42
BE (Semi–arid)	Stable	Top	132	0.92	0.29
		Sub	137	0.75	0.36
	Colluvial	Top	126	0.71	0.36
		Sub	124	1.31	0.37
SC (Wet)	Stable	Top	58	1.23	0.73
		Sub	101	1.93	0.68
	Colluvial	Top	48	0.70	0.69
		Sub	65	0.68	0.75

*Kaolinite (K) has been recognized as one of the end products in weathering sequences and Illite (I) as one of the earlier formed clay minerals. Hence, higher K/I ratios were interpreted as indicators of advanced chemical weathering (Liu et al., 2007). Fe_d/Fe_t, representing the proportion of pedogenic iron oxides to total iron, was expected to increase with weathering (Arduino et al., 1986). Total reserve in bases (TRB), a measure of four alkaline and alkaline–earth cations, was expected to decrease as cations are leached during weathering (Herbillon, 1986). Abbreviations are listed in Table 2–2.

Bibliography

Bibliography

Aitchison, J., 1986. The statistical analysis of compositional data, Journal of the Royal Statistical Society: Series B (Methodological). Wiley Online Library.

Ali, R.S., Kandeler, E., Marhan, S., Demyan, M.S., Ingwersen, J., Mirzaeitalarposhti, R., Rasche, F., Cadisch, G., Poll, C., 2018. Controls on microbially regulated soil organic carbon decomposition at the regional scale. Soil Biol. Biochem. https://doi.org/10.1016/j.soilbio.2017.12.007

Amelung, W., Bossio, D., de Vries, W., Kögel-Knabner, I., Lehmann, J., Amundson, R., Bol, R., Collins, C., Lal, R., Leifeld, J., Minasny, B., Pan, G., Paustian, K., Rumpel, C., Sanderman, J., van Groenigen, J.W., Mooney, S., van Wesemael, B., Wander, M., Chabbi, A., 2020. Towards a global-scale soil climate mitigation strategy. Nat. Commun. https://doi.org/10.1038/s41467-020-18887-7

An, F.Y., Lai, Z.P., Liu, X.J., Fan, Q.S., Wei, H.C., 2018. Abnormal Rb/Sr ratio in lacustrine sediments of Qaidam Basin, NE Qinghai–Tibetan Plateau: A significant role of aeolian dust input. Quat. Int. 469, 44–57. https://doi.org/10.1016/j.quaint.2016.12.050

Angst, G., Mueller, K.E., Nierop, K.G.J., Simpson, M.J., 2021. Plant- or microbial-derived? A review on the molecular composition of stabilized soil organic matter. Soil Biol. Biochem. https://doi.org/10.1016/j.soilbio.2021.108189

Antle, J.M., Stoorvogel, J.J., Valdivia, R.O., 2007. Assessing the economic impacts of agricultural carbon sequestration: Terraces and agroforestry in the Peruvian Andes. Agric. Ecosyst. Environ. 122, 435–445. https://doi.org/10.1016/j.agee.2007.02.003

Arduino, E., Barberis, E., Ajmone Marsan, F., Zanini, E., Franchini, M., 1986. Iron oxides and clay minerals within profiles as indicators of soil age in Northern Italy. Geoderma 37, 45–55. https://doi.org/10.1016/0016-7061(86)90042-X

Bailey, V.L., Pries, C.H., Lajtha, K., 2019. What do we know about soil

carbon destabilization? Environ. Res. Lett. https://doi.org/10.1088/1748-9326/ab2c11

Baldock, J.A., Hawke, B., Sanderman, J., Macdonald, L.M., 2013. Predicting contents of carbon and its component fractions in Australian soils from diffuse reflectance mid-infrared spectra. Soil Res. 51, 577–595.

Bascomb, C.L., 1968. Distribution of Pyrophosphate-Extractable Iron and Organic Carbon in Soils of Various Groups. J. Soil Sci. 19, 251–268. https://doi.org/10.1111/j.1365-2389.1968.tb01538.x

Baumann, P., Helfenstein, A., Gubler, A., Keller, A., Meuli, R.G., Wachter, D., Lee, J., Viscarra Rossel, R.A., Six, J., 2021. Developing the Swiss mid-infrared soil spectral library for local estimation and monitoring. Soil 7, 525–546.

Bellon-Maurel, V., Fernandez-Ahumada, E., Palagos, B., Roger, J.-M., McBratney, A., 2010. Critical review of chemometric indicators commonly used for assessing the quality of the prediction of soil attributes by NIR spectroscopy. TrAC Trends Anal. Chem. 29, 1073–1081.

Berhe, A.A., Harden, J.W., Torn, M.S., Kleber, M., Burton, S.D., Harte, J., 2012. Persistence of soil organic matter in eroding versus depositional landform positions. J. Geophys. Res. Biogeosciences 117, 1–16. https://doi.org/10.1029/2011JG001790

Berhe, A.A., Harte, J., Harden, J.W., Torn, M.S., 2007. The Significance of the Erosion-induced Terrestrial Carbon Sink. Bioscience 57, 337–346. https://doi.org/10.1641/b570408

Beuselinck, L., Govers, G., Poesen, J., Degraer, G., Froyen, L., 1998. Grain-size analysis by laser diffractometry: Comparison with the sieve-pipette method. Catena. https://doi.org/10.1016/S0341-8162(98)00051-4

Blakemore, L.C., Searle, P.L., Daly, B.K., 1987. Methods for chemical analysis of soils, Second Rev. ed. New Zealand Soil Bureau Scientific Report 10 A, Lower Hutt, New Zealand.

Blume, H.-P., Brümmer, G.W., Horn, R., Kandeler, E., Kögel-Knabner, I., Kretzschmar, R., Stahr, K., Wilke, B.-M., Thiele-Bruhn, S., Welp, G., 2016. Scheffer/Schachtschabel Soil Science. Springer.

https://doi.org/10.1007/978-3-642-30942-7

Borrelli, P., Robinson, D.A., Fleischer, L.R., Lugato, E., Ballabio, C., Alewell, C., Meusburger, K., Modugno, S., Schütt, B., Ferro, V., Bagarello, V., Oost, K. Van, Montanarella, L., Panagos, P., 2017. An assessment of the global impact of 21st century land use change on soil erosion. Nat. Commun. 8, 1–13. https://doi.org/10.1038/s41467-017-02142-7

Bosatta, E., Ågren, G.I., 1999. Soil organic matter quality interpreted thermodynamically. Soil Biol. Biochem. 31, 1889–1891. https://doi.org/10.1016/S0038-0717(99)00105-4

Brady, N.C., Weil, R.R., Weil, R.R., 2008. The nature and properties of soils. Prentice Hall Upper Saddle River, NJ.

Briedis, C., Baldock, J., de Moraes Sá, J.C., dos Santos, J.B., Milori, D.M.B.P., 2020. Strategies to improve the prediction of bulk soil and fraction organic carbon in Brazilian samples by using an Australian national mid-infrared spectral library. Geoderma. https://doi.org/10.1016/j.geoderma.2020.114401

Brown, A.G., Fallu, D., Walsh, K., Cucchiaro, S., Tarolli, P., Zhao, P., Pears, B.R., van Oost, K., Snape, L., Lang, A., Albert, R.M., Alsos, I.G., Waddington, C., 2021. Ending the Cinderella status of terraces and lynchets in Europe: The geomorphology of agricultural terraces and implications for ecosystem services and climate adaptation. Geomorphology. https://doi.org/10.1016/j.geomorph.2020.107579

Bukombe, B., Fiener, P., Hoyt, A.M., Kidinda, L.K., Doetterl, S., 2021. Heterotrophic soil respiration and carbon cycling in geochemically distinct African tropical forest soils. SOIL. https://doi.org/10.5194/soil-7-639-2021

Carvalhais, N., Forkel, M., Khomik, M., Bellarby, J., Jung, M., Migliavacca, M., Mu, M., Saatchi, S., Santoro, M., Thurner, M., Weber, U., Ahrens, B., Beer, C., Cescatti, A., Randerson, J.T., Reichstein, M., 2014. Global covariation of carbon turnover times with climate in terrestrial ecosystems. Nature. https://doi.org/10.1038/nature13731

Chakraborty, S., Li, B., Deb, S., Paul, S., Weindorf, D.C., Das, B.S., 2017. Predicting soil arsenic pools by visible near infrared diffuse reflectance

spectroscopy. Geoderma. https://doi.org/10.1016/j.geoderma.2017.02.015

Chang, C.-W., Laird, D., Mausbach, M.J., Hurburgh Jr, C.R., 2001. Near-infrared reflectance spectroscopy–principal components regression analyses of soil properties. Soil Sci. Soc. Am. J. 65, 480.

Chao, T.T., Sanzolone, R.F., 1992. Decomposition techniques. J. Geochemical Explor. 44, 65–106.

Chaplot, V., Bouahom, B., Valentin, C., 2010. Soil organic carbon stocks in Laos: Spatial variations and controlling factors. Glob. Chang. Biol. https://doi.org/10.1111/j.1365-2486.2009.02013.x

Chapman, H.D., 1969. Cation exchange capacity. Methods of soil analysis. Am. Soc. A g ronomy 1, 891–900.

Chappell, A., Baldock, J., Sanderman, J., 2016. The global significance of omitting soil erosion from soil organic carbon cycling schemes. Nat. Clim. Chang. https://doi.org/10.1038/nclimate2829

Chen, D., Wei, W., Daryanto, S., Tarolli, P., 2020. Does terracing enhance soil organic carbon sequestration? A national-scale data analysis in China. Sci. Total Environ. 721, 137751. https://doi.org/10.1016/j.scitotenv.2020.137751

Chen, S., Xu, D., Li, S., Ji, W., Yang, M., Zhou, Y., Hu, B., Xu, H., Shi, Z., 2020. Monitoring soil organic carbon in alpine soils using in situ vis-NIR spectroscopy and a multilayer perceptron. L. Degrad. Dev. 31, 1026–1038.

Coblinski, J.A., Giasson, É., Demattê, J.A.M., Dotto, A.C., Costa, J.J.F., Vašát, R., 2020. Prediction of soil texture classes through different wavelength regions of reflectance spectroscopy at various soil depths. Catena 189, 104485.

Contreras-Cisneros, A.J., Mata-González, R., Trejo-Calzada, R., Pedroza-Sandoval, A., Prado-Tarango, D., Abdallah, M.A.B., 2022. Carbon and nitrogen stocks through time in abandoned croplands of the Comarca Lagunera, Mexico. Agric. Ecosyst. Environ. 327, 107828.

Cozzolino, D., Morón, A., 2006. Potential of near-infrared reflectance spectroscopy and chemometrics to predict soil organic carbon

fractions. Soil Tillage Res. 85, 78–85.

Craine, J., Spurr, R., McLauchlan, K., Fierer, N., 2010. Landscape-level variation in temperature sensitivity of soil organic carbon decomposition. Soil Biol. Biochem. https://doi.org/10.1016/j.soilbio.2009.10.024

Craine, J.M., Fierer, N., McLauchlan, K.K., 2010. Widespread coupling between the rate and temperature sensitivity of organic matter decay. Nat. Geosci. 3, 854–857. https://doi.org/10.1038/ngeo1009

Cucchiaro, S., Fallu, D.J., Zhang, H., Walsh, K., Oost, K. Van, Brown, A.G., Tarolli, P., 2020a. Multiplatform-SfM and TLS data fusion for monitoring agricultural terraces in complex topographic and landcover conditions. Remote Sens. https://doi.org/10.3390/rs12121946

Cucchiaro, S., Fallu, D.J., Zhao, P., Waddington, C., Cockcroft, D., Tarolli, P., Brown, A.G., 2020b. SfM photogrammetry for GeoArchaeology, in: Developments in Earth Surface Processes. Elsevier, pp. 183–205. https://doi.org/10.1016/B978-0-444-64177-9.00006-0

Cui, J., Li, Z., Liu, Z., Ge, B., Fang, C., Zhou, C., Tang, B., 2014. Physical and chemical stabilization of soil organic carbon along a 500-year cultived soil chronosequence originating from estuarine wetlands: Temporal patterns and land use effects. Agric. Ecosyst. Environ. 196, 10–20. https://doi.org/10.1016/j.agee.2014.06.013

Curtaz, F., Stanchi, S., D'Amico, M.E., Filippa, G., Zanini, E., Freppaz, M., 2015. Soil evolution after land-reshaping in mountains areas (Aosta Valley, NW Italy). Agric. Ecosyst. Environ. 199, 238–248. https://doi.org/10.1016/j.agee.2014.09.013

Dahlgren, R.A., 1994. Quantification of allophane and imogolite. Quant. methods soil Mineral. 430–451.

Davidovich, U., Porat, N., Gadot, Y., Avni, Y., Lipschits, O., 2012. Archaeological investigations and OSL dating of terraces at Ramat Rahel, Israel. J. F. Archaeol. https://doi.org/10.1179/0093469012Z.00000000019

Davidson, E.A., Janssens, I.A., 2006. Temperature sensitivity of soil carbon decomposition and feedbacks to climate change. Nature.

https://doi.org/10.1038/nature04514

Davidson, E.A., Samanta, S., Caramori, S.S., Savage, K., 2012. The Dual Arrhenius and Michaelis-Menten kinetics model for decomposition of soil organic matter at hourly to seasonal time scales. Glob. Chang. Biol. https://doi.org/10.1111/j.1365-2486.2011.02546.x

De Blécourt, M., Hänsel, V.M., Brumme, R., Corre, M.D., Veldkamp, E., 2014. Soil redistribution by terracing alleviates soil organic carbon losses caused by forest conversion to rubber plantation. For. Ecol. Manage. 313, 26–33. https://doi.org/10.1016/j.foreco.2013.10.043

Deiss, L., Franzluebbers, A.J., de Moraes, A., 2017. Soil texture and organic carbon fractions predicted from near-infrared spectroscopy and geostatistics. Soil Sci. Soc. Am. J. 81, 1222–1234.

Denef, K., Six, J., 2005. Clay mineralogy determines the importance of biological versus abiotic processes for macroaggregate formation and stabilization. Eur. J. Soil Sci. 56, 469–479.

Doetterl, S., Asifiwe, R.K., Baert, G., Bamba, F., Bauters, M., Boeckx, P., Bukombe, B., Cadisch, G., Cooper, M., Cizungu, L.N., 2021. Organic matter cycling along geochemical, geomorphic, and disturbance gradients in forest and cropland of the African Tropics-project TropSOC database version 1.0. Earth Syst. Sci. Data 13, 4133–4153.

Doetterl, S., Berhe, A.A., Arnold, C., Bodé, S., Fiener, P., Finke, P., Fuchslueger, L., Griepentrog, M., Harden, J.W., Nadeu, E., Schnecker, J., Six, J., Trumbore, S., Van Oost, K., Vogel, C., Boeckx, P., 2018. Links among warming, carbon and microbial dynamics mediated by soil mineral weathering. Nat. Geosci. 11, 589–593. https://doi.org/10.1038/s41561-018-0168-7

Doetterl, S., Berhe, A.A., Nadeu, E., Wang, Z., Sommer, M., Fiener, P., 2016. Erosion, deposition and soil carbon: A review of process-level controls, experimental tools and models to address C cycling in dynamic landscapes. Earth-Science Rev. https://doi.org/10.1016/j.earscirev.2015.12.005

Doetterl, S., Cornelis, J.T., Six, J., Bodé, S., Opfergelt, S., Boeckx, P., Van Oost, K., 2015a. Soil redistribution and weathering controlling the fate

of geochemical and physical carbon stabilization mechanisms in soils of an eroding landscape. Biogeosciences 12, 1357–1371. https://doi.org/10.5194/bg-12-1357-2015

Doetterl, Sebastian, Stevens, A., Six, J., Merckx, R., Van Oost, K., Casanova Pinto, M., Casanova-Katny, A., Muñoz, C., Boudin, M., Zagal Venegas, E., Boeckx, P., 2015b. Soil carbon storage controlled by interactions between geochemistry and climate. Nat. Geosci. 8, 780–783. https://doi.org/10.1038/ngeo2516

Dotto, A.C., Dalmolin, R.S.D., ten Caten, A., Grunwald, S., 2018. A systematic study on the application of scatter-corrective and spectral-derivative preprocessing for multivariate prediction of soil organic carbon by Vis-NIR spectra. Geoderma 314, 262–274.

Duiker, S.W., Rhoton, F.E., Torrent, J., Smeck, N.E., Lal, R., 2003. Iron (hydr)oxide crystallinity effects on soil aggregation. Soil Sci. Soc. Am. J.

Dümig, A., Smittenberg, R., Kögel-Knabner, I., 2011. Concurrent evolution of organic and mineral components during initial soil development after retreat of the Damma glacier, Switzerland. Geoderma. https://doi.org/10.1016/j.geoderma.2011.04.006

Dunjó, G., Pardini, G., Gispert, M., 2003. Land use change effects on abandoned terraced soils in a Mediterranean catchment, NE Spain. Catena 52, 23–37. https://doi.org/10.1016/S0341-8162(02)00148-0

Egozcue, J.J., Pawlowsky-Glahn, V., Mateu-Figueras, G., Barcelo-Vidal, C., 2003. Isometric logratio transformations for compositional data analysis. Math. Geol. 35, 279–300.

Feng, W., Liang, J., Hale, L.E., Jung, C.G., Chen, J., Zhou, J., Xu, M., Yuan, M., Wu, L., Bracho, R., Pegoraro, E., Schuur, E.A.G., Luo, Y., 2017. Enhanced decomposition of stable soil organic carbon and microbial catabolic potentials by long-term field warming. Glob. Chang. Biol. https://doi.org/10.1111/gcb.13755

Finke, P., Opolot, E., Balesdent, J., Berhe, A.A., Boeckx, P., Cornu, S., Harden, J., Hatté, C., Williams, E., Doetterl, S., 2019. Can SOC modelling be improved by accounting for pedogenesis? Geoderma.

https://doi.org/10.1016/j.geoderma.2018.10.018

Fisher, B.A., Aufdenkampe, A.K., Yoo, K., Aalto, R.E., Marquard, J., 2018. Soil carbon redistribution and organo-mineral associations after lateral soil movement and mixing in a first-order forest watershed. Geoderma 319, 142–155. https://doi.org/10.1016/j.geoderma.2018.01.006

Frodsham, P., Waddington, C., 2004. The Breamish Valley Archaeology Project 1994-2002. Archaeol. Northumberl. Natl. Park. Counc. Br. Archaeol. Res. Rep. 136, 171–189.

Gao, X., Li, W., Salman, A., Wang, R., Du, L., Yao, L., Hu, Y., Guo, S., 2020. Impact of topsoil removal on soil CO2 emission and temperature sensitivity in Chinese Loess Plateau. Sci. Total Environ. 708, 135102. https://doi.org/10.1016/j.scitotenv.2019.135102

Gareth, J., Daniela, W., Trevor, H., Robert, T., 2013. An introduction to statistical learning: with applications in R. Spinger.

Gillabel, J., Cebrian-Lopez, B., Six, J., Merckx, R., 2010. Experimental evidence for the attenuating effect of SOM protection on temperature sensitivity of SOM decomposition. Glob. Chang. Biol. 16, 2789–2798. https://doi.org/10.1111/j.1365-2486.2009.02132.x

Godfray, H.C.J., Beddington, J.R., Crute, I.R., Haddad, L., Lawrence, D., Muir, J.F., Pretty, J., Robinson, S., Thomas, S.M., Toulmin, C., 2010. Food security: The challenge of feeding 9 billion people. Science (80-.). https://doi.org/10.1126/science.1185383

Haaf, D., Six, J., Doetterl, S., 2021. Global patterns of geo-ecological controls on the response of soil respiration to warming. Nat. Clim. Chang. https://doi.org/10.1038/s41558-021-01068-9

Hall, S.J., Ye, C., Weintraub, S.R., Hockaday, W.C., 2020. Molecular trade-offs in soil organic carbon composition at continental scale. Nat. Geosci. https://doi.org/10.1038/s41561-020-0634-x

Hamdan, J., Burnham, C.P., Ruhana, B., 2000. Degradation effect of slope terracing on soil quality for Elaeis guineensis Jacq. (oil palm) cultivation. L. Degrad. Dev. https://doi.org/10.1002/(sici)1099-145x(200003/04)11:2<181::aid-ldr377>3.3.co;2-l

Harden, J.W., Sharpe, J.M., Parton, W.J., Ojima, D.S., Fries, T.L.,

Bibliography

Huntington, T.G., Dabney, S.M., 1999. Dynamic replacement and loss of soil carbon on eroding cropland. Global Biogeochem. Cycles 13, 885–901. https://doi.org/10.1029/1999GB900061

Hemingway, J.D., Rothman, D.H., Grant, K.E., Rosengard, S.Z., Eglinton, T.I., Derry, L.A., Galy, V. V., 2019. Mineral protection regulates long-term global preservation of natural organic carbon. Nature. https://doi.org/10.1038/s41586-019-1280-6

Henaka Arachchi, M.P.N.K., Field, D.J., McBratney, A.B., 2016. Quantification of soil carbon from bulk soil samples to predict the aggregate-carbon fractions within using near- and mid-infrared spectroscopic techniques. Geoderma. https://doi.org/10.1016/j.geoderma.2015.12.030

Herbillon, A.J., 1986. Chemical estimation of weatherable minerals present in the diagnostic horizons of low activity clay soils, in: Proceedings of the 8th International Clay Classification Workshop: Classification, Characterization and Utilization of Oxisols (Part 1)[Beinroth, FH, Camargo, MN and Eswaran (Ed)][39–48](Rio de Janeiro, 1986).

Hobley, E.U., Prater, I., 2019. Estimating soil texture from vis–NIR spectra. Eur. J. Soil Sci. https://doi.org/10.1111/ejss.12733

Hong, Y., Chen, S., Liu, Yaolin, Zhang, Y., Yu, L., Chen, Y., Liu, Yanfang, Cheng, H., Liu, Yi, 2019. Combination of fractional order derivative and memory-based learning algorithm to improve the estimation accuracy of soil organic matter by visible and near-infrared spectroscopy. Catena. https://doi.org/10.1016/j.catena.2018.10.051

Howel, D., 2007. Multivariate data analysis of pollutant profiles: PCB levels across Europe. Chemosphere 67, 1300–1307.

Igne, B., Reeves, J.B., McCarty, G., Hively, W.D., Lund, E., Hurburgh, C.R., 2010. Evaluation of spectral pretreatments, partial least squares, least squares support vector machines and locally weighted regression for quantitative spectroscopic analysis of soils. J. Near Infrared Spectrosc. 18, 167–176.

IPCC, 2021. Summary for Policymakers. Cambridge University Press.

Islam, K., Singh, B., McBratney, A., 2003. Simultaneous estimation of

several soil properties by ultra-violet, visible, and near-infrared reflectance spectroscopy. Aust. J. Soil Res. https://doi.org/10.1071/SR02137

Jaconi, A, Poeplau, C., Ramirez‐Lopez, L., Van Wesemael, B., Don, A., 2019. Log-ratio transformation is the key to determining soil organic carbon fractions with near-infrared spectroscopy. Eur. J. Soil Sci. 70, 127–139.

Jaconi, Angélica, Vos, C., Don, A., 2019. Near infrared spectroscopy as an easy and precise method to estimate soil texture. Geoderma 337, 906–913.

Jolliffe, I.T., 1995. Rotation of principal components: choice of normalization constraints. J. Appl. Stat. 22, 29–35.

Jukić, D., Denić-Jukić, V., 2015. Investigating relationships between rainfall and karst-spring discharge by higher-order partial correlation functions. J. Hydrol. 530, 24–36.

Kagabo, D.M., Stroosnijder, L., Visser, S.M., Moore, D., 2013. Soil erosion, soil fertility and crop yield on slow-forming terraces in the highlands of Buberuka, Rwanda. Soil Tillage Res. 128, 23–29. https://doi.org/10.1016/j.still.2012.11.002

Kinnaird, T., Bolòs, J., Turner, A., Turner, S., 2017. Optically-stimulated luminescence profiling and dating of historic agricultural terraces in Catalonia (Spain). J. Archaeol. Sci. https://doi.org/10.1016/j.jas.2016.11.003

Kirschbaum, M.U.F., 1995. The temperature dependence of soil organic matter decomposition, and the effect of global warming on soil organic C storage. Soil Biol. Biochem. 27, 753–760. https://doi.org/10.1016/0038-0717(94)00242-S

Kleber, M., 2010. What is recalcitrant soil organic matter? Environ. Chem. 7, 320–332. https://doi.org/10.1071/EN10006

Knorr, W., Prentice, I.C., House, J.I., Holland, E.A., 2005. Long-term sensitivity of soil carbon turnover to warming. Nature 433, 298–301. https://doi.org/10.1038/nature03226

Knox, N.M., Grunwald, S., McDowell, M.L., Bruland, G.L., Myers, D.B.,

Bibliography

Harris, W.G., 2015. Modelling soil carbon fractions with visible near-infrared (VNIR) and mid-infrared (MIR) spectroscopy. Geoderma. https://doi.org/10.1016/j.geoderma.2014.10.019

Kodinariya, T.M., Makwana, P.R., 2013. Review on determining number of Cluster in K-Means Clustering. Int. J. 1, 90–95.

Kögel-Knabner, I., Guggenberger, G., Kleber, M., Kandeler, E., Kalbitz, K., Scheu, S., Eusterhues, K., Leinweber, P., 2008. Organo-mineral associations in temperate soils: Integrating biology, mineralogy, and organic matter chemistry. J. Plant Nutr. Soil Sci. 171, 61–82. https://doi.org/10.1002/jpln.200700048

Kopittke, P.M., Dalal, R.C., Hoeschen, C., Li, C., Menzies, N.W., Mueller, C.W., 2020. Soil organic matter is stabilized by organo-mineral associations through two key processes: The role of the carbon to nitrogen ratio. Geoderma 357. https://doi.org/10.1016/j.geoderma.2019.113974

Lair, G.J., Zehetner, F., Hrachowitz, M., Franz, N., Maringer, F.J., Gerzabek, M.H., 2009. Dating of soil layers in a young floodplain using iron oxide crystallinity. Quat. Geochronol. https://doi.org/10.1016/j.quageo.2008.11.003

Lang, A., Hatté, C., Rousseau, D.D., Antoine, P., Fontugne, M., Zöller, L., Hambach, U., 2003. High-resolution chronologies for loess: Comparing AMS 14C and optical dating results, in: Quaternary Science Reviews. https://doi.org/10.1016/S0277-3791(03)00035-0

Li, J., Wan, H., Shang, S., 2020. Comparison of interpolation methods for mapping layered soil particle-size fractions and texture in an arid oasis. Catena. https://doi.org/10.1016/j.catena.2020.104514

Li, Y., Quine, T.A., Yu, H.Q., Govers, G., Six, J., Gong, D.Z., Wang, Z., Zhang, Y.Z., Van Oost, K., 2015. Sustained high magnitude erosional forcing generates an organic carbon sink: Test and implications in the Loess Plateau, China. Earth Planet. Sci. Lett. 411, 281–289. https://doi.org/10.1016/j.epsl.2014.11.036

Liu, Y., Wang, C., He, N., Wen, X., Gao, Y., Li, S., Niu, S., Butterbach-Bahl, K., Luo, Y., Yu, G., 2017. A global synthesis of the rate and

temperature sensitivity of soil nitrogen mineralization: latitudinal patterns and mechanisms. Glob. Chang. Biol. 23, 455–464. https://doi.org/10.1111/gcb.13372

Luo, Y., Ahlström, A., Allison, S.D., Batjes, N.H., Brovkin, V., Carvalhais, N., Chappell, A., Ciais, P., Davidson, E.A., Finzi, A., Georgiou, K., Guenet, B., Hararuk, O., Harden, J.W., He, Y., Hopkins, F., Jiang, L., Koven, C., Jackson, R.B., Jones, C.D., Lara, M.J., Liang, J., McGuire, A.D., Parton, W., Peng, C., Randerson, J.T., Salazar, A., Sierra, C.A., Smith, M.J., Tian, H., Todd-Brown, K.E.O., Torn, M., Van Groenigen, K.J., Wang, Y.P., West, T.O., Wei, Y., Wieder, W.R., Xia, J., Xu, Xia, Xu, Xiaofeng, Zhou, T., 2016. Toward more realistic projections of soil carbon dynamics by Earth system models, in: Global Biogeochemical Cycles. https://doi.org/10.1002/2015GB005239

Luo, Z., Feng, W., Luo, Y., Baldock, J., Wang, E., 2017. Soil organic carbon dynamics jointly controlled by climate, carbon inputs, soil properties and soil carbon fractions. Glob. Chang. Biol. https://doi.org/10.1111/gcb.13767

Luo, Z., Wang, G., Wang, E., 2019. Global subsoil organic carbon turnover times dominantly controlled by soil properties rather than climate. Nat. Commun. 10, 1–10. https://doi.org/10.1038/s41467-019-11597-9

Lützow, M. V., Kögel-Knabner, I., Ekschmitt, K., Matzner, E., Guggenberger, G., Marschner, B., Flessa, H., 2006. Stabilization of organic matter in temperate soils: Mechanisms and their relevance under different soil conditions - A review. Eur. J. Soil Sci. https://doi.org/10.1111/j.1365-2389.2006.00809.x

Masiello, C.A., Chadwick, O.A., Southon, J., Torn, M.S., Harden, J.W., 2004. Weathering controls on mechanisms of carbon storage in grassland soils. Global Biogeochem. Cycles 18, 1–9. https://doi.org/10.1029/2004GB002219

Mayrink, G.O., Valente, D.S.M., Queiroz, D.M., Pinto, F.A.C., Teofilo, R.F., 2019. Determination of chemical soil properties using diffuse reflectance and ion-exchange resins. Precis. Agric. https://doi.org/10.1007/s11119-018-9597-y

Bibliography

McGuire, K.L., Treseder, K.K., 2010. Microbial communities and their relevance for ecosystem models: Decomposition as a case study. Soil Biol. Biochem. https://doi.org/10.1016/j.soilbio.2009.11.016

Meersmans, J., van Wesemael, B., Goidts, E., Van Molle, M., De Baets, S., De Ridder, F., 2011. Spatial analysis of soil organic carbon evolution in Belgian croplands and grasslands, 1960–2006. Glob. Chang. Biol. 17, 466–479.

Mehra, O.P., Jackson, M.L., 1958. Iron Oxide Removal from Soils and Clays by a Dithionite-Citrate System Buffered with Sodium Bicarbonate. Clays Clay Miner. 7, 317–327. https://doi.org/10.1346/CCMN.1958.0070122

Mesfin, A., 2016. A Field Guideline on Bench Terrace Design and Construction. Minist. Agric. Nat. Resour. Nat. Resour. Manag. Dir.

Metzen, D., Sheridan, G.J., Benyon, R.G., Bolstad, P. V., Griebel, A., Lane, P.N.J., 2019. Spatio-temporal transpiration patterns reflect vegetation structure in complex upland terrain. Sci. Total Environ. https://doi.org/10.1016/j.scitotenv.2019.07.357

Minella, J.P.G., Merten, G.H., Walling, D.E., Moro, M., 2012. Using 137Cs measurements and sediment yield monitoring to document catchment-scale sediment dynamics and budgets, in: Chengdu Symposium on Erosion and Sediment Yields in the Changing Environment. pp. 338–344.

Minella, J.P.G., Walling, D.E., Merten, G.H., 2014. Establishing a sediment budget for a small agricultural catchment in southern Brazil, to support the development of effective sediment management strategies. J. Hydrol. 519, 2189–2201. https://doi.org/10.1016/j.jhydrol.2014.10.013

Moore, D.M., Reynolds, R.C. j., 1997. X-Ray Diffraction and the Identification and Analysis of Clay Minerals, second edition, Oxford University Press. https://doi.org/10.1038/srep26532

Muñoz-Salinas, E., Bishop, P., Sanderson, D.C., Zamorano, J.J., 2011. Interpreting luminescence data from a portable OSL reader: Three case studies in fluvial settings. Earth Surf. Process. Landforms 36, 651–660. https://doi.org/10.1002/esp.2084

Bibliography

Muzzamal, M., Huang, J., Nielson, R., Sefton, M., Triantafilis, J., 2018. Mapping soil particle-size fractions using additive log-ratio (ALR) and isometric log-ratio (ILR) transformations and proximally sensed ancillary data. Clays Clay Miner. https://doi.org/10.1346/CCMN.2017.064074

Ng, W., Minasny, B., Jones, E., McBratney, A., 2022. To spike or to localize? Strategies to improve the prediction of local soil properties using regional spectral library. Geoderma. https://doi.org/10.1016/j.geoderma.2021.115501

Nocita, M., Stevens, A., Toth, G., Panagos, P., van Wesemael, B., Montanarella, L., 2014. Prediction of soil organic carbon content by diffuse reflectance spectroscopy using a local partial least square regression approach. Soil Biol. Biochem. https://doi.org/10.1016/j.soilbio.2013.10.022

Nussbaum, M., Spiess, K., Baltensweiler, A., Grob, U., Keller, A., Greiner, L., Schaepman, M.E., Papritz, A., 2018. Evaluation of digital soil mapping approaches with large sets of environmental covariates. SOIL. https://doi.org/10.5194/soil-4-1-2018

Nyssen, J., Clymans, W., Poesen, J., Vandecasteele, I., de Baets, S., Haregeweyn, N., Naudt, J., Hadera, A., Moeyersons, J., Haile, M., Deckers, J., 2009. How soil conservation affects the catchment sediment budget - A comprehensive study in the north Ethiopian highlands. Earth Surf. Process. Landforms 34, 1216–1233. https://doi.org/10.1002/esp.1805

Otero, N., Tolosana-Delgado, R., Soler, A., Pawlowsky-Glahn, V., Canals, A., 2005. Relative vs. absolute statistical analysis of compositions: a comparative study of surface waters of a Mediterranean river. Water Res. 39, 1404–1414.

Palarea-Albaladejo, J., Martín-Fernández, J.A., 2015. zCompositions—R package for multivariate imputation of left-censored data under a compositional approach. Chemom. Intell. Lab. Syst. 143, 85–96.

Palarea-Albaladejo, J., Martín-Fernández, J.A., Buccianti, A., 2014. Compositional methods for estimating elemental concentrations below

the limit of detection in practice using R. J. Geochemical Explor. 141, 71–77.

Parent, E.J., Parent, S.É., Parent, L.E., 2021. Determining soil particle-size distribution from infrared spectra using machine learning predictions: Methodology and modeling. PLoS One. https://doi.org/10.1371/journal.pone.0233242

Paul, E.A.A., Morris, S.J.J., Böhm, S., 2001. The determination of soil C pool sizes and turnover rates: biophysical fractionation and tracers. Assess. methods soil carbon 14, 193–206.

Pawlowsky-Glahn, V., Egozcue, J.J., 2006. Compositional data and their analysis: An introduction. Geol. Soc. Spec. Publ. https://doi.org/10.1144/GSL.SP.2006.264.01.01

Poeplau, C., Kätterer, T., Leblans, N.I.W., Sigurdsson, B.D., 2017. Sensitivity of soil carbon fractions and their specific stabilization mechanisms to extreme soil warming in a subarctic grassland. Glob. Chang. Biol. 23, 1316–1327. https://doi.org/10.1111/gcb.13491

Porat, N., López, G.I., Lensky, N., Elinson, R., Avni, Y., Elgart-Sharon, Y., Faershtein, G., Gadot, Y., 2019. Using portable OSL reader to obtain a time scale for soil accumulation and erosion in archaeological terraces, the Judean Highlands, Israel. Quat. Geochronol. 49, 65–70.

Portenga, E.W., Bishop, P., Gore, D.B., Westaway, K.E., 2016. Landscape preservation under post-European settlement alluvium in the south-eastern Australian tablelands, inferred from portable OSL reader data. Earth Surf. Process. Landforms 41, 1697–1707.

Quijano, L., Beguería, S., Gaspar, L., Navas, A., 2016. Estimating erosion rates using 137Cs measurements and WATEM/SEDEM in a Mediterranean cultivated field. Catena. https://doi.org/10.1016/j.catena.2015.11.009

Rakhsh, F., Golchin, A., Beheshti Al Agha, A., Alamdari, P., 2017. Effects of exchangeable cations, mineralogy and clay content on the mineralization of plant residue carbon. Geoderma 307, 150–158. https://doi.org/10.1016/j.geoderma.2017.07.010

Ramirez-Lopez, L., Behrens, T., Schmidt, K., Stevens, A., Demattê, J.A.M.,

Bibliography

Scholten, T., Jaconi, A., Vos, C., Don, A., 2013. The spectrum-based learner: A new local approach for modeling soil vis–NIR spectra of complex datasets. Geoderma 195, 268–279.

Ramirez-Lopez, L., Stevens, A., Viscarra Rossel, R., Lobsey, C., Wadoux, A., Breure, T., 2020. resemble: Regression and similarity evaluation for memory-based learning in spectral chemometrics. R Packag. Vignette R Packag. version 2.0.0. 1, 2.

Reda, R., Saffaj, T., Derrouz, H., Itqiq, S.E., Bouzida, I., Saidi, O., Lakssir, B., El Hadrami, E.M., 2021. Comparing CalReg performance with other multivariate methods for estimating selected soil properties from Moroccan agricultural regions using NIR spectroscopy. Chemom. Intell. Lab. Syst. https://doi.org/10.1016/j.chemolab.2021.104277

Reichenbach, M., Fiener, P., Garland, G., Griepentrog, M., Six, J., Doetterl, S., 2021. The role of geochemistry in organic carbon stabilization against microbial decomposition in tropical rainforest soils. SOIL 7, 453–475.

Reimann, C., Filzmoser, P., Hron, K., Kynčlová, P., Garrett, R.G., 2017. A new method for correlation analysis of compositional (environmental) data – a worked example. Sci. Total Environ. https://doi.org/10.1016/j.scitotenv.2017.06.063

Robert, M., Tessier, D., 1974. Méthode de préparation des argiles des sols pour des études minéralogiques, in: Annales Agronomiques.

Sağlam, M., 2015. Evaluation of the physicochemical properties of alluvial and colluvial soils formed under ustic moisture regime using multivariate geostatistical techniques. Arch. Agron. Soil Sci. 61, 943–957.

Sagova-Mareckova, M., Zadorova, T., Penizek, V., Omelka, M., Tejnecky, V., Pruchova, P., Chuman, T., Drabek, O., Buresova, A., Vanek, A., Kopecky, J., 2016. The structure of bacterial communities along two vertical profiles of a deep colluvial soil. Soil Biol. Biochem. https://doi.org/10.1016/j.soilbio.2016.06.026

Sanderman, J., Berhe, A.A., 2017. Biogeochemistry: The soil carbon erosion paradox. Nat. Clim. Chang. https://doi.org/10.1038/nclimate3281

Bibliography

Sandor, J.A., Eash, N.S., 1995. Ancient Agricultural Soils in the Andes of Southern Peru. Soil Sci. Soc. Am. J. https://doi.org/10.2136/sssaj1995.03615995005900010026x

Savitzky, A., Golay, M.J.E., 1964. Smoothing and differentiation of data by simplified least squares procedures. Anal. Chem. 36, 1627–1639.

Scharlemann, J.P.W., Tanner, E.V.J., Hiederer, R., Kapos, V., 2014. Global soil carbon: Understanding and managing the largest terrestrial carbon pool. Carbon Manag. https://doi.org/10.4155/cmt.13.77

Schmidt, M.W.I., Torn, M.S., Abiven, S., Dittmar, T., Guggenberger, G., Janssens, I.A., Kleber, M., Kögel-Knabner, I., Lehmann, J., Manning, D.A.C., Nannipieri, P., Rasse, D.P., Weiner, S., Trumbore, S.E., 2011. Persistence of soil organic matter as an ecosystem property. Nature. https://doi.org/10.1038/nature10386

Shenk, J.S., Westerhaus, M.O., Berzaghi, P., 1997. Investigation of a LOCAL calibration procedure for near infrared instruments. J. Near Infrared Spectrosc. 5, 223–232.

Sherrod, L.A., Dunn, G., Peterson, G.A., Kolberg, R.L., 2002. Inorganic carbon analysis by modified pressure-calcimeter method. Soil Sci. Soc. Am. J. 66, 299–305.

Shi, P., Castaldi, F., van Wesemael, B., Van Oost, K., 2020. Vis-NIR spectroscopic assessment of soil aggregate stability and aggregate size distribution in the Belgian Loam Belt. Geoderma. https://doi.org/10.1016/j.geoderma.2019.113958

Shi, P., Zhang, Y., Li, P., Li, Z., Yu, K., Ren, Z., Xu, G., Cheng, S., Wang, F., Ma, Y., 2019. Distribution of soil organic carbon impacted by land-use changes in a hilly watershed of the Loess Plateau, China. Sci. Total Environ. 652, 505–512. https://doi.org/10.1016/j.scitotenv.2018.10.172

Six, J., Bossuyt, H., Degryze, S., Denef, K., 2004. A history of research on the link between (micro)aggregates, soil biota, and soil organic matter dynamics. Soil Tillage Res. https://doi.org/10.1016/j.still.2004.03.008

Six, J., Conant, R.T., Paul, E.A., Paustian, K., 2002. Stabilization mechanisms of soil organic matter: Implications for C-saturation of soils. Plant Soil 241, 155–176.

https://doi.org/10.1023/A:1016125726789

Six, J., Elliott, E.T., Paustian, K., Doran, J.W., 1998. Aggregation and Soil Organic Matter Accumulation in Cultivated and Native Grassland Soils. Soil Sci. Soc. Am. J. 62, 1367. https://doi.org/10.2136/sssaj1998.03615995006200050032x

Sollins, P., Homann, P., Caldwell, B.A., 1996. Stabilization and destabilization of soil organic matter: Mechanisms and controls. Geoderma 74, 65–105. https://doi.org/10.1016/S0016-7061(96)00036-5

Souza, E. de, Fernandes Filho, E.I., Schaefer, C.E.G.R., Batjes, N.H., Santos, G.R. dos, Pontes, L.M., 2016. Pedotransfer functions to estimate bulk density from soil properties and environmental covariates: Rio Doce basin. Sci. Agric. 73, 525–534. https://doi.org/10.1590/0103-9016-2015-0485

Stavi, I., Fizik, E., Argaman, E., 2015. Contour bench terrace (shich/shikim) forestry systems in the semi-arid Israeli Negev: Effects on soil quality, geodiversity, and herbaceous vegetation. Geomorphology. https://doi.org/10.1016/j.geomorph.2014.12.028

Stavi, I., Gusarov, Y., Halbac-Cotoara-Zamfir, R., 2019. Collapse and failure of ancient agricultural stone terraces: On-site geomorphic processes, pedogenic mechanisms, and soil quality. Geoderma 344, 144–152. https://doi.org/10.1016/j.geoderma.2019.03.007

Steinhof, A., Altenburg, M., Machts, H., 2017. Sample Preparation at the Jena 14C Laboratory, in: Radiocarbon. https://doi.org/10.1017/RDC.2017.50

Stevens, A., Ramirez-Lopez, L., 2020. An introduction to the prospectr package. R Packag. Vignette R Packag. version 0.2.1.

Stucki, J.W., Goodman, B.A., Schwertmann, U., 2012. Iron in soils and clay minerals. Springer Science & Business Media.

Stuiver, M., Polach, H.A., 1977. Discussion Reporting of 14 C Data . Radiocarbon 19, 355–363. https://doi.org/10.1017/s0033822200003672

Summerauer, L., Baumann, P., Ramirez-Lopez, L., Barthel, M., Bauters, M.,

Bibliography

Bukombe, B., Reichenbach, M., Boeckx, P., Kearsley, E., Van Oost, K., 2021. The Central African Soil Spectral Library: A new soil infrared repository and a geographical prediction analysis. SOIL 7, 693–715.

Tang, J., Riley, W.J., 2015. Weaker soil carbon-climate feedbacks resulting from microbial and abiotic interactions. Nat. Clim. Chang. https://doi.org/10.1038/nclimate2438

Tarolli, P., Sofia, G., Calligaro, S., Prosdocimi, M., Preti, F., Dalla Fontana, G., 2015. Vineyards in Terraced Landscapes: New Opportunities from Lidar Data. L. Degrad. Dev. 26, 92–102. https://doi.org/10.1002/ldr.2311

Thevenot, M., Dignac, M.F., Rumpel, C., 2010. Fate of lignins in soils: A review. Soil Biol. Biochem. https://doi.org/10.1016/j.soilbio.2010.03.017

Thompson, A., Chadwick, O.A., Rancourt, D.G., Chorover, J., 2006. Iron-oxide crystallinity increases during soil redox oscillations. Geochim. Cosmochim. Acta 70, 1710–1727. https://doi.org/10.1016/j.gca.2005.12.005

Thuiller, W., Lavorel, S., Araújo, M.B., Sykes, M.T., Prentice, I.C., 2005. Climate change threats to plant diversity in Europe. Proc. Natl. Acad. Sci. U. S. A. https://doi.org/10.1073/pnas.0409902102

Todd-Brown, K.E.O., Randerson, J.T., Post, W.M., Hoffman, F.M., Tarnocai, C., Schuur, E.A.G., Allison, S.D., 2013. Causes of variation in soil carbon simulations from CMIP5 Earth system models and comparison with observations. Biogeosciences. https://doi.org/10.5194/bg-10-1717-2013

Toma, Y., Clifton-Brown, J., Sugiyama, S., Nakaboh, M., Hatano, R., Fernández, F.G., Ryan Stewart, J., Nishiwaki, A., Yamada, T., 2013. Soil carbon stocks and carbon sequestration rates in seminatural grassland in Aso region, Kumamoto, Southern Japan. Glob. Chang. Biol. https://doi.org/10.1111/gcb.12189

Toraya, H., 2016. A new method for quantitative phase analysis using X-ray powder diffraction: Direct derivation of weight fractions from observed integrated intensities and chemical compositions of individual phases. J. Appl. Crystallogr. 49, 1508–1516.

https://doi.org/10.1107/S1600576716010451

Van De Broek, M., Temmerman, S., Merckx, R., Govers, G., 2016. Controls on soil organic carbon stocks in tidal marshes along an estuarine salinity gradient. Biogeosciences. https://doi.org/10.5194/bg-13-6611-2016

van den Boogaart, K.G., Tolosana, R., Bren, M., van den Boogaart, M.K.G., 2021. Compositions: compositional data analysis.

Van Oost, K., Quine, T.A., Govers, G., De Gryze, S., Six, J., Harden, J.W., Ritchie, J.C., McCarty, G.W., Heckrath, G., Kosmas, C., Giraldez, J. V., Marques Da Silva, J.R., Merckx, R., 2007. The impact of agricultural soil erosion on the global carbon cycle. Science (80-.). 318, 626–629. https://doi.org/10.1126/science.1145724

Van Oost, K., Verstraeten, G., Doetterl, S., Notebaert, B., Wiaux, F., Broothaerts, N., Six, J., 2012. Legacy of human-induced C erosion and burial on soil-atmosphere C exchange. Proc. Natl. Acad. Sci. U. S. A. https://doi.org/10.1073/pnas.1211162109

Vandenbygaart, A.J., Kroetsch, D., Gregorich, E.G., Lobb, D., 2012. Soil C erosion and burial in cropland. Glob. Chang. Biol. 18, 1441–1452. https://doi.org/10.1111/j.1365-2486.2011.02604.x

Viscarra Rossel, R.A., Lee, J., Behrens, T., Luo, Z., Baldock, J., Richards, A., 2019. Continental-scale soil carbon composition and vulnerability modulated by regional environmental controls. Nat. Geosci. https://doi.org/10.1038/s41561-019-0373-z

Viscarra Rossel, R.A., Walvoort, D.J.J., McBratney, A.B., Janik, L.J., Skjemstad, J.O., 2006. Visible, near infrared, mid infrared or combined diffuse reflectance spectroscopy for simultaneous assessment of various soil properties. Geoderma. https://doi.org/10.1016/j.geoderma.2005.03.007

Vohland, M., Ludwig, B., Seidel, M., Hutengs, C., 2022. Quantification of soil organic carbon at regional scale: Benefits of fusing vis-NIR and MIR diffuse reflectance data are greater for in situ than for laboratory-based modelling approaches. Geoderma 405, 115426.

Von Fromm, S.F., Hoyt, A.M., Lange, M., Acquah, G.E., Aynekulu, E., Berhe,

A.A., Haefele, S.M., Mcgrath, S.P., Shepherd, K.D., Sila, A.M., Six, J., Towett, E.K., Trumbore, S.E., Vägen, T.G., Weullow, E., Winowiecki, L.A., Doetterl, S., 2021. Continental-scale controls on soil organic carbon across sub-Saharan Africa. SOIL. https://doi.org/10.5194/soil-7-305-2021

von Lützow, M., Kögel-Knabner, I., Ekschmitt, K., Flessa, H., Guggenberger, G., Matzner, E., Marschner, B., 2007. SOM fractionation methods: Relevance to functional pools and to stabilization mechanisms. Soil Biol. Biochem. https://doi.org/10.1016/j.soilbio.2007.03.007

Walter, C., Merot, P., Layer, B., Dutin, G., 2003. The effect of hedgerows on soil organic carbon storage in hillslopes. Soil Use Manag. 19, 201–207. https://doi.org/10.1079/sum2002190

Wang, C., Zhao, L., Fang, H., Wang, L., Xing, Z., Zou, D., Hu, G., Wu, X., Zhao, Y., Sheng, Y., Pang, Q., Du, E., Liu, G., Yun, H., 2021. Mapping surficial soil particle size fractions in alpine permafrost regions of the qinghai-tibet plateau. Remote Sens. https://doi.org/10.3390/rs13071392

Wang, Q., Liu, S., Tian, P., 2018. Carbon quality and soil microbial property control the latitudinal pattern in temperature sensitivity of soil microbial respiration across Chinese forest ecosystems. Glob. Chang. Biol. 24, 2841–2849. https://doi.org/10.1111/gcb.14105

Wang, X., Sanderman, J., Yoo, K., 2018a. Climate-dependent topographic effects on pyrogenic soil carbon in southeastern Australia. Geoderma. https://doi.org/10.1016/j.geoderma.2018.02.025

Wang, X., Yoo, K., Wackett, A.A., Gutknecht, J., Amundson, R., Heimsath, A., 2018b. Soil organic carbon and mineral interactions on climatically different hillslopes. Geoderma 322, 71–80. https://doi.org/10.1016/j.geoderma.2018.02.021

Wang, Y., Wang, S., Adhikari, K., Wang, Q., Sui, Y., Xin, G., 2019. Effect of cultivation history on soil organic carbon status of arable land in northeastern China. Geoderma 342, 55–64.

Wang, Z., Hoffmann, T., Six, J., Kaplan, J.O., Govers, G., Doetterl, S., Van Oost, K., 2017. Human-induced erosion has offset one-third of carbon

emissions from land cover change. Nat. Clim. Chang. 7, 345–349. https://doi.org/10.1038/nclimate3263

Wang, Z., Shi, W., 2018. Robust variogram estimation combined with isometric log-ratio transformation for improved accuracy of soil particle-size fraction mapping. Geoderma 324, 56–66.

Wang, Z., Shi, W., 2017. Mapping soil particle-size fractions: A comparison of compositional kriging and log-ratio kriging. J. Hydrol. https://doi.org/10.1016/j.jhydrol.2017.01.029

Wang, Z., Van Oost, K., Govers, G., 2015. Predicting the long-term fate of buried organic carbon in colluvial soils. Global Biogeochem. Cycles 29, 65–79. https://doi.org/10.1002/2014GB004912

Wang, Z., Van Oost, K., Lang, A., Quine, T., Clymans, W., Merckx, R., Notebaert, B., Govers, G., 2014. The fate of buried organic carbon in colluvial soils: A long-term perspective. Biogeosciences. https://doi.org/10.5194/bg-11-873-2014

Wei, W., Chen, D., Wang, L., Daryanto, S., Chen, L., Yu, Y., Lu, Y., Sun, G., Feng, T., 2016. Global synthesis of the classifications, distributions, benefits and issues of terracing. Earth-Science Rev. https://doi.org/10.1016/j.earscirev.2016.06.010

Welemariam, M., Kebede, F., Bedadi, B., Birhane, E., 2018. Exclosures backed up with community-based soil and water conservation practices increased soil organic carbon stock and microbial biomass carbon distribution, in the northern highlands of Ethiopia. Chem. Biol. Technol. Agric. 5, 12. https://doi.org/10.1186/s40538-018-0124-1

Wiaux, F., Vanclooster, M., Cornelis, J.T., Van Oost, K., 2014. Factors controlling soil organic carbon persistence along an eroding hillslope on the loess belt. Soil Biol. Biochem. https://doi.org/10.1016/j.soilbio.2014.05.032

Wiaux, F., Vanclooster, M., Van Oost, K., 2015. Vertical partitioning and controlling factors of gradient-based soil carbon dioxide fluxes in two contrasted soil profiles along a loamy hillslope. Biogeosciences 12, 4637–4649. https://doi.org/10.5194/bg-12-4637-2015

Wilke, F., Sommer, M., Van Oost, K., Bens, O., Fiener, P., 2017. Process-

oriented modelling to identify main drivers of erosion-induced carbon fluxes. SOIL. https://doi.org/10.5194/soil-3-83-2017

Xia, S., Song, Z., Li, Q., Guo, L., Yu, C., Singh, B.P., Fu, X., Chen, C., Wang, Y., Wang, H., 2021. Distribution, sources, and decomposition of soil organic matter along a salinity gradient in estuarine wetlands characterized by C:N ratio, δ13C-δ15N, and lignin biomarker. Glob. Chang. Biol. https://doi.org/10.1111/gcb.15403

Xu, G., Lu, K., Li, Z., Li, P., Wang, T., Yang, Y., 2015. Impact of soil and water conservation on soil organic carbon content in a catchment of the middle Han River, China. Environ. Earth Sci. 74, 6503–6510. https://doi.org/10.1007/s12665-015-4749-0

Yassoglou, N., Tsadilas, C., Kosmas, C., 2017. Colluvial Soils, in: The Soils of Greece. Springer International Publishing, Cham, p. 53. https://doi.org/10.1007/978-3-319-53334-6_5

Zádorová, T., Pení žek, V., 2018. Formation, morphology and classification of colluvial soils: a review. Eur. J. Soil Sci. https://doi.org/10.1111/ejss.12673

Zádorová, T., Penížek, V., Vašát, R., Žížala, D., Chuman, T., Vaněk, A., 2015. Colluvial soils as a soil organic carbon pool in different soil regions. Geoderma. https://doi.org/10.1016/j.geoderma.2015.04.012

Zhang, M., Shi, W., Xu, Z., 2020. Systematic comparison of five machine-learning models in classification and interpolation of soil particle size fractions using different transformed data. Hydrol. Earth Syst. Sci. https://doi.org/10.5194/hess-24-2505-2020

Zhang, S.H., Li, S., Wu, B., Yan, P., Wei, X.H., 2011. Study of soil erosion using 137Cs method in rocky desertification region of northern Guangdong. For. Res.

Zhao, M., Jacobs, L., Bouillon, S., Govers, G., 2021. Rapid soil organic carbon decomposition in river systems: Effects of the aquatic microbial community and hydrodynamical disturbance. Biogeosciences. https://doi.org/10.5194/bg-18-1511-2021

Zhao, P., Fallu, D.J., Cucchiaro, S., Tarolli, P., Waddington, C., Cockcroft, D., Snape, L., Lang, A., Doetterl, S., Brown, A.G., Van Oost, K., 2021.

Bibliography

Soil organic carbon stabilization mechanisms and temperature sensitivity in old terraced soils. Biogeosciences 18, 6301–6312. https://doi.org/10.5194/bg-18-6301-2021

Zheng, G., Ryu, D., Jiao, C., Xie, X., Cui, X., Shang, G., 2019. Visible and near-infrared reflectance spectroscopy analysis of a coastal soil chronosequence. Remote Sens. https://doi.org/10.3390/rs11202336